Metamorphic microtextures and mineral assemblages in orthogneisses in NW Skåne – how do they correlate with technical properties?

Maria Eleni Taxopoulou

Dissertations in Geology at Lund University,
Master's thesis, no 607
(45 hp/ECTS credits)

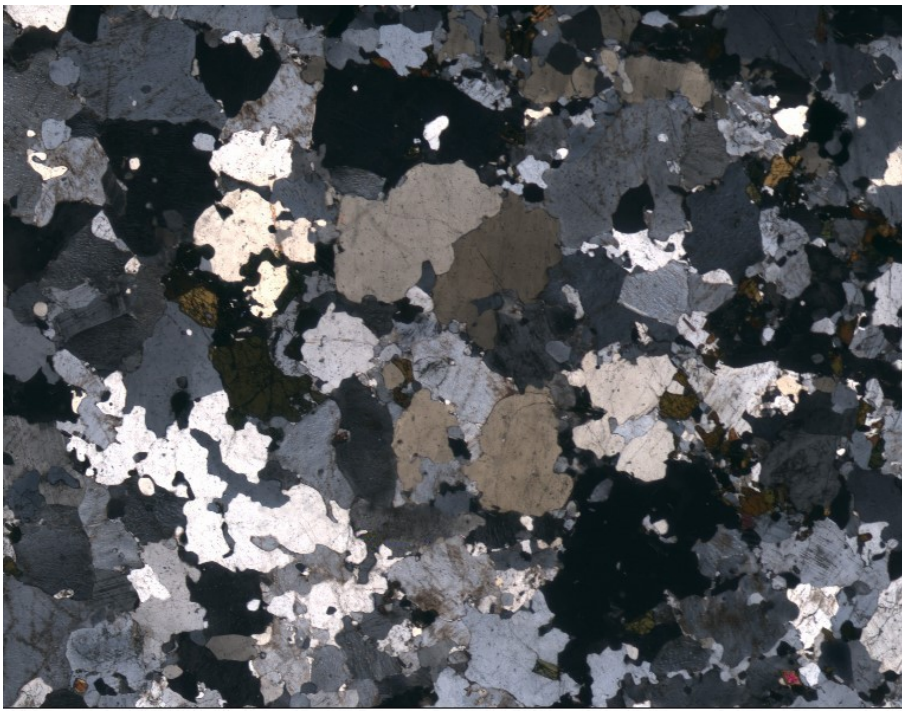

Department of Geology
Lund University
2020

Metamorphic microtextures and mineral assemblages in orthogneisses in NW Skåne – how do they correlate with technical properties?

Master's thesis

Maria Eleni Taxopoulou

Department of Geology
Lund University
2020

Contents

Cover Picture: Microphotograph of sample MGO075116.

Metamorphic micro-textures and mineral assemblages in orthogneisses in NW Skåne – how do they correlate with technical properties?

MARIA ELENI TAXOPOULOU

Taxopoulou, M., 2020: Metamorphic micro-textures and mineral assemblages in orthogneisses in NW Skåne – how do they correlate with technical properties? *Dissertations in Geology at Lund University*, No. 607, 54 pp. 45 hp (45 ECTS credits).

Abstract: Glaciofluvial deposits used to be the most common source for construction aggregates in Sweden during the past decades; however, their source is limited and they must be preserved, as they also act as aquifers. Gravel has largely been replaced by crushed rock materials, but the technical properties of crushed rock depend on many factors, some of which can reduce the quality.

This study deals with granitic rocks in the Söderåsen area in northwest Skåne, south Sweden. Nineteen orthogneiss samples from the Eastern Segment of the Sveconorwegian Province have been analyzed. The primary goal was to investigate whether there is a correlation between their technical quality and their petrographic characteristics. The suitability of these rocks as aggregates, estimated from technical standard test values performed by the Geological Survey of Sweden (Los Angeles, MicroDeval, Studded Tyre), was compared with mineral content, metamorphic conditions, fabric, and micro-textures.

The study area was exposed to metamorphic conditions of upper amphibolite- up to granulite-facies. Most of the samples of higher quality (classes 1 and 2) are located in the northwest part of the study area. This area belongs to zone 6 (Möller & Andersson, 2018) that has higher metamorphic grade, as also indicated by the presence of orthopyroxene in the one metagabbro that was studied. On the other hand, the southeast part of the study area that includes the lower quality samples (mostly class 3), is located in zone 5 and has undergone slightly lower metamorphic conditions. A low average grain size and higher degree of strain also show good correlation with low Los Angeles values. Another important factor is the amount of very fine-grained material, as well as the grain boundary complexity. The latter factor contributes to a higher degree of interlocking between the grains, resulting in better technical properties. In this study, higher quality samples show higher amounts of very fine grains and medium- to high grain boundary complexity.

The samples located in the northwest part of the study area have higher proportion of quartz and perthitic exsolution in K-feldspar; garnet is present in very small, rounded crystals. In these samples, titanite is absent and tartan twinning in feldspars is rare, whereas apatite is more abundant.

The present investigation reveals that the samples located in the north and northwest part of the study area belong to the metamorphic zone 6 of the Eastern Segment and they are the most suitable for road and railway construction. The geological conditions are of high importance, as the metamorphic grade and the degree of deformation have a direct effect on the mineralogy and the fabrics, and therefore affect the technical quality in various ways.

Keywords: granitic gneiss, Eastern Segment, Söderåsen, rock quality, quantitative analyses, grain size, aspect ratio, circularity, mineralogy

Supervisor(s): Charlotte Möller

Subject: Bedrock Geology

Maria Eleni Taxopoulou, Department of Geology, Lund University, Sölvegatan 12, SE-223 62 Lund, Sweden. E-mail: ma3733ta-s@student.lu.se

Metamorfa mikrotexturer och mineralsammansättningar i ortognejs i NV Skåne - hur korrelerar de med tekniska egenskaper?

MARIA ELENI TAXOPOULOU

Taxopoulou, M., 2020: Metamorfa mikrotexturer och mineralsammansättningar i ortognejs i NV Skåne - hur korrelerar de med tekniska egenskaper? *Examensarbeten i geologi vid Lunds universitet*, Nr. 607, 54 sid. 45 hp.

Sammanfattning: Glacifluviala avlagringar har varit de vanligaste källorna för byggmaterial i Sverige under de senaste decennierna. De är dock ändliga resurser som måste bevaras eftersom de också fungerar som akvifärer. Krossat bergmaterial har i stor utsträckning ersatt naturgrus, men standarderna för deras tekniska egenskaper beror på många faktorer av vilka en del kan försämra deras kvalitet.

Denna studie behandlar granitiska bergarter i området i och runt Söderåsen i nordvästra Skåne, vilket geologiskt sett är en del av det Östra segmentet i den Svekonorvegiska provinsen. Nitton prover av granitisk ortognejs har undersökts. Det primära målet var att undersöka om det finns ett samband mellan deras tekniska kvalitet och deras petrografiska egenskaper. Lämpligheten för dessa bergarter som aggregat, uppskattat från tekniska standardtestvärden (Los Angeles-, MicroDeval-, Studded Tyre-tester utförda av Sveriges geologiska undersökning), jämfördes med mineralinnehåll, metamorfa förhållanden, struktur och mikrotexturer.

Studieområdet har geonmgått metamorfos i övre amfibolitfacies till högtrycks-granulitfacies. De flesta bergarter av högre kvalitet (klass 1 och 2) är belägna i den nordvästra delen av studieområdet. Detta område tillhör metamorfa zon 6 (Möller & Andersson, 2018) som har högst metamorf grad, vilket också indikeras av närvaron av ortopyroxen i det prov av metagabbro som studerades. Den sydöstra delen av studieområdet, som innehåller prover av lägre kvalitet (mestadels klass 3), har klassats som zon 5 (Möller & Andersson, 2018) och har genomgått metamorfa förhållanden av något lägre grad än zon 6. Låg genomsnittlig kornstorlek och höga deformationsgrad korrelerar med låga Los Angeles-värden, dvs. god kvalitet. En annan viktig faktor är mängden mycket finkornigt material såväl som korngränsernas komplexitet. Den senare påverkar sammanväxningen mellan kornen, där komplexa former resulterar i bättre tekniska egenskaper. I den här studien visar prover av högre kvalitet större mängder mycket fina korn och medelhög till hög korngränskomplexitet.

Proverna i den nordvästra delen av studieområdet har större andel kvarts och pertitisk avblandning i K-fältspat; granat förekommer som mycket små, rundade kristaller. I dessa prover saknas titanit och gallertvillingar i kalifältspat är sällsynt, medan apatit är vanligare.

Denna undersökning poängterar att proverna i den norra och nordvästra delen av studieområdet tillhör metamorf zon 6 i Östra segmentet och att dessa är bäst lämpade för väg- och järnvägsbyggande. Områdets geologiska förhållanden, såsom metamorf grad och deformationsgrad har en direkt inverkan på tekniska kvaliteter hos granitiska bergarter.

Nyckelord: granitisk gnejs, Östra segmentet, Svekonorvegiska orogenen, bergkvalitet, Los Angeles-test, dubbdäckprov, MicroDeval-test, petrografi

Handledare: Charlotte Möller

Ämnesinriktning: Berggrundsgeologi

Maria Eleni Taxopoulou, Geologiska institutionen, Lunds Universitet, Sölvegatan 12, 223 62 Lund, Sverige. E-post: ma3733ta-s@student.lu.se

1. Introduction

Sweden is one of the leading countries in Europe in the construction sector. The state and the municipalities are responsible for maintenance and expansion of the public road network, which had a total length of 215400 km in 2017 (European Commission, 2019). The demand for construction material is constantly increasing, in order to maintain the high quality and the continuous development of the road network.

One important goal of the industry is to locate the most suitable bedrock for road and railway aggregates, preferably close to where it will be used, to reduce the cost of transportation which can be very high. The most common source for aggregates in Sweden has been sand and gravel from glaciofluvial deposits (Figure 1). However, these deposits also store water, and it is vital that they are preserved. An alternative source of aggregates are granitic rocks, but they can vary in technical properties, and some are less suitable for construction material in highways or railroads.

In order to meet the expanding demand for crushed rock for road and construction and to locate sustainable materials, it is crucial to understand the variations in technical properties within the Swedish bedrock. The reasons for rocks having good or bad technical properties are affected by their geological history (metamorphic conditions, degree of deformation etc.), composition (mineral content) and microstructure (size, shapes and orientation of grains, fractures etc.). Therefore, it is necessary to study the geology of the area and analyze the mineral structures and textures of the rocks under microscope.

The study area in northwest Skåne was investigated for determination of technical quality by the Geological Survey of Sweden (SGU) in 2010, based on previous bedrock mapping (Persson & Göransson, 2010). All rock quality measurements were executed in the laboratory at SGU in Uppsala. Quantitative analyses included Studded Tyre test (A_N), MicroDeval test (M_{DE}), and Los Angeles test (LA). The results demonstrated a wide range of technical properties, despite that the rocks are of similar type (granitic gneisses) and are situated in a restricted area (20 x 40 km).

The primary purpose of this study is to determine the factors that drive the variation in technical properties between metagranitic rocks in the Söderåsen area. Is there a correlation with metamorphic conditions, mineral contents, grain size or grain shape? Deeper understanding of how different geological processes steer technical properties, has the potential to greatly facilitate the identification of sustainable materials. The basis of this understanding is the correlation of technical properties to mineralogy, petrography, and petrology, and this study attempts to provide such a basis for the orthogneisses of Söderåsen in Skåne.

2. Background

2.1 Geological setting

2.1.1 Regional geology

The Sveconorwegian Orogen

The Sveconorwegian Orogen represents the reworked southwest boundary of the Baltic Shield, formed after the collision (Figures 2, 3a, 3b) between Baltica and another major continent, possibly Amazonia, at the end of the Mesoproterozoic (1.14-0.90 Ga; Bingen et al., 2008). It is an orogenic belt of ca. 500 km width across southern Scandinavia and includes the present study area in NW Skåne (Figure 3c). The orogen consists of large lithotectonic segments, separated by N-S-trending ductile deformation zones (Bingen et al., 2008).

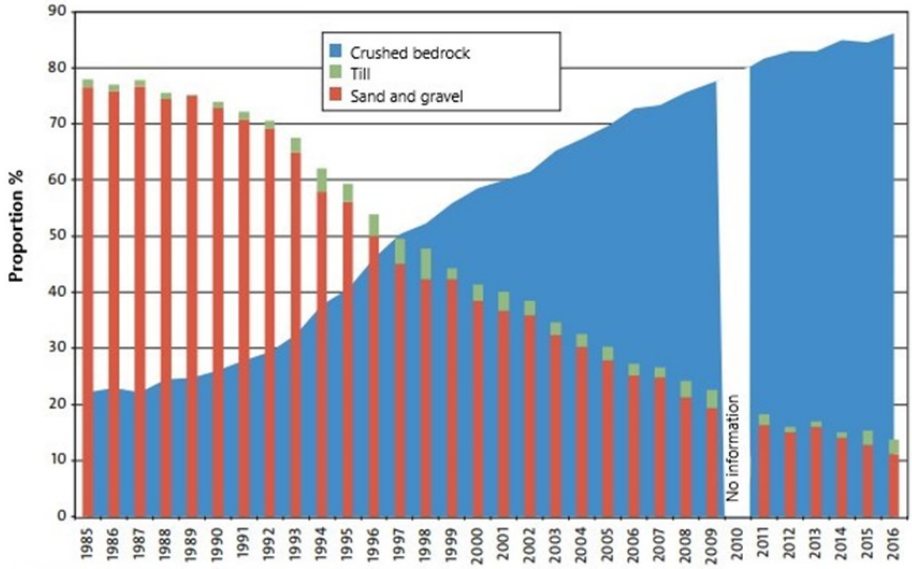

Figure 1. Percentage of sand and gravel, till and crushed bedrock in Sweden, during 1985-2016. The graph reveals that the amount of natural gravel being used as aggregates for construction has been reduced steadily through the last few decades. Figure modified after the Geological Survey of Sweden (Periodiska publikationer 2017:2).

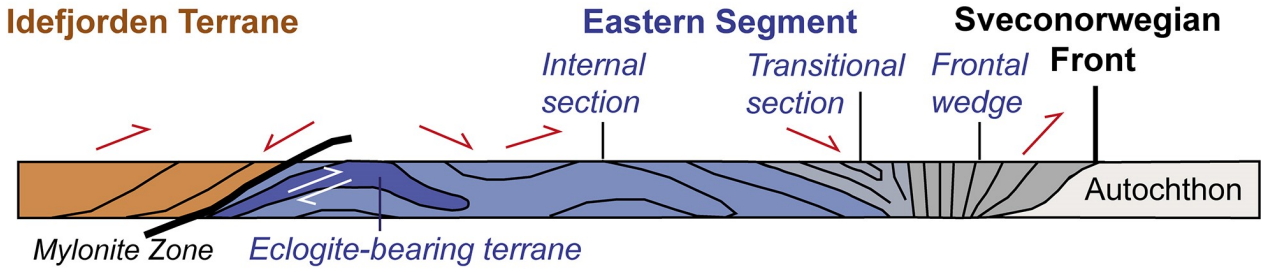

Figure 2: E-W cross-section of the eastern part of the Sveconorwegian Orogen, at the time of collision (0.98 Ga). Violet= underthrusting continental crust; light yellow = orogenic prism; orange = overriding plate. The blue dashed line marks the approximate location of the present erosion depth. Figure and figure text from Möller & Andersson (2018).

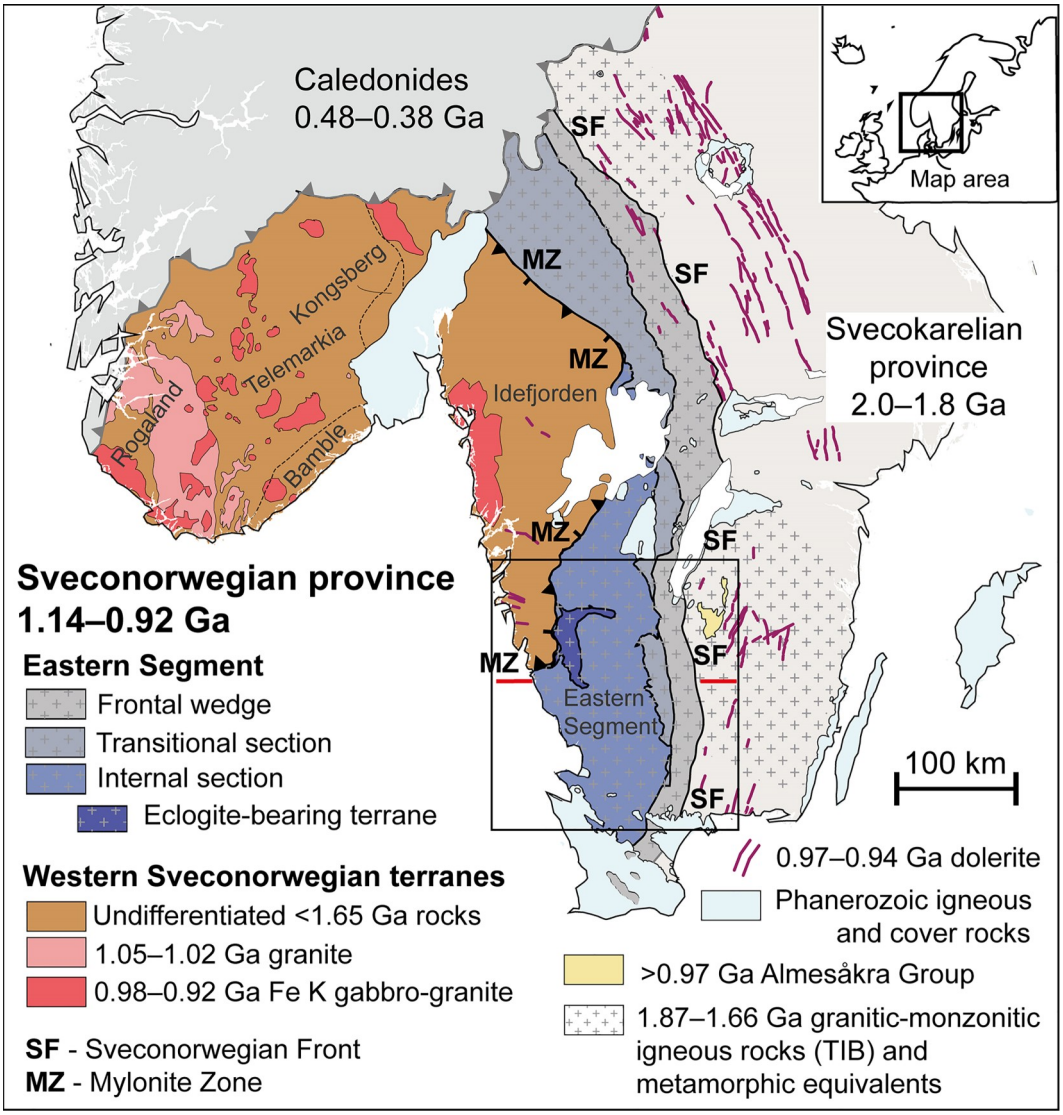

Figure 3: Tectonic and regional setting of the Sveconorwegian orogen (Möller & Andersson, 2018). (a) Plate reconstruction at the end of the Grenvillian–Sveconorwegian orogeny (unpublished compilation by B. Bingen, based on the reconstruction by Cawood et al. (2007); metamorphic subdivisions following Rivers (2008)). (b) Schematic representation of continent Baltica, inset to scale (transparent white with the Sveconorwegian orogen in pink), at two alternative positions in a collisional orogen: India-style v. intracontinental underthrusting. Modified from Möller et al. (2015). Composite satellite photograph of Asia in orthographic projection (source: NASA). (c) Tectonic map of the Sveconorwegian orogen (based on Geological Surveys of Sweden and Norway databases; distribution of 1.05–1.02 Ga granites from Laurent et al. (2016), with the Eastern Segment in violet to medium dark grey shades and a schematic cross-section. Internal subdivision of the Eastern Segment after Möller et al. (2015); eclogite-bearing nappe in darkest violet. Figure and figure text from Möller & Andersson (2018).

The Eastern Segment

The Eastern Segment is a continuation of bedrock which is unmetamorphosed east of the orogen. It consists of 1.81-1.66 Ga deformed gneissic granitoids originated from the Transcandinavian Igneous Belt (TIB; e.g. Lundqvist, 1979; Söderlund et al., 1999; Högdahl et al., 2004; Möller et al., 2007), with minor gabbroic to syenitoid intrusions 1.56-1.20 Ga old (Andersson et al., 1999; Söderlund et al., 2004; Larsson & Söderlund, 2005; Söderlund & Ask, 2006).

The southern part of the Eastern Segment underwent a pre-Sveconorwegian, high-grade metamorphic event, known as the Hallandian orogeny at 1.47-1.38 Ga (Hubbard, 1978; Möller et al., 2007). The Sveconorwegian orogeny resulted in penetrative deformation of the rocks under high–grade metamorphism of high-pressure granulite- and amphibolite-facies at ca. 0.98 Ga (Johansson et al., 1991; Xiang-Dong, 1996; Möller & Söderlund, 1997; Möller & Andersson, 2018); remnants of eclogite are present in one part of the Eastern Segment (Möller et al., 2015). The degree of the Sveconorwegian metamorphism increases from north to south and from east to west (Johansson et al., 1991; Söderlund et al., 1999). Cooling initiated at 0.97 Ga, followed by extensional movements along the regional deformation zones, a possible collapse of the orogeny and exhumation as a metamorphic core complex before or at 0.90 Ga (Bingen et al., 2008).

By examining the metamorphic assemblages of Fe-Ti-rich metagabbro, Möller & Andersson (2018) proposed eight metamorphic zones in the area (Figure 4). The internal section is marked mainly by the presence of leucosome in both felsic and mafic rocks. In zone 5, the main mineral assemblage in non-migmatitic metagabbro includes olive-green hornblende, plagioclase, garnet, biotite and Fe-Ti oxides, together with small, light-green metamorphic clinopyroxene, sometimes appearing as rims around relict igneous clinopyroxene crystals. In zone 6, orthopyroxene and antiperthitic plagioclase appear in the assemblage (Möller & Andersson, 2018). The Söderåsen area is located in the internal section, in zones 5 and 6.

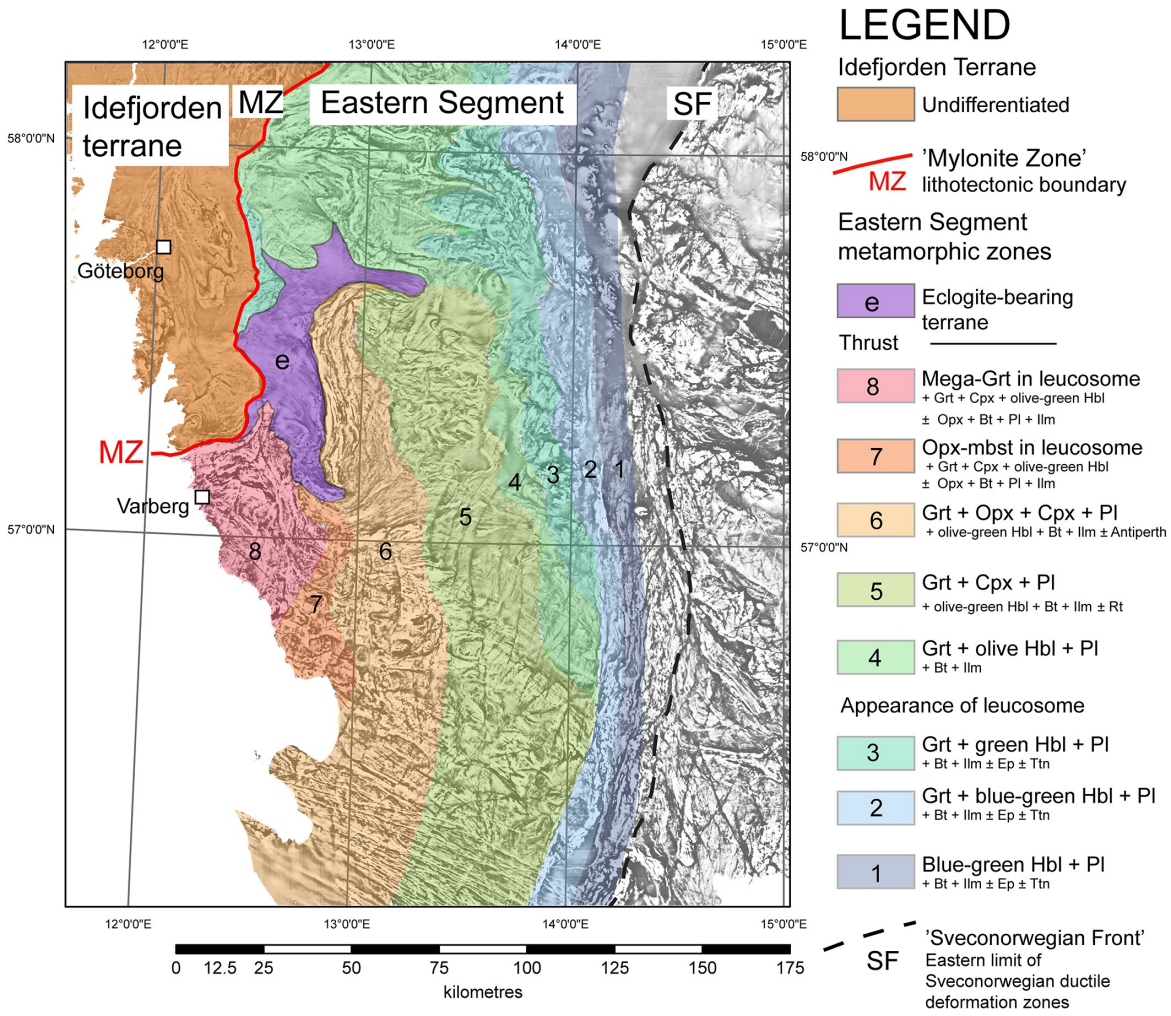

Figure 4: Metamorphic zones of the Eastern Segment (black square in Figure 3c), overlain on grayscale airborne magnetic anomaly map (differential field; source: Geological Survey of Sweden; softened contrast). Zones 1-8 represent gradually increasing metamorphic grade, from ≈550 ºC in the east part, to ≈850 ºC in the west part. Metamorphic zones are based on assemblages of Fe-Ti-rich metagabbro (n=276) of a c. 75 km wide profile between the coastal areas and 130 km towards ENE; zones are preliminary extrapolated to areas north and south of this profile. Figure and figure text from Möller & Andersson (2018).

The Tornquist Zone

The Sorgenfrei - Tornquist Zone (STZ) is a broad tectonic belt that cuts across Skåne in a NW - SE direction (Norling & Bergström, 1987), and it is a prolongation of the Teisseyre – Tornquist Zone (TTZ) that extends from the Black Sea to the Baltic Sea (Bergerat et al., 2007). The zone forms a boundary between the Precambrian crystalline bedrock in the north, and the Paleozoic sedimentary rocks in the south. The area underwent two main tectonic periods. The first one was an extensional episode during the Early Permian to the end of Mesozoic (299-66 Ma), resulting in normal faulting and major intrusion of diabase dykes. The second was a compressional episode during the Late Cretaceous to Tertiary, resulting in structural inversion characterized by strike-slip and reverse faulting (Bergerat et al., 2007).

2.1.2 Geology of the Söderåsen area

The study area is part of the Söderåsen project area of the Geological Survey of Sweden. The survey has created thematic maps of rock quality for different areas of Sweden, based on SGU's bedrock maps at 1:50000 scale, aiming at assessment of the rocks as aggregate materials.

The Söderåsen project area is 400 km^2 large in total and includes parts of the municipalities Bjuv, Klippan, Svalöv Åstorp, Ängelholm and Örkelljunga, in addition to smaller areas of Ljungbyhed, Stridsvig, Åstorp and Östra Ljungby (Figure 5; Persson & Göransson, 2010). The project area has four active quarries: Bjärsgård, Mölletofta, Össjö and Åstorp.

The Söderåsen project area comprises two NW-SE trending blocks of Precambrian bedrock, where the southern is horst Söderåsen and the northern is the NW extension of horst Linderödsåsen. The two parts are connected in the southeast. The bedrock is dominated by granitic to granodioritic gneisses with a generally good strength as reflected in technical properties (Persson & Göransson, 2010). However, in the southeastern parts of the analyzed area, the strength decreases (Sivhed & Wikman, 1986; Norling & Wikman, 1990; Wikman & Sivhed, 1992; Wikman et al., 1993).

The bedrock in the Söderåsen project area (Persson & Göransson, 2010) consists of meta-granitic rocks of the Eastern Segment, together with smaller bodies of amphibolite and metagabbro. The area is also host of unmetamorphosed Permian NW-SW-trending dolerite dykes. The dominating rocks are gneisses and gneissic granites to granodiorites. The granitic gneisses of

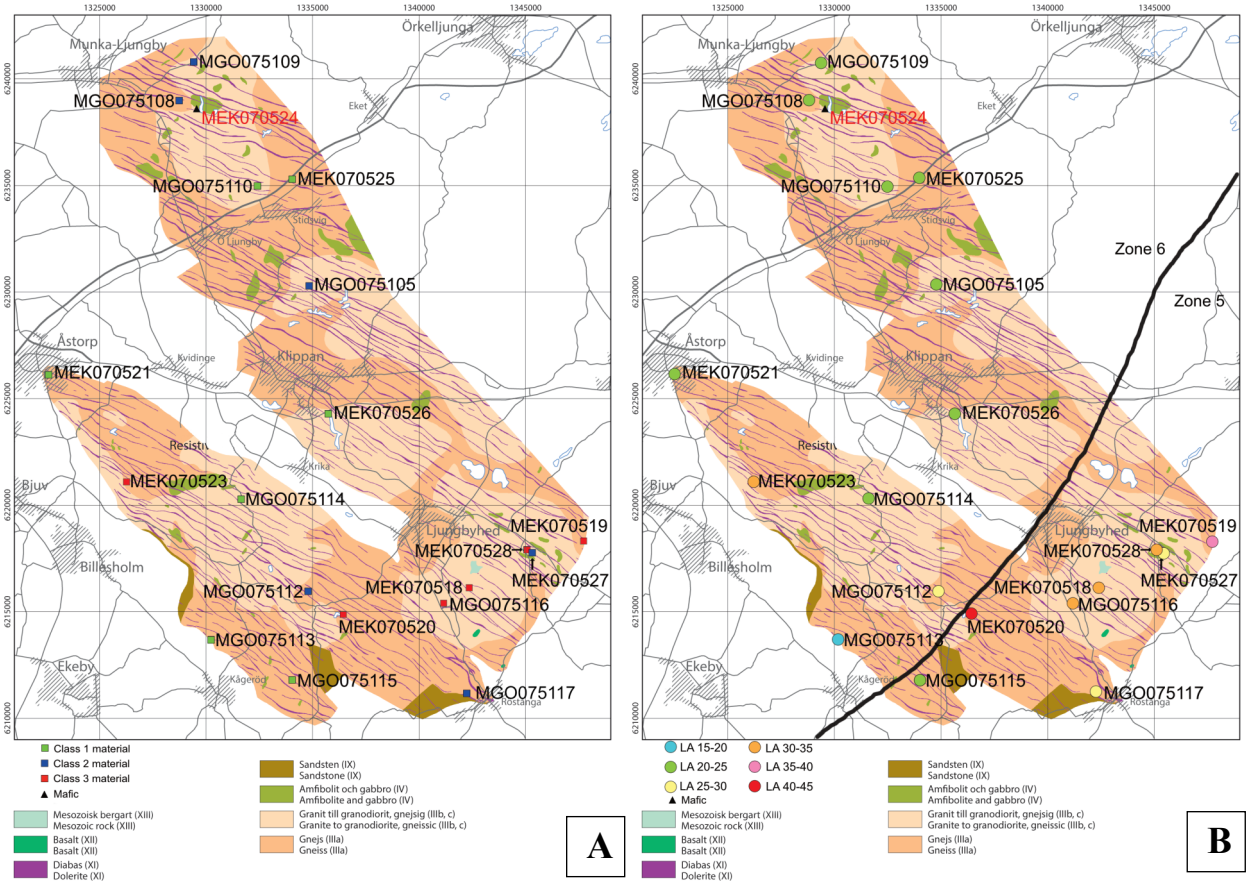

Figure 5: (A) Simplified bedrock map and sample sites for technical analyses, modified from Persson & Göransson (2010; based on Norling & Wikman (1990), Wikman et. al. (1993), Sivhed & Wikman (1986) and Wikman & Sivhed (1992)). Black labels mark samples of meta-granitic rocks; red label MEK070524 marks a sample of mafic granulite. (B) Same map with the LA values for each sample (Persson & Göransson, 2010). The black dashed line represents the south extension of the border between metamorphic zone 5 and 6 (after Möller & Andersson, 2018).

Söderåsen are fine to medium grained and have igneous protoliths, thus termed orthogneisses. The degree of deformation varies among the orthogneisses, from weak foliation to intensely deformed (Norling & Wikman, 1990; Wikman & Sivhed, 1992). Locally, orthogneisses show migmatitic structures which are stronger developed in some areas. Amphibolite bodies occur locally as inclusions, lenses or thin layers in gneisses, and less frequently as sizeable bodies. Characteristic for the area is northwest-trending diabase intrusions of Permian-Carboniferous age, dipping steeply to the southwest. The dolerite dykes are dark gray to black, fine grained and they can reach up to 50 meters wide (Persson & Göransson, 2010). The youngest rocks in the area are of basaltic composition and intruded during Jurassic time. Fracture zones or crushed zones which are oriented in a north direction generally occur in connection to contacts between the Precambrian bedrock and the younger sedimentary rocks (Sivhed & Wikman, 1986; Norling & Wikman, 1990; Wikman & Sivhed, 1992; Wikman et al., 1993).
The study area is located between the metamorphic zones 5 and 6, as proposed after Möller & Andersson (2018). The approximate extension of the limit between these metamorphic zones is drawn in Figure 5B.

2.2 Technical analyses

In order to evaluate whether a rock is appropriate to be exploited for industrial purposes, a series of standardized methods should be applied to measure the technical properties of this rock. The correlation between these methods is useful for estimation of the other when one of them is calculated (Göransson et al., 2008). These analyses were performed by the Geological Survey of Sweden in 2010 and will be described below. Approximately 70 kg of rock material were taken from each locality, in order to perform the technical analyses. Crushing, sieving and weighting were completed in the same way for the Los Angeles test, The MicroDeval test and the Studded Tyre test. The material was placed in a rotary jaw crusher with a 30 mm outlet gap and in a laboratory crusher with the outlet gap set at 16 mm. Sieving was done in a machine siever and fine sieving according to FAS-method 221-98 (Föreningen för asfaltsbeläggningar i Sverige, 1998). The fraction analyzed is 10-16 mm. The results from the technical analyses for all samples are presented in the Appendix.

2.2.1 Los Angeles Value Test (LA)

The Los Angeles value is an index of the rock's resistance to brittle fragmentation. High values indicate low resistance to fragmentation, thus poor technical properties.
The Los Angeles value (LA value) was determined in accordance with SS-EN 1097-2 (Swedish Standards Institute, 1997b). Around 5000 g of the analyzed material is required, and the material is crushed into 10 -14 mm size fractions prior to performing the test. The dry sample is placed in the Los Angeles steel drum, together with 11 steel spheres, each with a diameter of 47-49 mm, and rotated 500 times (approximately 30 minutes). Then, the sample is sieved through a 1.6 mm sieve, in a machine shaker for 10 minutes. The content (except for the fraction 0-1.6 mm) is weighted after the sieving.
The Los Angeles test value is calculated as a percentage of the original mass of the sample, following the equation:

$$\mathrm{LA} = \frac{5000 - m_1}{50}$$

where m_1 represents the sample weight in grams after the fragmentation process.

2.2.2 Studded Tyre Test (A_N)

The Studded Tyre Test value (A_N) is a measure of the rock's resistance to wear by abrasion from studded tyres and it is required by the Swedish Road Administration on ballast (material that is used to provide stability to a structure), among other things in road layers. High values indicate low resistance to abrasion, thus poor technical properties.

The A_N value has been performed according to the FAS Method 259-02 (Swedish Standards Institute, 2004). The sample is crushed in two steps by a rotational jaw crusher and a smaller jaw crusher. Following that, the sample is sieved, and the different fractions are weighed. Then the sample is placed in a ball mill together with steel spheres (7000 g) and 2 *l* of water. The ball mill rotates the sample for 5400 revolutions (ca. 1 hour), and when it is completed the steel spheres are removed and the sample is sieved again, dried and weighted in different fractions. The Studded Tyre Test value is calculated in relation to these fractions.

2.2.3 MicroDeval Test (M_{DE})

The MicroDeval value is an index of the rock's resistance to abrasion. High values indicate low resistance to abrasion, thus poor technical properties.

The M_{DE} value was determined in accordance with SS-EN 1097-1 (Swedish Standards Institute, 1997a). The process of crushing, sieving and weighing is the same as for the Studded Tyre Test. 500 g of the sample are placed in a mill together with steel spheres (5000 g) and 2,5 *l* of water and rotated for 12000 revolutions (ca. 2 hours). Then the steel spheres are removed, and the sample is sieved through an 8 mm and a 1.6 mm sieve plane. The different fractions are dried and weighted.

The MicroDeval value is calculated as a percentage of the original mass of the sample, following the equation:

$$\mathrm{M_{DE}} = \frac{m_1 - m_2}{5}$$

where m_1 and m_2 represent the sample weight in g before and after the procedure, respectively.

2.2.4 Classification of the samples based on the technical analyses

The Swedish National Transport administration (Trafikverket) lays down the demands on the bedrock which can be used in asphalt layers and for unbound road constructions (Vägverket, 2005a; Vägverket, 2005b). The Studded Tyre Test value (resistance to abrasion caused by studded tyres) and the Los Angeles value (resistance to brittle fragmentation) are important properties for the highway roads, in order to preserve the sustainability of the road top surface – the asphalt layer; the unbound layers have similar requirements. In Table 1 there is a list with the requirements for each type of road.

Road Type	A_N	M_{DE}	LA
Highway asphalt layers	<7 or <9%	<15%	<25%
Other asphalt layers	<11 or <14%	<15%	<25%
Base course	-	<20 or <25%	<40%
Sub layer	-	<25 or <30%	No demand

Table 1: Standards for Studded Tyre Test, MicroDeval Test and Los Angeles value for different road types (Mattias Göransson, personal communication, 22/06/2020).

The Geological Survey of Sweden (SGU) has classified the aggregate quality of the samples, in relation to their suitability for road construction, railway or concrete (Persson & Göransson, 2010). In general, aggregate quality class 1 corresponds to the most suitable rock as road construction material, whereas aggregate quality class 4 is not suitable at all as a road construction material. Table 2 shows the requirements for each class, and Figure 6 presents the results from the classification.

SGU Road	Road Type	A_N	M_{DE}	LA
Class 1	Most asphalt layers, unbound layers	<10%	<7%	<30%
Class 2	Only in roads with less traffic & in unbound layers	10-18%	7-14%	<30%
Class 3	Only in unbound layers	>18%	>14%	30-50%
Class 4	Should not be used as a road stone at all	-	>30%	>50%

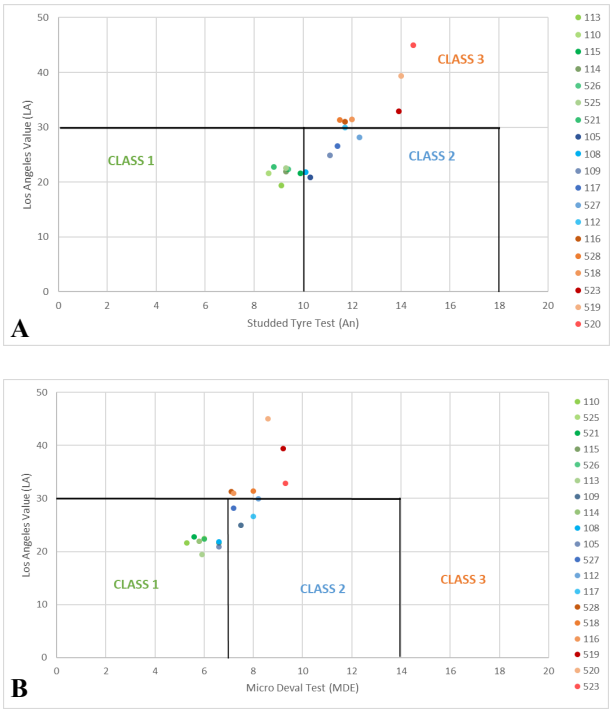

Figure 6: Diagrams showing the technical test results for metagranitic rocks in the Söderåsen area, from Persson & Göransson (2010), with sample color code added for road-material based on LA and AN /MDE (greens= class 1; blues= class 2; reds class 3), (A) Studded Tyre Test value (AN) vs Los Angeles-value (LA), (B) MicroDeval (MDE) value vs Los Angeles-value (LA).

2.3 Petrography

2.3.1 Mineral species

The mineral content of a rock is one of the most important factors affecting the technical properties. The most essential properties of a mineral species in a rock are the chemical composition, shape, density, strength and cleavage. In granitic rocks, the dominant minerals are quartz, K-feldspar, plagioclase, amphibole and micas, so their properties and proportions affect the technical properties, as well as the texture, which refers to how the minerals are arranged in the rock.

Quartz crystals have high hardness and low cleavage, providing the rock with better resistance to wear (lower M_{DE} and A_N values). They are also anhedral, and they usually crystallize in the remaining space between other grains, resulting in lowering the rock's porosity (Goodman, 1989; Tugrul & Zarif, 1999; Jo-

Table 2: Classification for Studded Tyre Test, MicroDeval Test and Los Angeles value for different road types (Mattias Göransson, personal communication, 22/06/2020).

hansson, 2011). Additionally, quartz is easy to recrystallize and they can create crystals with complex grain boundaries and good interlocking, making the rock more resistant to fragmentation (lower LA value; Hellman et al., 2011). Increased quartz content results in better interlocking of the individual grains, increasing the rock's strength (Merriam et al., 1970; Johansson, 2011).

Feldspar has relatively high hardness, and it generally increases the rock's resistance to abrasion. However, it usually has two cleavage plains that intersect at 90º, negatively influencing the resistance to brittle fragmentation of the rock (Brattli, 1992; Miskovsky et al., 2004). Plus, feldspar is connected with microcrack presence and therefore decreasing the rock's strength (Johansson, 2011). The sericite that might form as alteration product causes the feldspar to be less brittle, increasing the rock's resistance to brittle fragmentation (Åkesson et al., 2004). The reason is that sericite micas usually grow perpendicular to the cleavage planes so they tend to propagate cracks.

The phyllosilicate minerals found in rocks may diminish or raise the technical properties of the rock, and they are considered to be very important in controlling the overall behavior of the rock (Lanin et al., 2019). Micas (in orthogneisses there is mostly biotite, sericite and chlorite) usually form flaky grains. They are quite soft and flexible, giving the rock higher resistance to fragmentation but low resistance to abrasion. The spatial arrangement of those minerals is crucial, because if they are randomly oriented in relation to the fabric, they can act as barriers of the (micro) fractures, but when they are oriented parallel to the fabric, they lower the rock's strength by causing fracture initiation and propagation (Åkesson et al., 2004). Increasing mica content has a negative impact on the MicroDeval and the Studded Tyre test values, resulting in lower technical properties (Johansson, 2011). Nonetheless, chlorite sometimes act almost similar to holes in the rock, and the cracking might disappear in the chlorite and appear again on the other side of the crystal (Jan-Erik Lindqvist, personal communication, 17/11/2020).

The amphibole usually appears long, prismatic or fibrous. The inosilicate minerals generally increase the rock's flakiness and brittleness but in high percentage it can decrease the total strength of the rock (Brattli, 1992).

2.3.2 Textures

Exsolution textures

When there is a change in the metamorphic conditions, the minerals that are solid solutions of two or more phases can have exsolution structures. The presence of *perthitic exsolution* in K-feldspar shows that the rock experienced high (igneous or metamorphic) temperatures, such that there was increased solid solution of albite in K-feldspar. The exsolution texture is the result of slow cooling, since below a certain temperature there is a miscibility gap between the albitic and the anorthitic component. In K-feldspar, local increase of exsolution may be caused by deformation of old crystals in lower-grade conditions (Passchier & Trouw, 1997). In plagioclase, the corresponding exsolution of K-feldspar is known as *anti-perthitic exsolution*. Other temperature indicators are tartan twinning in K-feldspar, which is typical of microcline (low- temperature polymorph), and Carlsbad twinned K-feldspar, which occurs in orthoclase and is the higher-temperature polymorph.

The vermicular intergrowth of quartz in feldspar is a bulbous type of symplectite called *myrmekite.* It is usually found in high-grade metamorphic and igneous rocks (Passchier & Trouw, 1997). The formation of the myrmekites is caused by the breakdown of feldspar during retrograde metamorphism (Phillips, 1974; Smith, 1974; Phillips, 1981; Shelley, 1993), but they can also appear in progressive deformation, where there might be an area of higher stress (Simpson & Wintsch, 1989). In the second case, the myrmekites are shear/deformation indicators.

Interlocking textures

The geometry of the grains is related to their degree of interlocking; if the grain boundaries are straight, including anhedral or subhedral grains, the rock has a *polygonal texture*. Grains with irregular or lobate grain boundaries form an *interlobate texture*, and when a rock consists of strongly curved grains, it has an *amoeboid texture*. As for the shape of grain aggregates, the term *granoblastic* is used for a metamorphic rock that looks like a mosaic that is formed by equidimensional grains, having the lowest degree of interlocking. Lastly, the term *porphyroblastic* refers to an inequigranular texture that includes many large grains that have formed during metamorphism in a finer-grained matrix (Passchier & Trouw, 1997).

Foliation and lineation textures

The foliation describes any flat texture that develops penetratively in a rock. Fossen (2010) uses the definition of foliation as *"a planar structure formed by tectonic processes and includes cleavages, schistosity and mylonitic foliations". Cleavage* is mostly found in low -grade metamorphic rocks and mica-rich gneisses or schists, describing the splitting of the rock into almost parallel surfaces. A special type of cleavage is *crenulation cleavage*, a secondary tectonic fabric that is composed by microfolds developing on pre-existing folds. Schistosity appears in higher metamorphic conditions, when the foliation becomes less planar and is located around strong minerals or mineral aggregates. Finally, *mylonitic foliations* are connected to transposed layering and gneissic banding (Fossen, 2010).

The lineation describes any linear texture that develops penetratively in a rock and they are more common in metamorphic rocks. Fossen (2010) uses the definition of lineation as "*a fabric element in which one dimension is considerably longer than the other two".* The standard types of lineations are: (i) *mineral lineation* (a penetrative fabric formed due to alignment of prismatic or elongated minerals or mineral aggregates),

(ii) *stretching lineation* (plastically deformed minerals or mineral aggregates), (iii) *fiber lineation* (in low pressure and temperature metamorphic conditions, minerals like quartz and calcite can develop parallel fibrous crystals that specify linear elements), (iv) *intersection lineation* (a combination of more than one set of planar structures), (v) *crenulation lineation* (small-scale folds or crenulations occurring in phyllosilicate-rich metamorphic rocks) and (vi) *slicken lines or striations* (formed due to abrasion of hanging-wall rocks into the footwall, mostly found on shear fractures) (Fossen, 2010).

3. Methods

3.1 Field investigation

All sampling and geological interpretation has been made within mapping activities carried out by the Geological Survey of Sweden. Twenty-five samples were collected by the SGU in 2010 in order to perform technical analyses and create a geological map with the different classes of bedrock material. Nineteen samples out of them are of meta-granitic composition, and they have been selected for further analysis in this work (Figure 5). The coordinates are specified according to national grid RT90. The field work for the present MSc project involved visiting these sample sites in order to describe and document the outcrops and rocks, in October 2019 and May 2020.

3.2 Petrographic microscopy

The sawing of rock slabs for thin sections was performed by the SGU and the samples were sent to Lund University to be used in this study. One polished thin section exists per sample, a total of 23 thin sections. 19 of them are orthogneisses, whereas the remaining are mafic granulites and basalts. The thin sections dimensions range between 34 and 36 mm in length, and 19 and 21 mm in width.

The thin sections were studied under a standard polarizing microscope equipped with 2X, 4X, 10X and 40X objectives, in order to describe the mineral contents and textures. Photomicrographs were taken for each sample to illustrate the main mineralogy, the metamorphic texture, and possible alterations.

3.3 Point counting

Each sample was analyzed with the point counting method to determine the modal content of an area that is covered by a mineral. The basic method of point counting is that the thin section is placed under a polarizing microscope, where a point counter (a slide advance mechanism) is connected to the stage of the microscope. The machine moves the thin section on a specified distance (step) along a traverse line and when it stops, the mineral that appears on the cross is counted. A number of 500 points per thin section were counted, and the estimation of the proportion of the mineral is given as:

$$p_i = \frac{h_i}{N}$$

where p is the true proportion of a mineral i, h is the number of points hitting the mineral i and N is the total number of points counted (in this study N=500).

3.4 Grain size analysis

Grain size is a substantial criterion when analyzing the strength of a rock material. Generally, a fine-grained material is stronger than a coarse-grained material . Moreover, the association between the grain size distribution and the technical analyses show that the mechanical properties of a rock are controlled by the amount of fine-grained matrix, as even in small percentages, a fine-grained matrix can improve significantly the material's quality (Lundqvist & Göransson, 2001).

A series of measurements were carried out using polarized images and image analysis software. The thin sections were scanned with the aid of a plastic polarization filter. The sample was placed between two filters that acted as crossed polarizers. The photos cover the whole thin section, and they have the maximum resolution provided by the scanner (4000 dpi). These photos were used for the grain size analysis, using the ImageJ® software. The photo of the thin section was rescaled in mm.

First of all, it is required to decide how to count the mineral grains and how to show the grain size. In the present work, all grains were counted using the following specifications: (i) An altered crystal was counted as one grain, unless the alteration minerals could be clearly measured. (ii) Inclusions in minerals that were cut by the traverse line were counted separately. (iii) Small inclusions in minerals were not counted. (iv) Whether the sample appeared with a lineation fabric, the traverse lines were made both perpendicular and parallel to the fabric, in order to prevent any bias. (v) Grains on the borders of the thin section were not measured, because they were not complete.

A standard way to quantify the grain size, in accordance with the examination of the thin section under the optical microscope, is to perform two-dimensional measurements along a line of traverse. In this study, 300 grains per thin section were counted manually. The difficulty of using polarized photos on image analysis software is that each mineral appears with different hues and intensities under crossed nicols due to the angle of extinction, so any attempt of automatic calculation of grain size would create a significant error.

From the grain size measurements we can extract information regarding, among others: (i) the grain size,

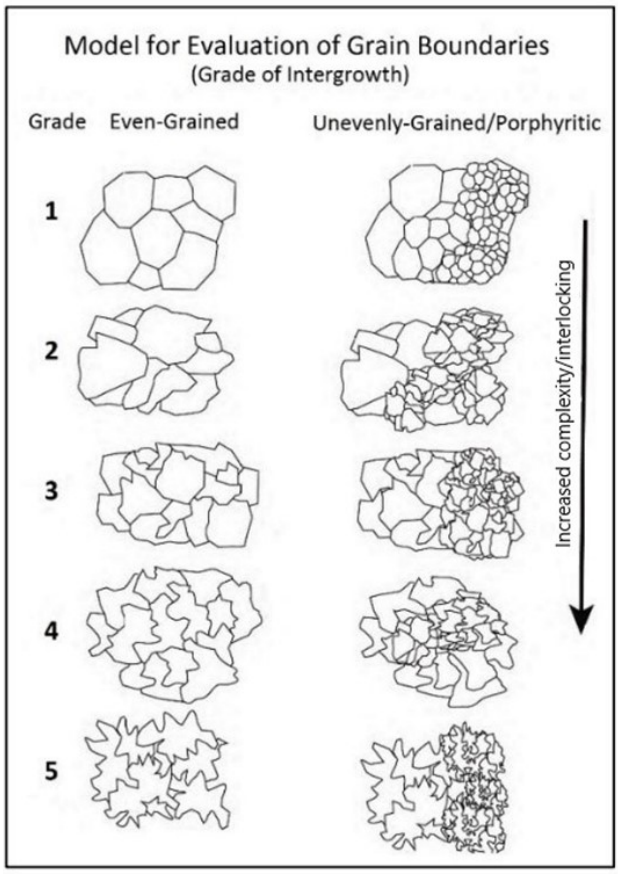

Figure 7: Scheme for evaluation of grain boundary complexity (degree of interlocking). From Hellman et al., (2011).

(ii) the grain boundary complexity, (iii) the degree of elongated grains, (iv) the circularity of the grains, (v) the area of the grains (mm^2).

3.5 Visual Classification of Grain Boundary Complexity (VC)

All 19 thin sections were analyzed microscopically to determine the amount of intergrowth between the grains and the grain complexity. Visual description of the degree of grain interlocking is described according to a five-point scale (Figure 7; Hellman et al., 2011). A straight grain joint is evaluated as scale 1 while a heavily lobed and irregular is evaluated as scale 5.

For these samples, the visual classification for grain boundary complexity was performed separately for the coarse-grained and the fine-grained material.

3.6 Microfracture analysis

Simmons & Richter (1976) give the definition for the word microcrack as *"an opening that occurs in rocks and has one or two dimensions smaller than the third. For flat microcracks, one dimension is much less than the other two and the width to length ratio, termed crack aspect ratio, much less than 10^{-2} and is typically 10^{-3} to 10^{-5}. The length… typically is of the order of 100 μm or less"*. They subcategorize the microcracks into *grain boundary cracks* (formed on the grain boundaries), *intragranular or intracrystalline cracks* (occurring within the grain) and *intergranular or intercrystalline cracks* (developing from a grain boundary into two or more grains). The term *transgranular crack* is used for cracks expanding across the grains or from one grain boundary and across a grain (Figure 8; Simmons & Richter, 1976; Kranz, 1983).

The rocks that consist of many light minerals like quartz and feldspar usually act in a brittle way, because these minerals have lower fracture energies and as a result, they can break easily. When that happens, the LA values retrieved are high (Lindqvist et al., 2007; Tavares & Neves, 2008). Microfractures are greatly dependent on the grain size, the mineral assemblage, the deformation fabric, and the microstructure of a rock, and they play a major role in the mechanical behavior of rocks used as aggregates (Åkesson et al., 2004). Microcracks in granitic rocks can be formed due to thermal changes in polymetamorphic rocks, tectonic stress during deformation and stress reduction

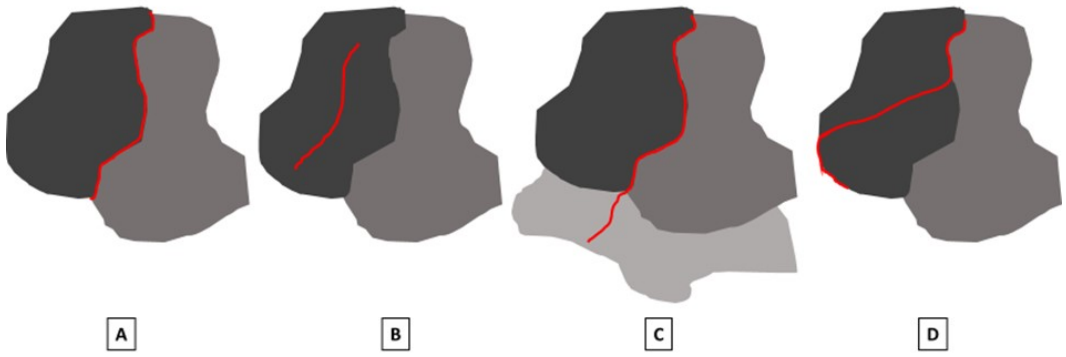

Figure 8: Schematic representation of: (A) a grain boundary crack, (B) an intragranular crack (occurring within the grain), (C) an intergranular crack (developing from a grain boundary into two or more grains), (D) α transgranular crack (expanding across the grain or from one grain boundary and across the grain) (Simmons & Richter, 1976; Kranz, 1983).

during uplift and unroofing (Kowallis & Wang, 1983; Hellman et al., 2011). The frequency of the microcracks can have a positive effect on the flakiness but a negative effect on the resistance to wear by abrasion from studded tyres (Miskovsky et al., 2004).

The microcrack analysis in this work was narrow because the thin sections were not impregnated with fluorescent epoxy, in order to be examined under the ultraviolet microscope. Four samples were selected for further analysis using a scanning electron microscope with a backscattered detector (SEM-BSE) in the Department of Geology of Lund University. The samples were coated with carbon (density of carbon coating 16 -19.5 nm) in order to increase the conductivity of the electrons. The first observation was successful and the microcracks were visible. However, these samples underwent the point counting after they got coated, resulting in alteration of the coat layer, and they had to be cleaned thoroughly with a 0.25 microns diamond paste, washed with rubbing alcohol and rerun the carbon coating. After this procedure, the microcracks were not visible, probably in most cases the excess carbon coating had filled the microcrack cavities, making it impossible to recognize them. Then, another set of four samples were selected for a second try, but after the first carbon coating the microcracks were not visible as well, probably for the same reason as before. The samples that could be analyzed are not representative. The photos obtained are limited and thus the interpretations are narrow.

4. Results

4.1 Sample sites

Individual sample sites are described macroscopically below, in the order of their technical properties, starting with class 1 samples. The coordinates of each outcrop, together with the results from the LA, MDE and AN analyses (performed by the SGU) are presented in the Appendix. The mafic granulite (sample MEK070524) is an indicator of the high metamorphic conditions of the area.

4.1.1 Samples of class 1

Sample MEK070525

North-east of Östra Ljungby, along highway E4, are exposures of gray-red granitic gneiss, fine- to medium-grained, with dm-long leucosome veins crosscutting the gneissic fabric (red arrow in Figure 9A). The veins are isotropic, thus younger than the gneissic fabric. The lineation here is the dominant texture and there is a weak foliation. Dark quartz is present primarily in the leucosome, and in lower amounts inside the host granitic gneiss. There is a high number of amphibole in the rock, which also has some signs of oxidation (Figure 9B).

Sample MGO075110

A quarry north-east of Östra Ljungby, exploited by Johanssons Grus & Mark Entreprenad AB, exposes red–gray, fine- to medium-grained granitic gneiss (Figure 9C). It is strongly deformed with various leucocratic parts rich in K-feldspar (Figure 9D) and shows variable strain within short distances (Figure 8E). Blasted boulders show that at least parts of the rock have a strong foliation defined by elongated aggregates of dark and light minerals, respectively, and we can macroscopically notice that the rock has a relict igneous fabric with very fine-grained feldspar aggregates, remnants of an igneous coarse feldspar grain. The rock contains dark-colored quartz (red arrows in Figure 9C).

Sample MEK070521

An abandoned quarry near Åstorp, run by Skanska AB and located in the westernmost part of the study area, exposes red, feldspar-rich granitic gneiss, fine-grained

with a gneissic fabric (Figure 9F). The rock has a strong lineation defined by elongated dark minerals, and the foliation fabric is weaker. Late fractures that cross-cut the rock have chlorite-covered surfaces. In the quarry, there are also fine- to medium-grained, folded meta-dolerite dykes and brecciated zones with hydrothermal deposits of pinkish carbonate.

Sample MEK070526

South-east of Klippan are exposures of grayish, fine- to medium-grained granitic gneiss with distinct lineation (Figure 9H). The rock is weakly foliated, and it contains dark quartz and mafic minerals (mostly amphibole) that define the gneissic fabric (Figure 9I).

Sample MGO075114

Close to Dragesholm, outcrops expose granitic gneiss of grayish-red color. This rock is fine- to medium-grained with a relict igneous coarse-grained texture, rich in K-feldspar, and has a distinct gneissic fabric (Figure 9J). Quartz is dark gray; dark minerals are dominantly hornblende and some fine-grained garnet.

Sample MGO075113

North of Kågeröd is a fine-grained dark gray granitic gneiss with a high amount of dark minerals (Figure 9K). The rock has a strong lineation (Figure 9L), and a slight foliation defined by the bands of dark minerals. Close to the coordinates of the sampled spot, a light red leucocratic granitic rock is exposed.

Sample MGO075115

East of Kågeröd are exposures of a gray-red granitic gneiss, fine-grained, with a strong gneissic fabric (Figure 9M). It has quartz veins and an increased amount of mafic minerals. The rock has a strong gneissic layering and foliation (Figure 9N). The reddish leucosome layers are coarser-grained and rich in feldspar and quartz, whereas the gray mesosome is more fine-grained and contains more mafic minerals.

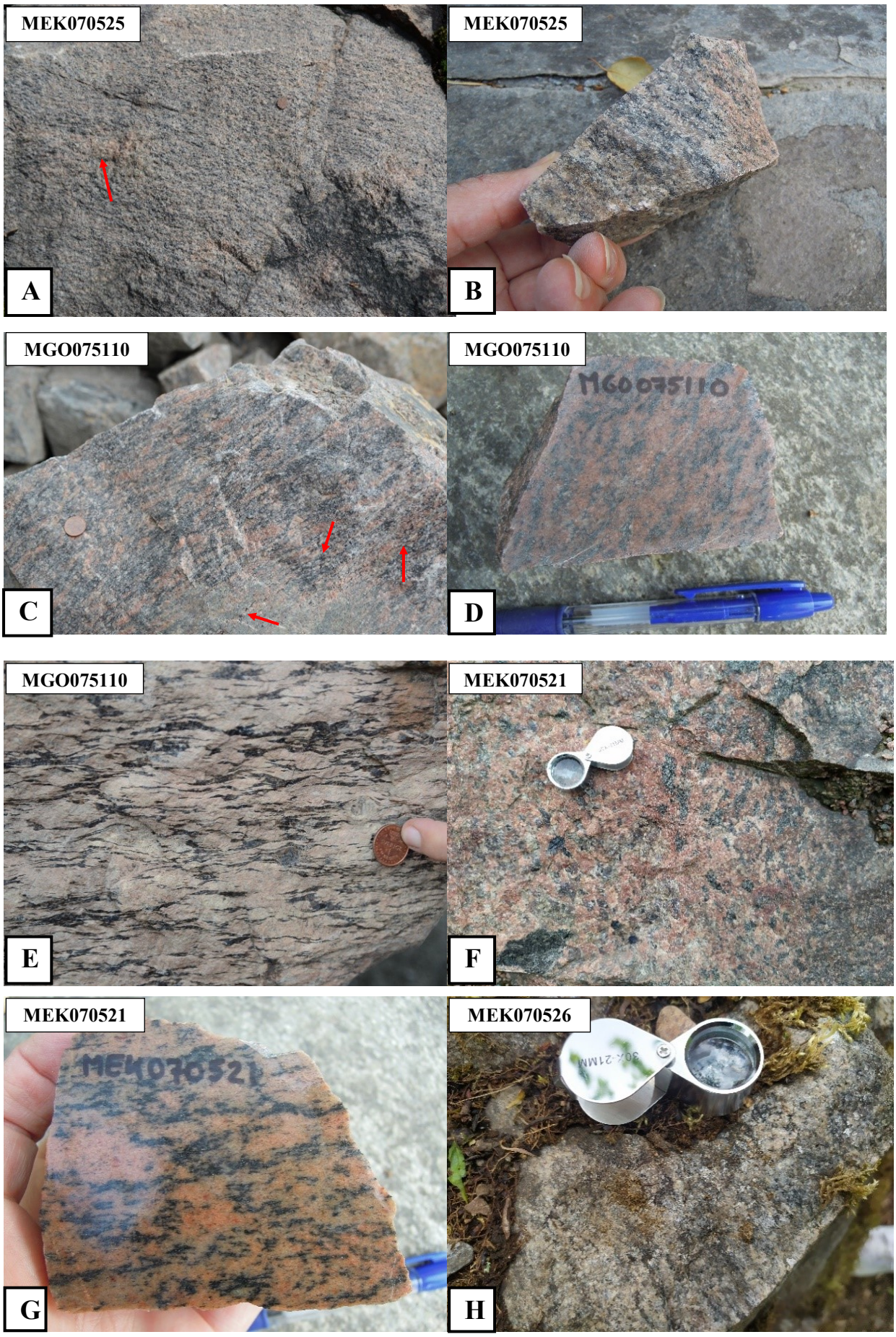
MEK070525
A
MEK070525
B
MGO075110
C
MGO075110
MGO075110
D
MGO075110
E
MEK070521
F
MEK070521
MEK070521
G
MEK070526
H

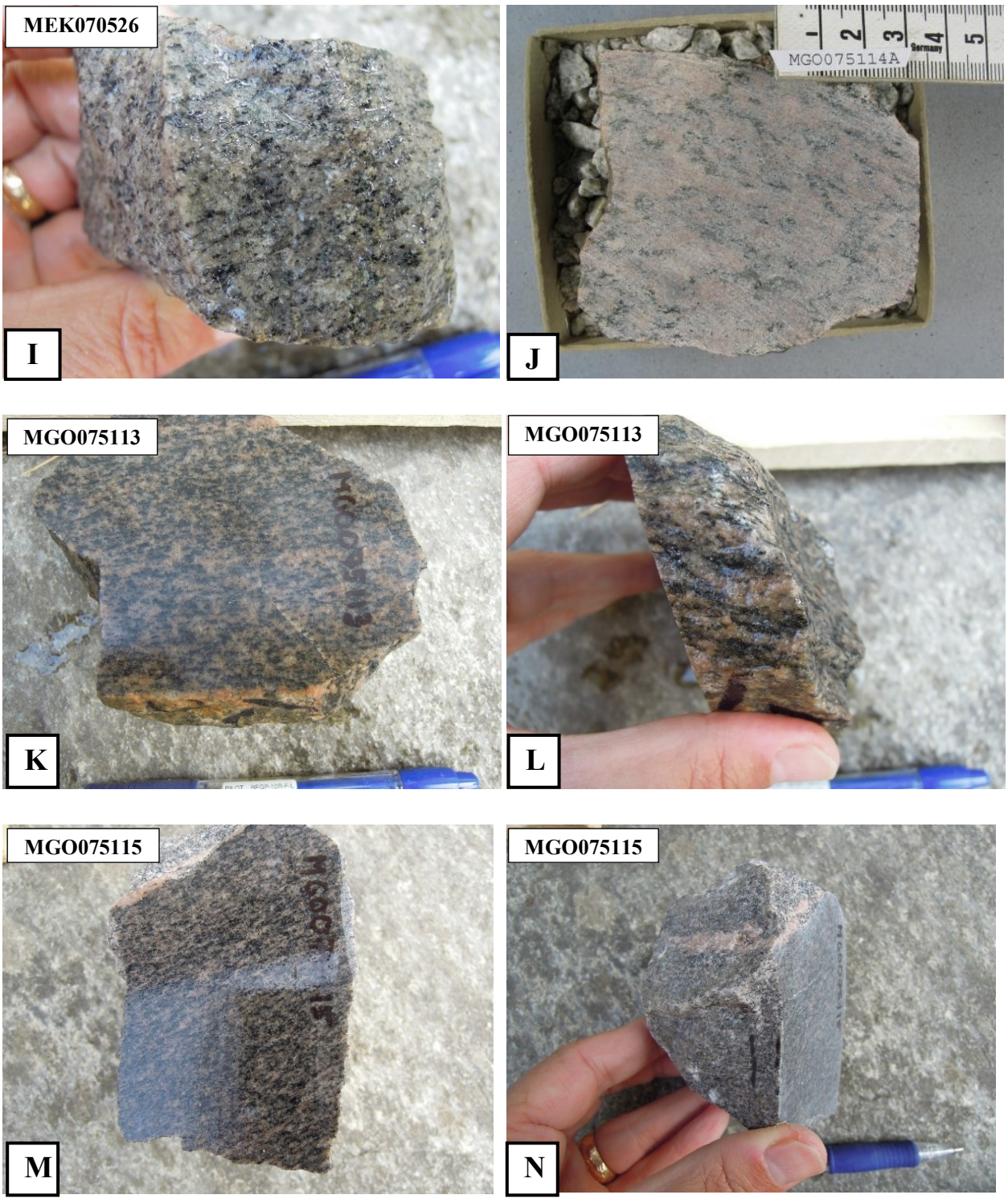

Figure 9: Field photographs and hand samples of class 1 samples. (A) Fine- to medium-grained granitic gneiss of gray-red color with a weak foliation. The red arrow shows a leucosome vein. (B) Hand sample cut parallel to the lineation plane. (C) Gneissic texture of relict medium-grained granitic gneiss. The red arrows show the dark quartz crystals that are scattered in the rock. (D) Hand sample. Some leucocratic parts of the rock are red in color, due to abundant K-feldspars. The rock has a strong foliation fabric. (E) Weathered surface illustrating the strong gneissic fabric and dark quartz domains. (F) A fine- to medium-grained granitic gneiss with dark quartz domains in Åstorp quarry. (G) Hand sample cut perpendicular to lineation, showing the well-developed gneissic texture. The rock has a strong lineation and medium foliation. (H) A gray, fine-grained granitic gneiss with weak foliation. (I) Hand sample showing the lineation plane. The dark minerals are primarily dark quartz and hornblende. (J) Hand sample of a gray granitic gneiss rich in feldspar porphyroblasts and with a well-developed gneissic texture. (K) Hand sample of fine-grained, massive granitic gneiss of dark gray-reddish color. The sample is cut perpendicular to the lineation. (L) Hand sample of the granitic gneiss, with the bands of mafic minerals defining the lineation plane. (M) Hand sample of gray granitic gneiss with a strong gneissic layering and foliation, having splits along the foliation planes. The sample is cut perpendicular to foliation. (N) The granitic gneiss has a fine-grained gray mesosome and reddish medium-grained leucosome. (Photographs for figures A, C, E by Charlotte Möller, B, D, G, I, K, L, M, N by Jenny Andersson, J by Mattias Göransson)

4.1.2 Samples of class 2

Sample MGO075109

At Hunseröd, east of Munka Ljungby, are exposures of a dark, red-gray granitic gneiss, with augen texture (showing that the rock was originally K-feldspar-megacrystic) and strong gneissic deformation fabric (Figure 10A). It is medium- to coarse-grained, and the gneissic fabric has a strong linear component, plunging gently towards NNW. Pre-deformational K-feldspar-rich granitic veins/ dykes are low-angle oblique to this fabric (Figure 10B).

Sample MGO075108

A quarry at Össjö, east of Munka Ljungby and that is run by Skanska AB exposes fine- to medium-grained granitic gneiss of grey color (Figure 10C). The rock is deformed and has a high amount of dark minerals (mostly amphibole). The gneiss is locally cut by Permian mafic dykes. The deformation fabric of the gneiss is an aggregate lineation defined by alternating dark minerals and light feldspar-rich bands with dark purple-gray quartz (Figures 10D, 10E).

Sample MGO075105

A quarry at Bjärstorp north of Klippan, run by Swerock, exposes gray-red granitic gneiss with relatively low amount of mafic minerals (Figure 10F). The rock does not appear deformed macroscopically. The gneiss is fine- to medium-grained with dark quartz and medium- to coarse-grained leucocratic veins (Figure 10G). A black, aphanitic dolerite is present near the sample site.

Sample MEK070527

An outcrop at Riseberga hosts a gray-red, medium-grained granitic gneiss with dark quartz (Figures 10H, 10I), and up to 5 mm large grains of dark minerals. The rock is not foliated and, in some places, it has a weak linear fabric. There are some dolerite dykes located close to the sample area.

Sample MGO075112

East of Stenestad there is an appearance of a fine- to medium-grained, massive granitic gneiss of red-gray color, having weak lineation (Figure 10J). It contains little mafic minerals (mostly biotite) that define the lineation. Near the outcrop there is a coarse-grained pegmatite with abundant feldspar porphyroblasts and dark quartz ribbons.

Sample MGO075117

At lake Odensjön, west of Röstånga, is the southernmost outcrop sampled from the Söderåsen study area and it is composed of red leucocratic granitic gneiss with weak foliation (Figure 10K). The rock is fine- to medium-grained, massive, and the strong lineation is defined by the dark quartz and mafic minerals (Figure 10L). The rock has a brownish hue due to its strong oxidation (it contains secondary reddish staining).

4.1.3 Samples of class 3

Sample MEK070523

East of Bjuv, a medium-grained, light greenish-grayish granitic gneiss is exposed (Figures 11A, 11B). The gneiss has an almost isotropic fabric and a very weak lineation defined by the amphibole and micas. There are local coarse-grained veins filled with recrystallized quartz and feldspar (red arrows in Figure 11A).

Sample MEK070519

East of Riseberga there is exposure of a gray-reddish, fine- to medium-grained granitic gneiss (Figure 11C). There are various pegmatite veins that cross-cut the weak foliation. In some places the rock looks coarse-grained, having signs of partial melting as there are some leucosomes parallel to the fabric (red arrows in Figure 11C). The rock has a strong lineation texture (Figure 11D).

Sample MEK070528

Two samples are located at a distance of only a few meters at Riseberga, MEK070527 and MEK070528. Sample MEK070528 (Figures 11E, 11F) is a medium-grained leucocratic granitic gneiss with a weak lineation fabric. It seems like there are some red (Fe-rich) inclusions inside quartz and a relict phase in this quartz, with a gray core and a recrystallized reddish rim.

Sample MEK070518

South of Riseberga is a gray to reddish gray, medium- to coarse-grained granitic gneiss with a relict igneous texture and a well-developed lineation (Figure 11G). The rock locally preserves remnants of igneous gray K -feldspar crystals, ca. 5 mm large. It is hornblende-bearing and contains very fine-grained garnet and some reddish Fe- and Mg-rich opaque minerals (Figure 11H). The rock has some reddish staining locally (red arrows in Figure 11G).

Sample MGO075116

An old quarry in Skäralid that has been transformed into a local camping site hosts gray-red, granitic gneiss with heterogeneously developed gneissic foliation and a weak lineation (Figure 11I). The rock is medium- to coarse-grained (Figure 11J) and has preserved igneous K-feldspar crystals (red arrows in Figure 11I), containing dark quartz and relatively low amount of dark minerals.

Sample MEK070520

East of Klåveröd is fine- to medium-grained, gray-red leucocratic granitic gneiss (Figure 11K). The rock is massive and has a very weak fabric (possibly lineation), containing sparse medium-grained leucocratic veins rich in feldspar, that are some mm-wide (Figure 11L).


MGO075109
A


MGO075109
B


MGO075108
C


MGO075108
D


MGO075108
E


MGO075105
F

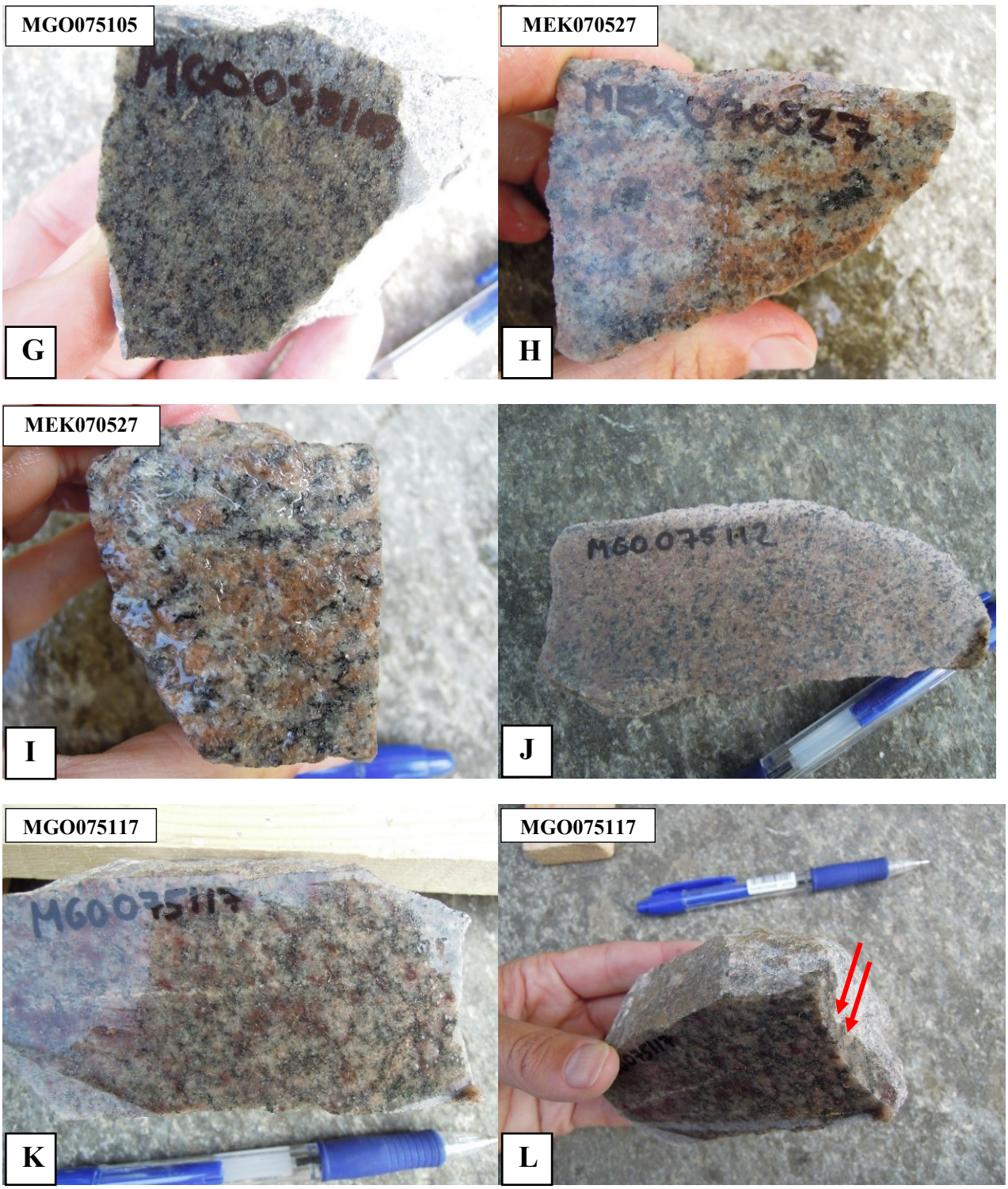

Figure 10: Field photographs and hand samples of class 2 samples. (A) Dark gray granitic gneiss with a well-developed gneissic fabric and pink feldspar crystals. (B) The rock has distinct reddish vein rich in K-feldspars that cut the lineation in a low angle. (C) Fine- to medium-grained, grayish granitic gneiss, strongly deformed. (D) The gneiss has various dark quartz domains and a strong lineation. (E) Freshly-cut granitic gneiss boulder showing the lineation fabric. (F) Fine-grained granitic gneiss that contains coarser-grained veins. (G) Hand sample of a granitic gneiss with no clear deformation fabric. (H) Hand sample of a medium-grained, reddish granitic gneiss. The rock has weak lineation. (I) Hand sample from the previous sample, that looks undeformed (cut perpendicular to the weak lineation). (J) Hand sample of a brown-red granitic gneiss with weak foliation. (K) Hand sample of a leucocratic, reddish- to grayish red granitic gneiss, fine- to medium-grained. The rock has a secondary red staining. (L) Hand sample of the previous sample. The red arrow shows the lineation. (Photographs for figures A, B, C, D by Charlotte Möller, G, H, I, J, K, L by Jenny Andersson)

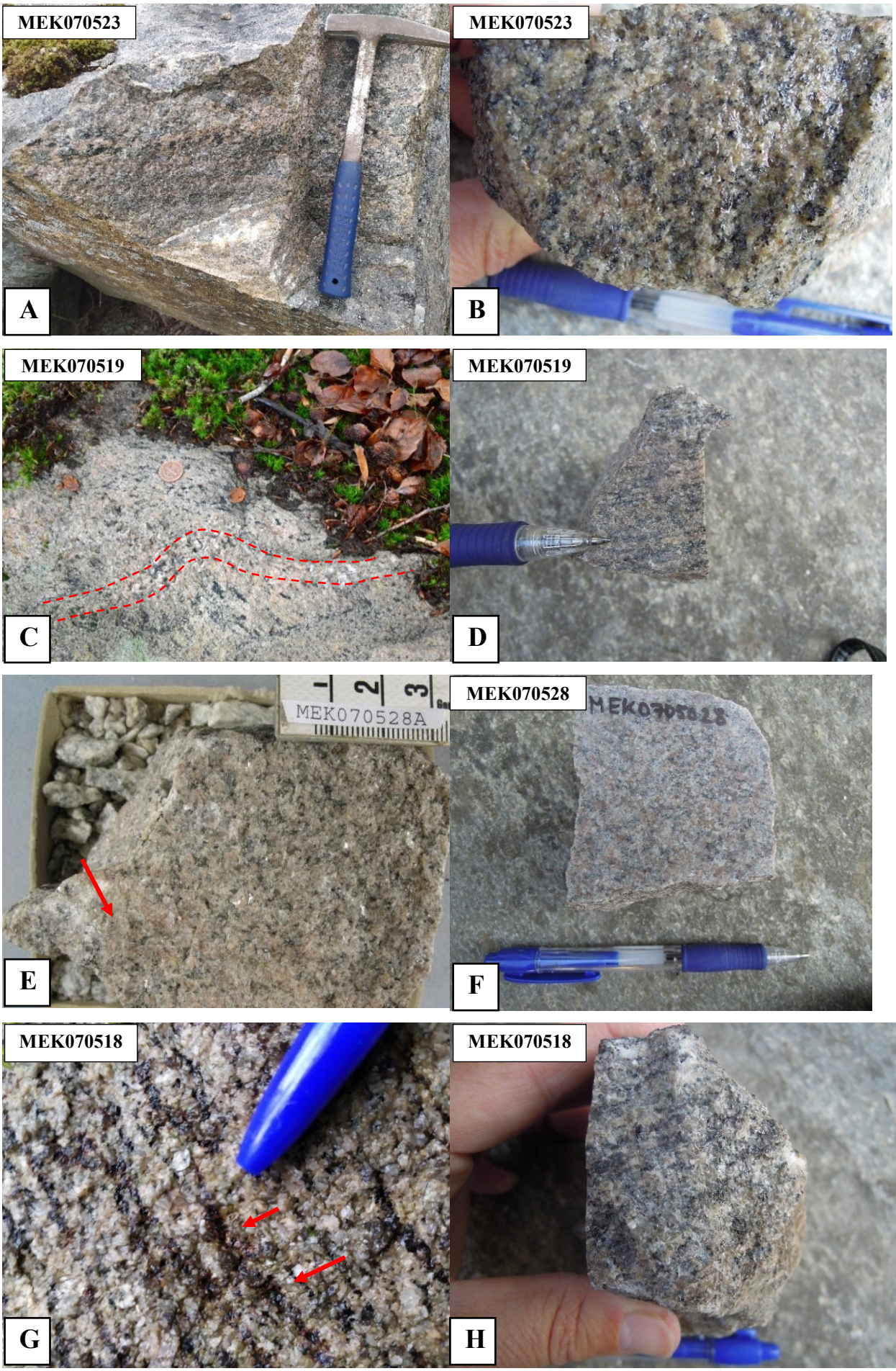
MEK070523
A
MEK070523
B
MEK070519
C
MEK070519
D
MEK070528A
E
MEK070528
F
MEK070518
G
MEK070518
H

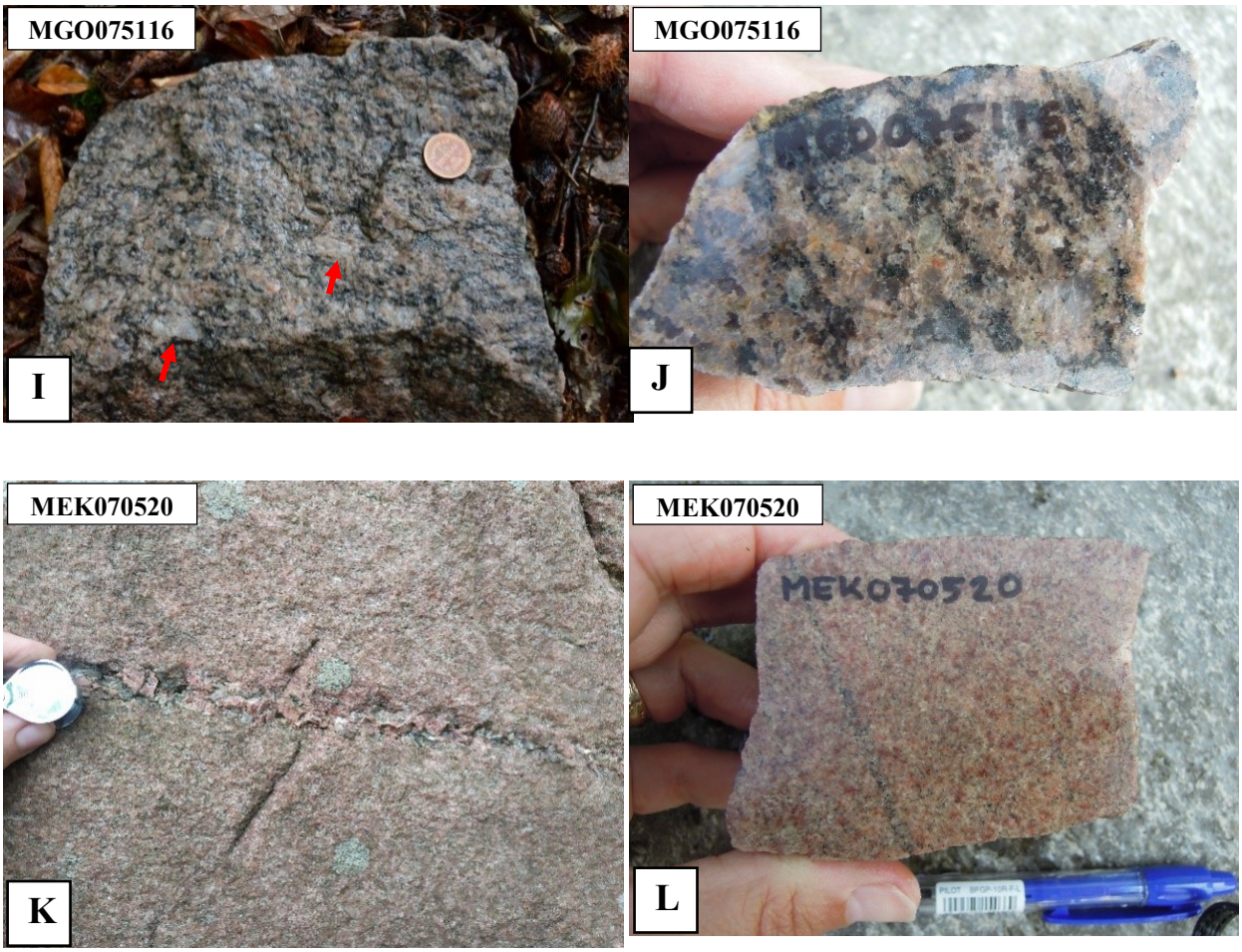

Figure 11: Field photographs and hand samples of class 3 samples. (A) A grayish granitic gneiss, with domains of coarser-grained quartz and feldspars (red arrows). (B) Hand sample of the previous sample. There is no obvious deformation fabric. The rock is medium-grained, and the dark minerals are primarily dark quartz and amphibole. (C) A fine- to medium-grained, red-gray granitic gneiss with reddish medium-grained leucosome veinlet cutting the deformation fabric (red dashed lines). (D) Hand sample of the previous sample, showing the strong lineation. (E) Hand sample of granitic gneiss, having some feldspar aggregates (red arrow). (F) Hand sample of the previous sample, showing the weak lineation. (G) A medium-grained granitic gneiss with high amount of garnet crystals. It has a strong lineation fabric. (H) Hand sample from the previous sample cut perpendicular to the lineation. (I) Medium- to coarse-grained, gray granitic gneiss. The rock has many coarse K-feldspar crystals (red arrows) and a weak lineation. (J) Hand sample of the same granitic gneiss, cut perpendicular to lineation. (K) Reddish, leucocratic granitic gneiss, weakly deformed. There are some mm-wide recrystallized veins of feldspar. (L) Hand sample of the previous fine-grained gneiss. The gray vein here contains feldspar and quartz and is fine-grained, like the host rock. (Photographs for figures C, I by Charlotte Möller, B, D, F, H, J, L by Jenny Andersson, E by Mattias Göransson)

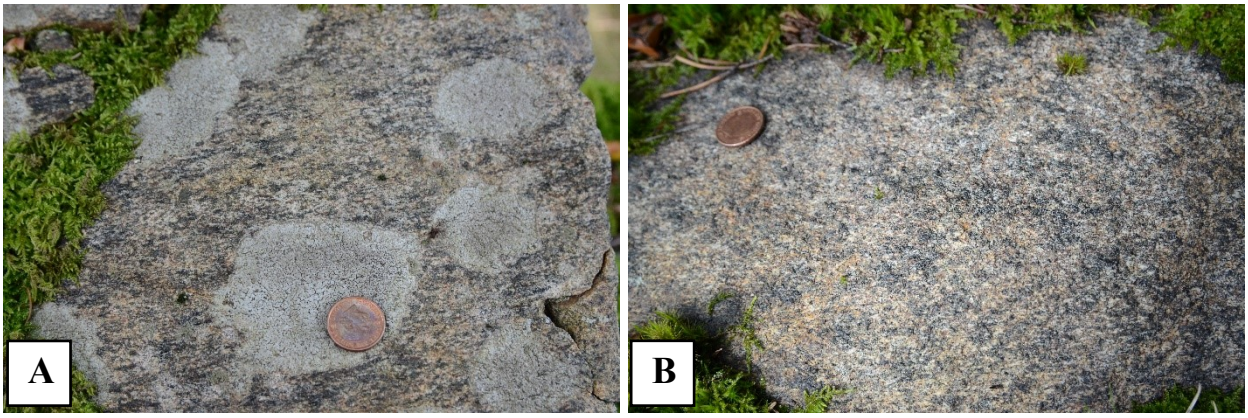

Figure 12: Field photographs of a garnet- and clinopyroxene-rich mafic granulite located E of Munka Ljungby (sample MEK070524). (A) The rock is dark gray, fine-grained and has a well-developed gneissic fabric. (B) The rock is rich in pyroxenes, amphibole and feldspars.

4.1.4 Metagabbro

Sample MEK070524

East of Munka Ljungby is a garnet- and pyroxene-rich metabasic rock that is also rich in plagioclase and amphibole (Figure 12). It has a dull, greenish-gray color. Clinopyroxene grains are recognized under the hand lens by their greenish gray color; amphibole form elongated black patches. The gneissic foliation dips towards the north.

4.2. Thin section descriptions

The description of thin sections below follows the same order as in chapter 4.1. The abbreviations for names of minerals follow Whitney & Evans (2010).

4.2.1 Samples of class 1

Sample MEK070525, granitic gneiss north-east of Östra Ljungby

Sample MEK070525 (Figure 13) is fine- to medium-grained gneiss with 21% plagioclase, 38% of K-feldspar and 24% quartz. Commonly, K-feldspar has perthitic exsolution (20%). The mafic minerals (amphibole dominating with 10%) are forming elongated aggregates that define the gneissic foliation, and biotite (2%) is locally replaced by chlorite. Individual amphibole grains have a maximum length of 1.6 mm. The largest grains can reach 2.3 mm, and the grain boundaries have an amoeboid texture. The accessory minerals include apatite, zircon, opaque minerals and garnet.

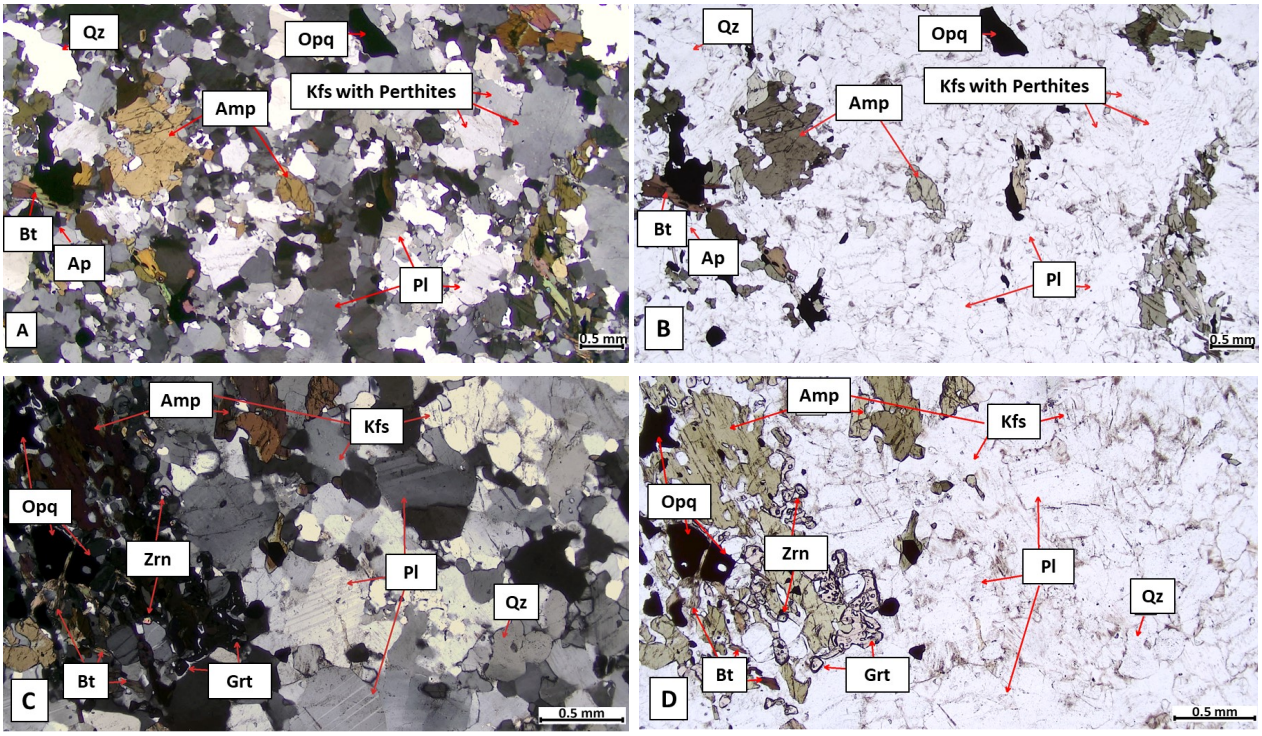

Figure 13: Photomicrographs of granitic gneiss (sample MEK070525) NE of Östra Ljungby. (A) and (C): Cross-polarized light (XPL) images. The large grains have complex grain boundaries, whereas the fine grains are more rounded. The coarse grains have amoeboid boundaries. Small garnet crystals are located in contact with amphibole or opaque grains. (B) and (D): Plain polarized light (PPL) images. The dark mineral aggregates are evenly distributed in the rock, and they are oriented (aggregate foliation).

Sample MGO075110, granitic gneiss at Mölletofta

Sample MGO075110 (Figure 14) is fine- to medium-grained gneiss with 42% K-feldspar (19% having perthitic exsolution), 3% plagioclase and 39% quartz. The biotite content is 1%. Quartz forms irregular grains that are elongated parallel to the foliation, having a maximum length of 3 mm. The mafic mineral grains are oriented parallel to the fabric, defining the foliation, and the size of the amphibole grains is less than 0.6 mm. The grains have variable degree of irregularity, ranging from irregular-shaped elongated aggregates of recrystallized quartz, to small (down to 0.04 mm), rounded crystals of quartz and feldspar. The accessory minerals are zircon, garnet, and opaque minerals.

Sample MEK070521, granitic gneiss at Åstorp

Sample MEK070521 (Figure 15) is a very fine-grained gneiss. It is richer in K-feldspar (48%) and has less quartz (25%) than other rocks in class 1. Perthitic exsolution in K-feldspar is common (19%), and they are usually microperthitic with almost submicroscopic lamellae. Plagioclase (10%) is rarely antiperthitic. Biotite (4%) and amphibole (6%) are present. Felspar is locally altered to sericite (4%). The sample is one of the finest-grained orthogneisses, with 98% of the grains being <1 mm long. The rock has a distinct gneissic fabric that is defined by elongated quartz and feldspar grains, up to

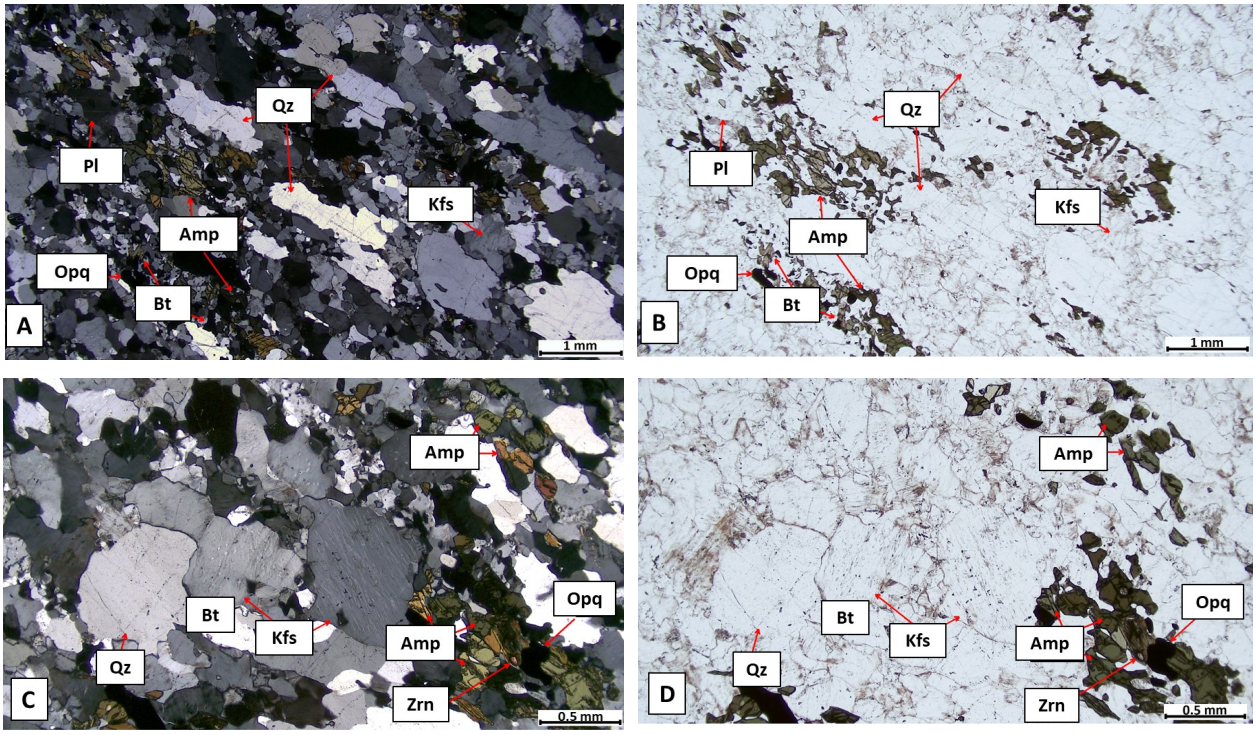

Figure 14: Photomicrographs of granitic gneiss (MGO075110) at Mölletofta. (A) and (C): XPL images. Alternating feldspar rich domains and domains with dark minerals defining the foliation. There are elongated individual quartz grains, and K-feldspar grains of various sizes that together form elongated domains. (B) and (D): PPL images. Individual grains and elongated aggregates rich in fine-grained biotite, amphibole and opaque minerals are oriented parallel to the foliation.

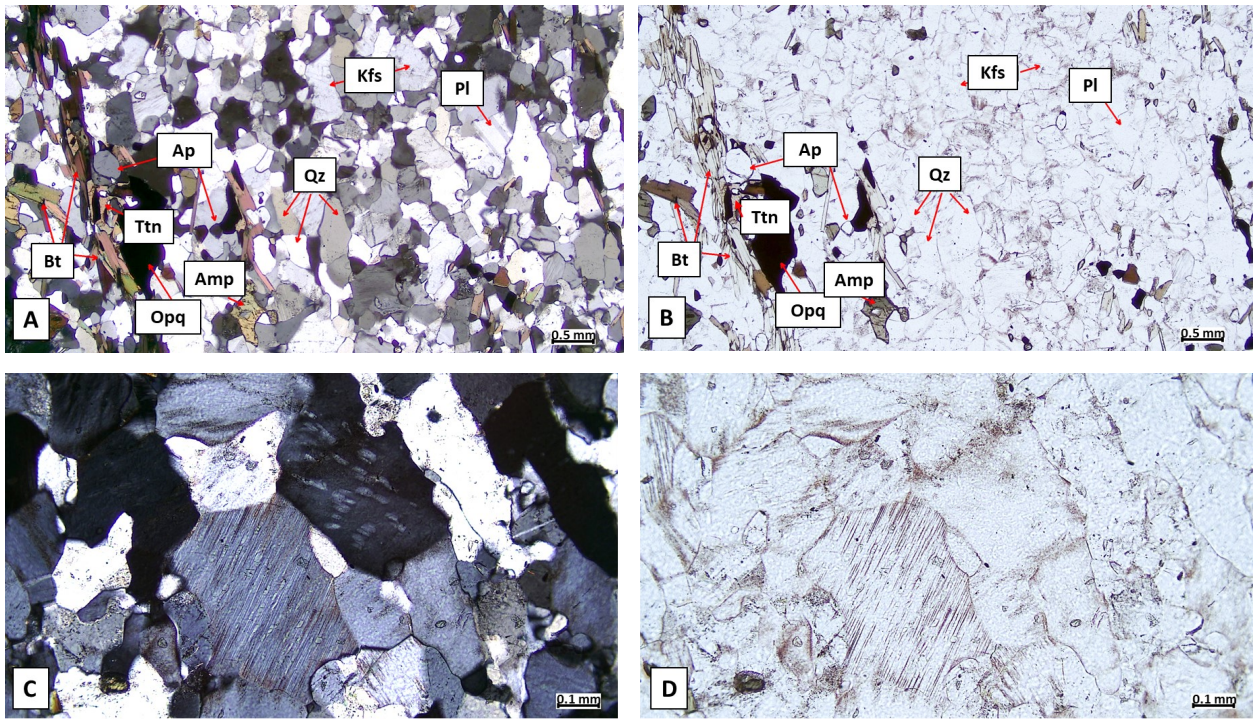

Figure 15: Photomicrographs of granitic gneiss (MEK070521) at Åstorp. Thin section cut perpendicular to lineation, cross-cutting foliation. (A): XPL image. The sample is fine-grained with gneissic fabric. There is some sericite as alteration product of the feldspar (yellow arrow). (B): PPL image. The mafic minerals are oriented parallel to the deformation fabric. The biotite crystals are fine-grained and elongated. (C): XPL image. Felsic domain composed of quartz, K-feldspar with perthitic exsolution lamellae, and plagioclase. Anti-perthitic plagioclase is rare in this sample (yellow arrow), and K-feldspar is commonly microperthitic. (D): PPL image showing the same microdomain as in (C).

1.5 mm long. Individual amphibole and biotite grains are oriented parallel to the fabric. The accessory minerals are zircon, titanite and opaque minerals.

Sample MEK070526, granitic gneiss at Forsmöllan

Sample MEK070526 (Figure 16) is a fine- to medium-grained granitic gneiss with the lowest quartz content (20%) among the class 1 samples. Feldspar content is high, with 44% K-feldspar and 18% plagioclase. K-feldspar is dominantly tartan twinned (14% of all minerals), with some containing microperthitic exsolution as well (11%); the size of K-feldspar grains reaches 2 mm in length. Locally, feldspar grains (mainly plagioclase) are altered to sericite (7%). The biotite content is 1% and chlorite (2%) is present locally as alteration product. The rock is fine- to medium-grained and has a fabric defined by the grain shape orientation of hornblende (6%) and (altered) biotite, while feldspar and quartz have complex grain boundaries. The accessory phases are zircon and opaque minerals.

Sample MGO075114, granitic gneiss at Dragesholm

Sample MGO075114 (Figure 17) is a relict granitic gneiss with the highest percentage in quartz among all samples (43%). K-feldspar (37%) has either tartan twinning (9%) or perthitic exsolution (9%), or a combination between the two (6%). Plagioclase makes up 5% of the rock. The rock has 5% of amphibole and less than 1% of fine-grained (up to 0.4 mm) garnet. There are local remnant crystals of igneous K-feldspar (1.2 cm long). The rock is generally fine- to medium-grained and has a distinct gneissic fabric defined by elongated quartz domains and elongated aggregates of dark minerals. The fine-grained minerals have an amoeboid shape, and the very fine-grained material is mostly rounded. There is local alteration of feldspar to sericite (4%) and alteration of biotite to very fine-grained chlorite (4%). The accessory minerals include zircon, garnet, apatite and opaque minerals.

Sample MGO075113, granitic gneiss north of Kågeröd

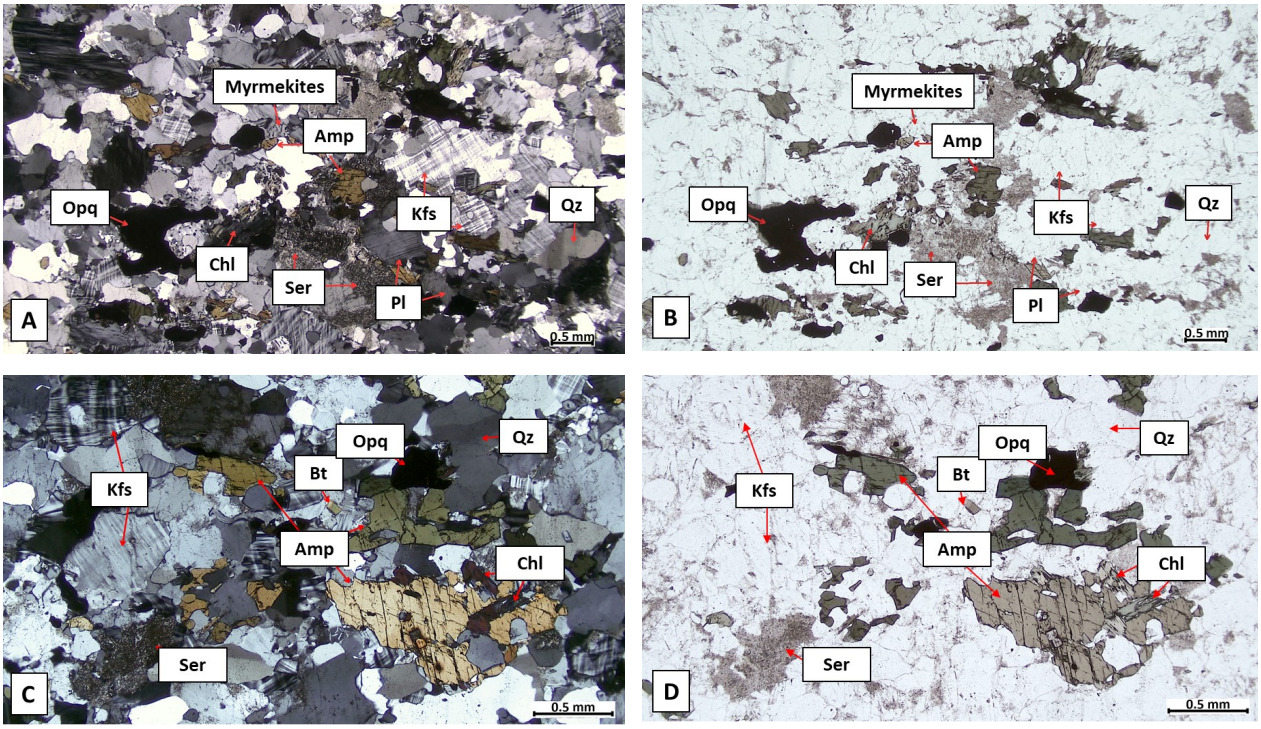

Figure 16: Photomicrographs of granitic gneiss (MEK070526) at Forsmöllan, SE of Klippan. (A) and (C): XPL images. The rock is dominated by quartz, K-feldspar, plagioclase and amphibole. K-feldspar has characteristic tartan (cross-hatched) twinning, and some grains are microperthitic. There are also some prismatic chlorite grains. (B) and (D): PPL images. The amphibole grains have a dark green color, and they are crystallized in patches together with biotite (and chlorite) and opaque minerals. Sericite is found as local alteration in feldspar.

Sample MGO075113 (Figure 18) is a very fine-grained granitic gneiss. The percentage of quartz and feldspar is 24% and 58%, respectively, where K-feldspar (40%) is locally perthitic or tartan twinned (6% and 3% of the total, respectively). The mafic minerals are oriented in bands between domains of felsic minerals, and they comprise amphibole (7%), biotite (5%) and opaque minerals (2%). The grain size measurements show that 50% of the grains have a length lower than 0.4 mm. The sample has a foliation defined by elongated aggregates of dark minerals and variably elongated quartz and feldspar crystals (their length does not exceed 2 mm). The felsic minerals have a slightly amoeboid shape. The biotite is locally altered to chlorite (2%). The accessory minerals are zircon, sericite and apatite.

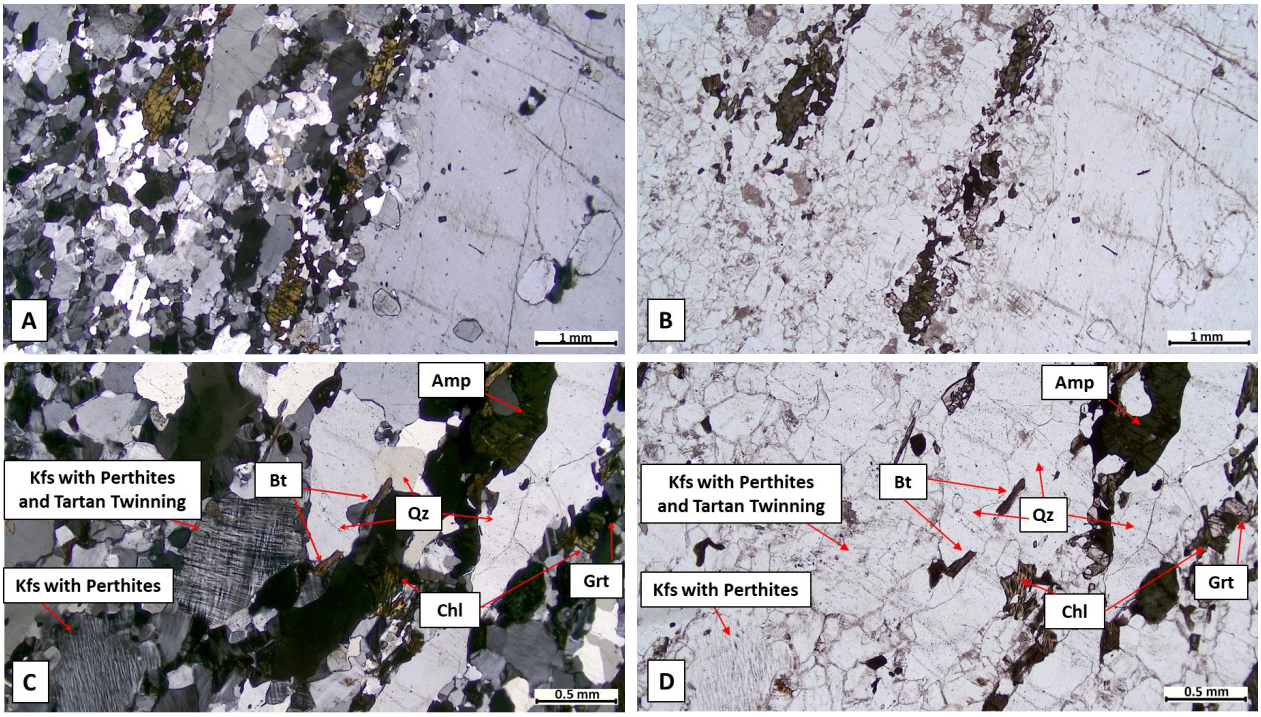

Figure 17: Photomicrographs of granitic gneiss (MGO075114) at Dragesholm. (A): XPL image. Remnant of igneous K-feldspar up to 1.2 cm long (lower right) with inclusions of rounded quartz and feldspar crystals and surrounded by very fine-grained material. (B): PPL image. Elongated mafic mineral aggregates define the gneissic fabric, and form horizons between the felsic minerals. (C): XPL image. The elongated and coarse quartz domains indicate recrystallization. Note K-feldspar with micro-perthitic exsolution lamellae and a grain with both tartan twinning and perthitic exsolution. (D): PPL image. The mafic minerals are aligned parallel to the fabric. There are some small (up to 0.4 mm), rounded garnet crystals.

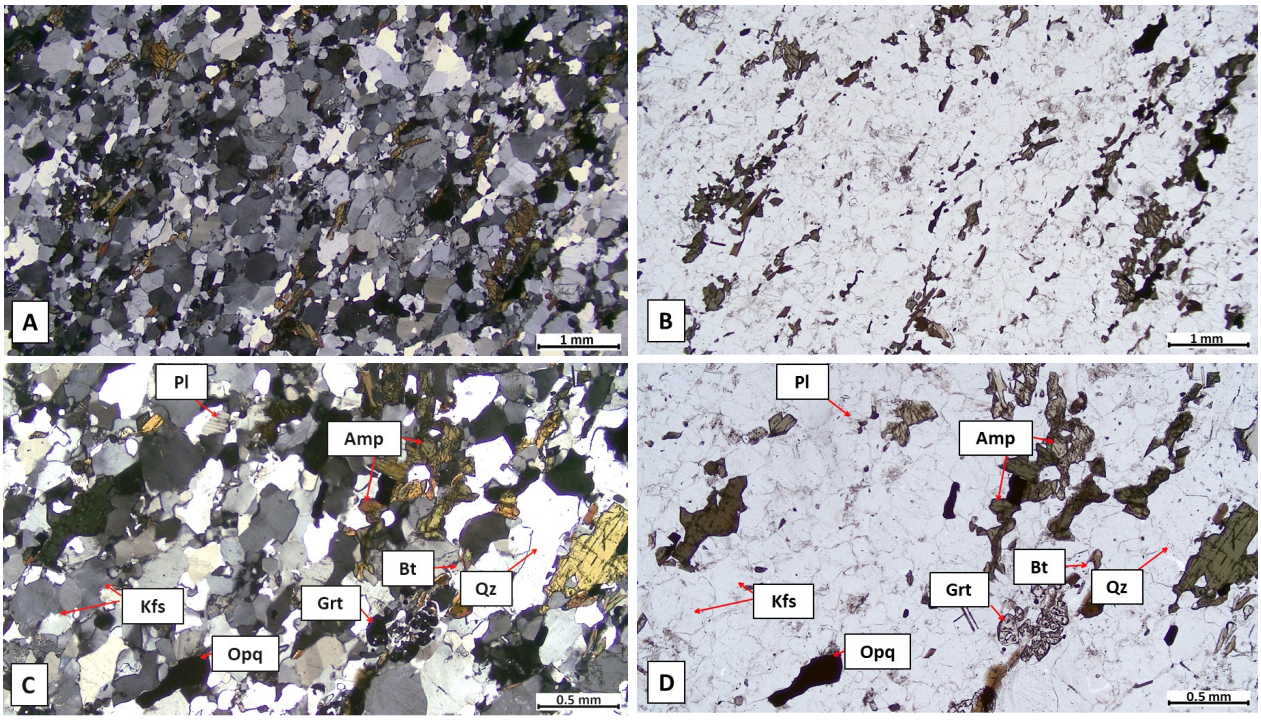

Figure 18: Photomicrographs of granitic gneiss (MGO075113), N of Kågeröd. Thin section cut perpendicular to lineation. (A) and (C): XPL images. The foliation is defined by the elongated dark mineral aggregates. This sample is one of the finest-grained. (B) and (D): PPL images. The mafic minerals are oriented parallel to the foliation, and they form bands that are alternating with the feldspar rich domains. There are some fine-grained garnet crystals present.

Sample MGO075115, migmatitic granitic gneiss north of Kågeröd

Sample MGO075115 (Figure 19) is a fine-grained, migmatitic granitic gneiss, and the thin section is of the mesosome only. The mesosome has high amount of mafic minerals, mainly amphibole (11%) and biotite (7%). The percentages of quartz and feldspar are 22% and 50%, respectively. The K-feldspar percentage is 43% of the total, with 7% having tartan twinning. The biotite is prismatic, and individual amphibole grains are elongated (they can reach 1.5 mm in length). The dark minerals are oriented in bands and they define a strong foliation fabric. Feldspar is locally sericitized (6%), and biotite locally altered to chlorite (0.4%). Accessory minerals are titanite and opaque minerals.

4.2.2 Samples of class 2

by elongated aggregates rich in dark minerals and in part by elongated domains of quartz (up to 5 mm long) and feldspar (up to 2 mm long). The largest quartz grains are up to 5 mm long and forms elongated lensoid domains. There is local alteration of feldspar to sericite (3%) and biotite to chlorite (3%). Accessory minerals are zircon, apatite and opaque minerals.

Sample MGO075108, granitic gneiss at Össjö, east of Munka Ljungby

Sample MGO075108 (Figure 21) is an uneven-grained, fine- to medium-grained granitic gneiss with well-developed gneissic fabric. It has a high percentage of amphibole (19%) compared to the rest of the samples in class 2, and 6% of biotite. Quartz percentage is 23% and they are relatively coarser grained than the remaining minerals of the rock. The percentage of feldspar is 45% and the K-feldspar have perthitic exso-

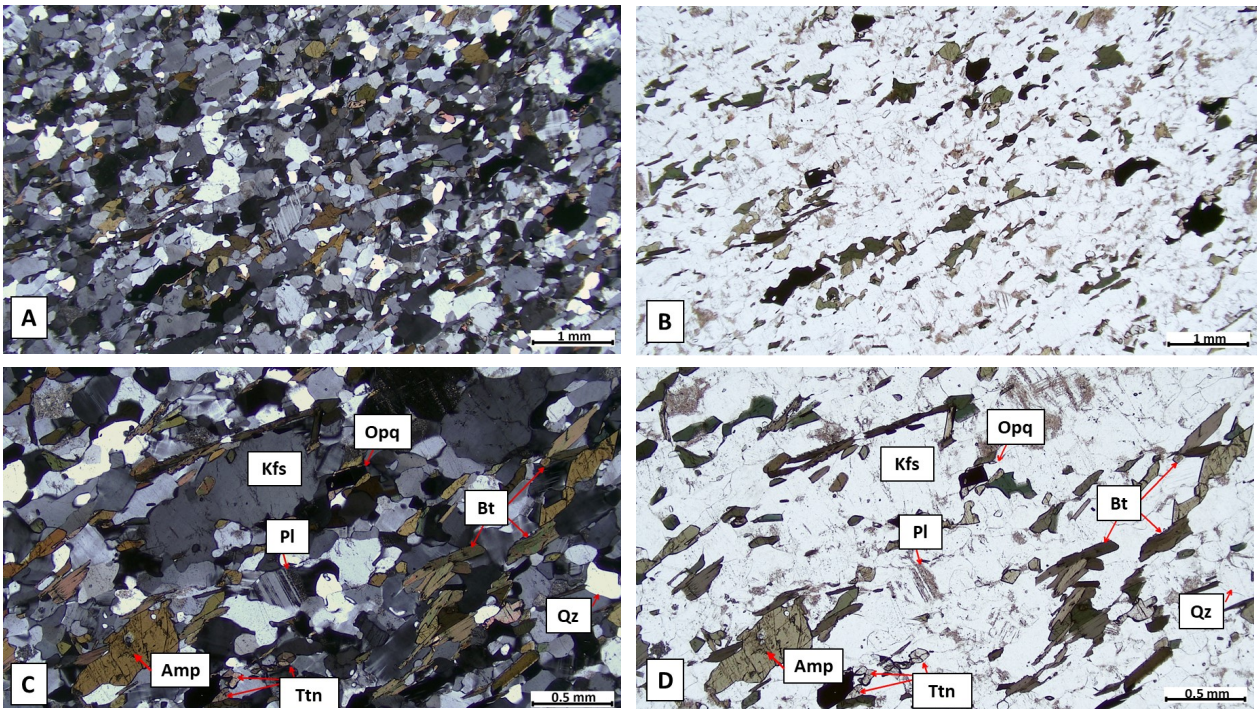

Figure 19: Photomicrographs of the mesosome of migmatitic granitic gneiss (MGO075115), N of Klåveröd. Thin section cut perpendicular to foliation. (A) and (C): XPL images. Individual felsic mineral grains are elongated, and they define the foliation fabric, together with elongated amphibole and biotite crystals. K-feldspar grains rarely have perthitic exsolution and some have tartan twins. (B) and (D): PPL images. The mafic minerals are oriented in thin bands, parallel to the foliation. Biotite is prismatic and can reach up to 0.8 mm long.

Sample MGO075109, granitic gneiss at Hunseröd, east of Munka Ljungby

Sample MGO075109 (Figure 20) is a granitic gneiss with high percentage of feldspar (60%). The rock consists of quartz (21%), K-feldspar (48%), plagioclase (12%), amphibole (8%) and little biotite (1%). Some 1 -2 mm large, elongated feldspar crystals have perthitic exsolution (19%). There are sparse myrmekites (~1%). The rock is uneven-grained, medium- to coarse-grained and the deformation fabric is defined in part

lution (13%). There are some antiperthitic plagioclase (Figure 21A, yellow arrow). The percentage of plagioclase is 9%, quite lower than the rest of the samples in class2. There is a 6x5 mm large remnant of igneous perthitic K-feldspar (yellow arrow in Figure 21C). The grains are elongated up to 2.5 mm long, but there is a high amount of very fine-grained material (50% of the grains have a length less than 0.4 mm). The accessory minerals are garnet, apatite, titanite and opaque minerals.

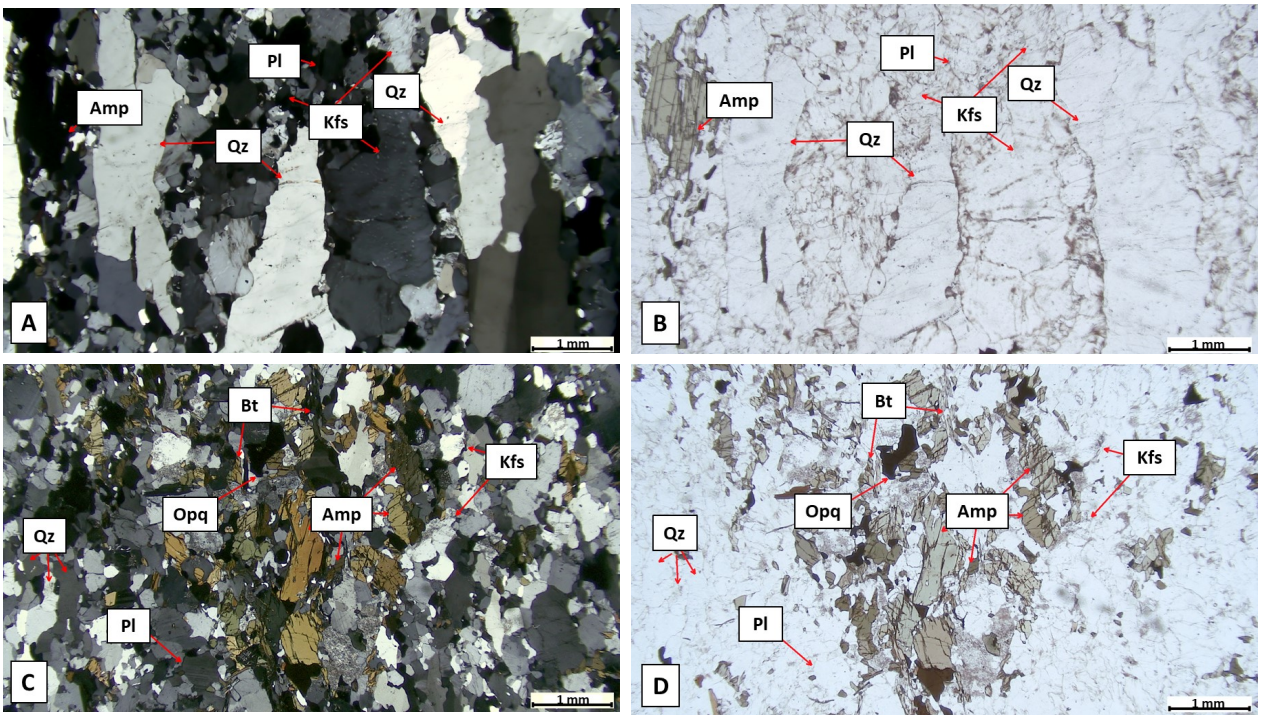

Figure 20: Photomicrographs of granitic gneiss (MGO075109) at Hunseröd, E of Munka Ljungby. Thin section cut perpendicular to lineation. (A) and (C): XPL images. (A): A felsic mineral domain consisting of coarse quartz and perthitic K-feldspar grains that form lenses parallel to the foliation fabric. (C): Aggregate rich in dark minerals consisting of fine-grained quartz, feldspar, amphibole, and accessory minerals. (B) and (D): PPL images of the same domains. Elongated quartz and K-feldspar grains occur in the felsic domains. The dark minerals are more fine-grained, and they form an aggregate foliation.

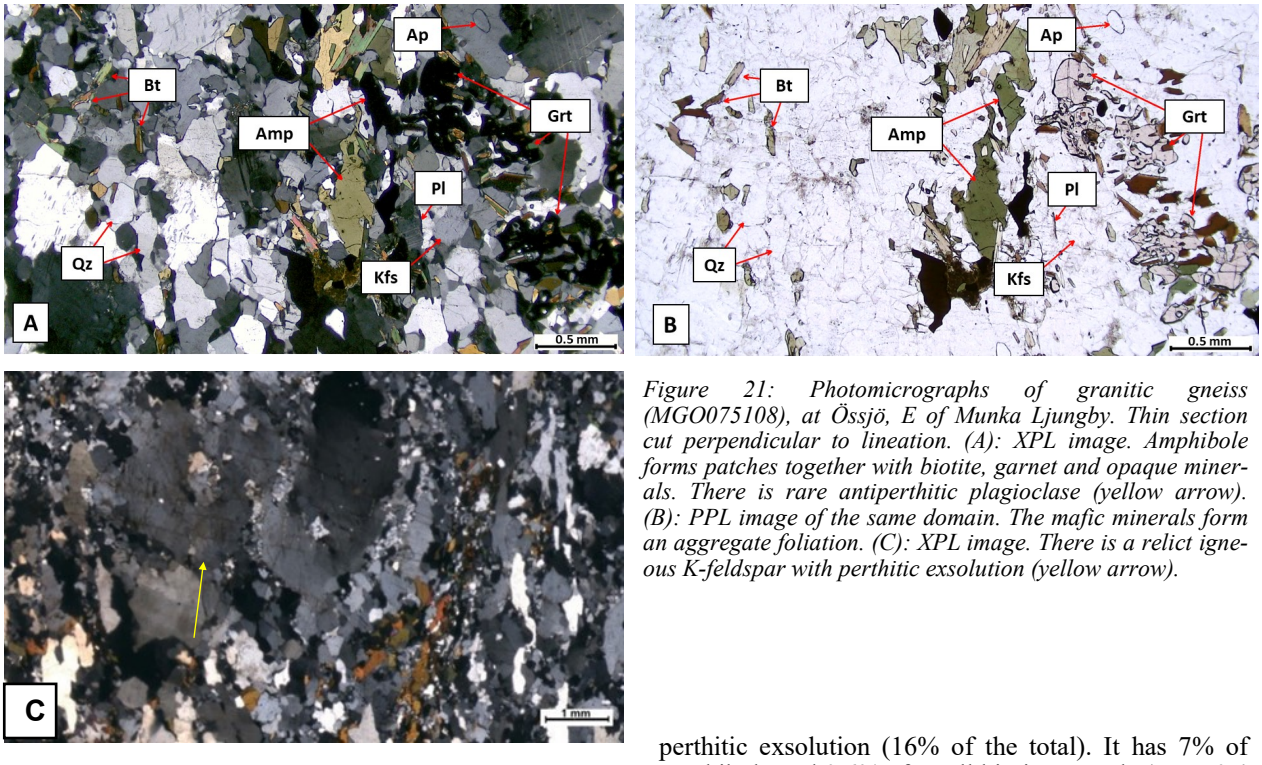

Figure 21: Photomicrographs of granitic gneiss (MGO075108), at Össjö, E of Munka Ljungby. Thin section cut perpendicular to lineation. (A): XPL image. Amphibole forms patches together with biotite, garnet and opaque minerals. There is rare antiperthitic plagioclase (yellow arrow). (B): PPL image of the same domain. The mafic minerals form an aggregate foliation. (C): XPL image. There is a relict igneous K-feldspar with perthitic exsolution (yellow arrow).

Sample MGO075105, granitic gneiss north of Klippan

The sample MGO075105 (Figure 22) is a fine- to medium-grained granitic gneiss with a gneissic texture. The percentages of quartz and feldspar are 25% and 56%, respectively. The K-feldspar (44%) shows perthitic exsolution (16% of the total). It has 7% of amphibole and 0.6% of small biotite crystals (up to 0.4 mm long) that are frequently altered to chlorite (2%). There is an increased amount of very fine-grained material (50% of the grains have a length less than 0.4 mm). There is rare myrmekite (1%). The mafic minerals are oriented parallel to the fabric. The accessory minerals are apatite, garnet and opaque minerals.

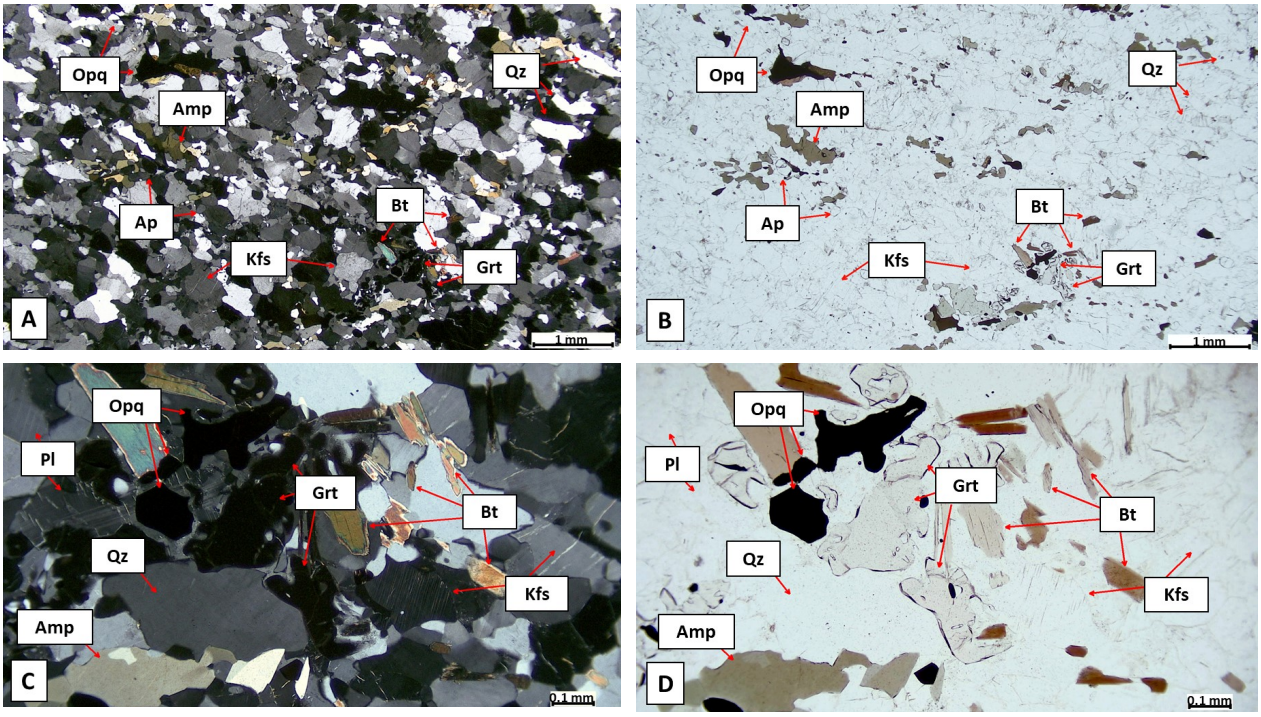

Figure 22: Photomicrographs of thin section MGO075105, located N of Klippan. (A): XPL image. The rock is fine- to medium-grained, and the quartz grains are elongated. The grains do not have complex boundaries, but there is a high amount of very fine-grained material. (B): PPL image. The mafic minerals are in small patches, sometimes following the weak deformation fabric. There is accessory apatite (rounded with high relief). (C): XPL image. The K-feldspars have microperthitic exsolution. (D): PPL image. the garnet crystals are small, subhedral and they are located close to the patches with opaque minerals, biotite, and amphibole.

Sample MEK070527, granitic gneiss at Riseberga

The sample MEK070527 (Figure 23) is a medium-grained granitic gneiss with a high amount of biotite (6%) in comparison with the rest of the samples of class 2. The percentage of quartz is low (18%), in relation to the rest of the samples, but there is increased feldspar content (67%). K-feldspar (50%) has either tartan twinning (4%) or perthitic exsolution (17%), or a combination between the two (13%). The rock has unclear deformation fabric, and the biotite crystals can reach up to 3 mm long. The felsic minerals are coarser grained, and their length can reach up to 4 mm. The K-feldspar is altered to sericite (2%) and the biotite is altered to chlorite (1%). The accessory minerals are zircon, titanite and opaque minerals.

Sample MGO075112, granitic gneiss east of Klåveröd

The sample MGO075112 (Figure 24) is a fine- to medium-grained granitic gneiss with high quartz content (39%). The feldspar percentage is 55% (37% K-feldspar and 18% plagioclase), and it appears either with tartan twinning (7%) or with perthitic exsolution (3%) or with a combination of the two (7%). The amphibole is absent, and the percentage of biotite is 5%. The weak fabric is formed by the elongated quartz that can reach up to 4 mm in length. The mafic minerals are very little and randomly oriented, and their maximum length is 0.8 mm. There is secondary sericite (2%) as alteration product of feldspar. The accessory minerals are garnet and opaque minerals.

Sample MGO075117, granitic gneiss west of Röstånga

The sample MGO075117 (Figure 25) is a fine- to medium-grained granitic gneiss with very low percentage of mafic minerals. The percentages of quartz and feldspar are 29% and 55%, respectively. It has higher percentage of plagioclase (24%) in comparison with the rest of the samples of class 2. The K-feldspar does not show perthitic exsolution and the tartan twinning is rare (3%). The weak foliation is defined by the elongated quartz and feldspar (maximum length 2 mm). The rock has 9% of chlorite but the biotite is absent. The K-feldspar is altered to sericite (4%). The accessory minerals are titanite and opaque minerals.

4.2.3 Samples of class 3

Sample MEK070523, granitic gneiss east of N Vram

The sample MEK070523 (Figure 26) is a fine- to medium-grained granitic gneiss with 21% of quartz and 64% of feldspar (35% of K-feldspar and 29% of plagioclase). The K-feldspar appears either with tartan twinning (6%) or with perthitic exsolution (4%) or with a combination of the two (3%). The K-feldspar is sericitized (6%). The amphibole percentage is low (4%), and the percentage of biotite is 3%. The rock has very weak or no fabric, and the grain boundaries have low complexity. The amount of fine-grained minerals

is quite low in this rock (15% of the grains have a length lower than 0.4 mm). There is secondary sericite (6%) from alteration of feldspar.

The accessory minerals are zircon, apatite and opaque minerals.

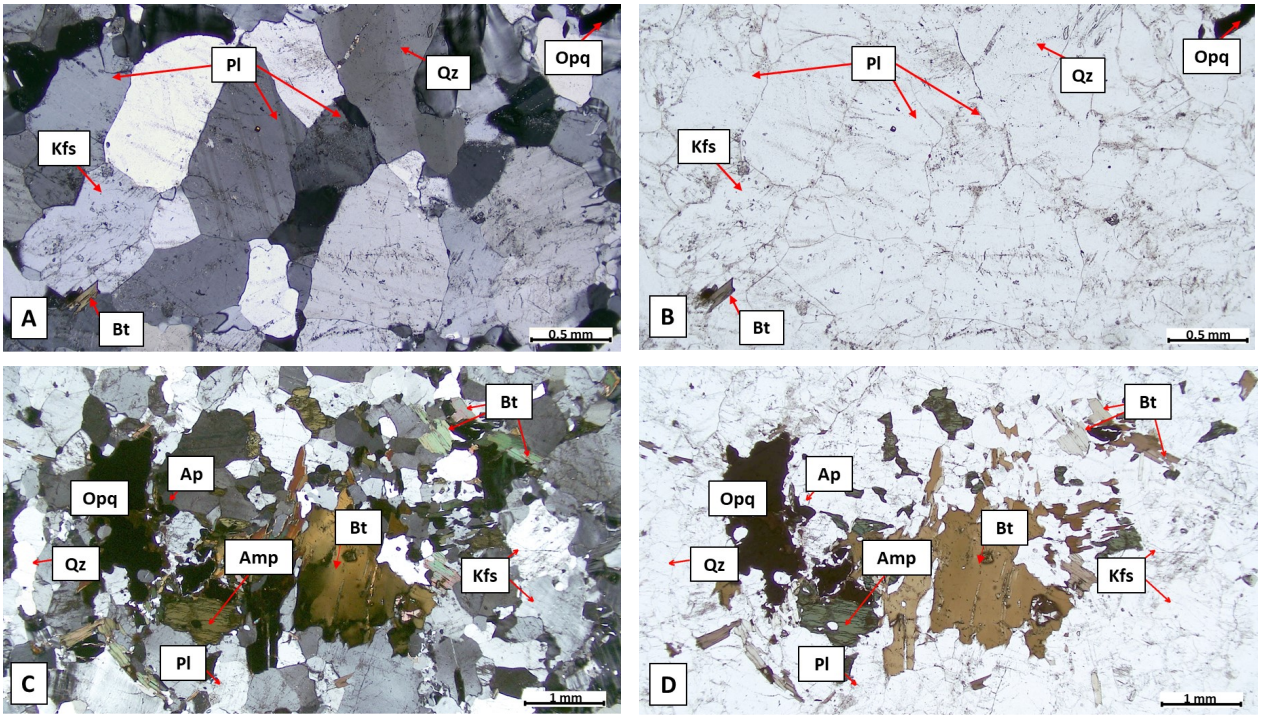

Figure 23: Photomicrographs of thin section MEK070527, in Riseberga. Thin section cut at an angle to the lineation. (A): XPL image. The plagioclase might have secondary alteration to sericite on the twinning lamellae. The felsic minerals have an almost granoblastic texture and there are some triple points between the grain boundaries. (B): PPL image of the same domain. (C): XPL image. Biotite is the dominant mafic mineral, forming patches together with amphibole and opaque minerals. Feldspar is altered to sericite. (D): PPL image of the same domain.

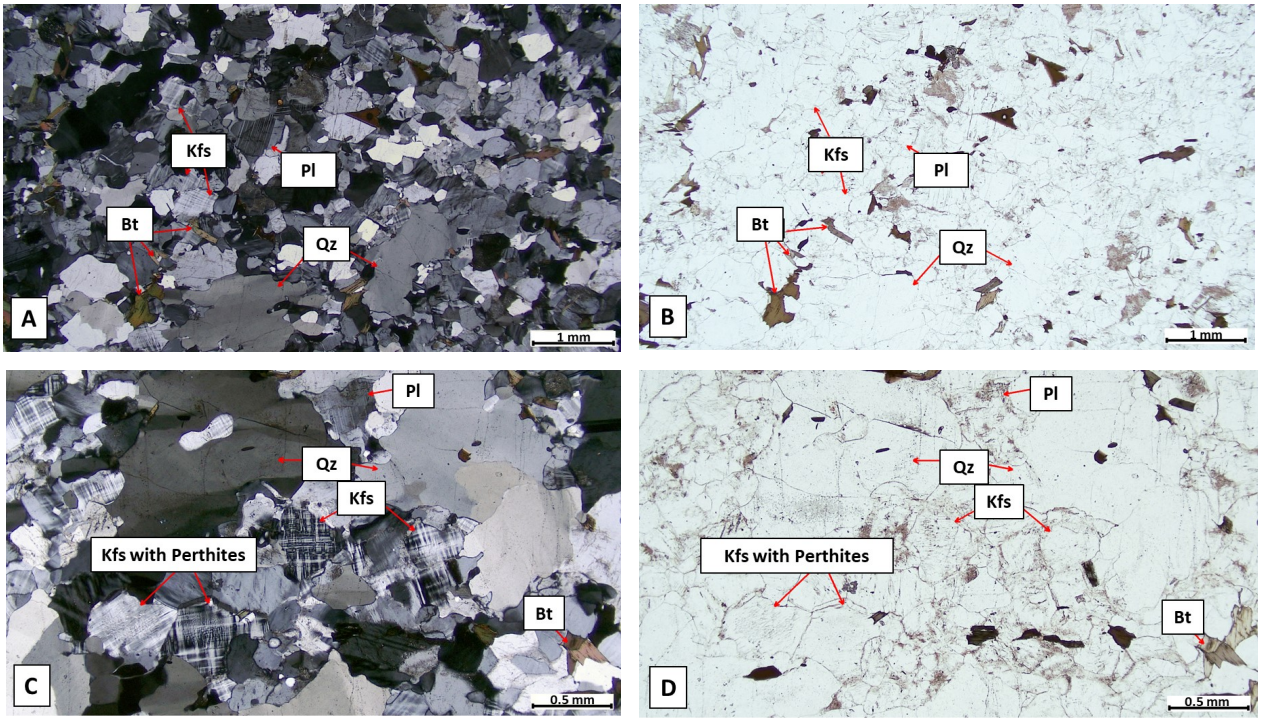

Figure 24: Photomicrographs of thin section MGO075112, located E of Stenestad. (A) and (C): XPL images. The rock has a weak fabric defined by the elongated quartz and feldspar grains. The K-feldspars have some perthitic exsolution or tartan twinning. (B) and (D): PPL images. The mafic minerals are sparse, small in size and they are oriented randomly. The biotite forms small, elongated crystals and the rock lacks amphibole.

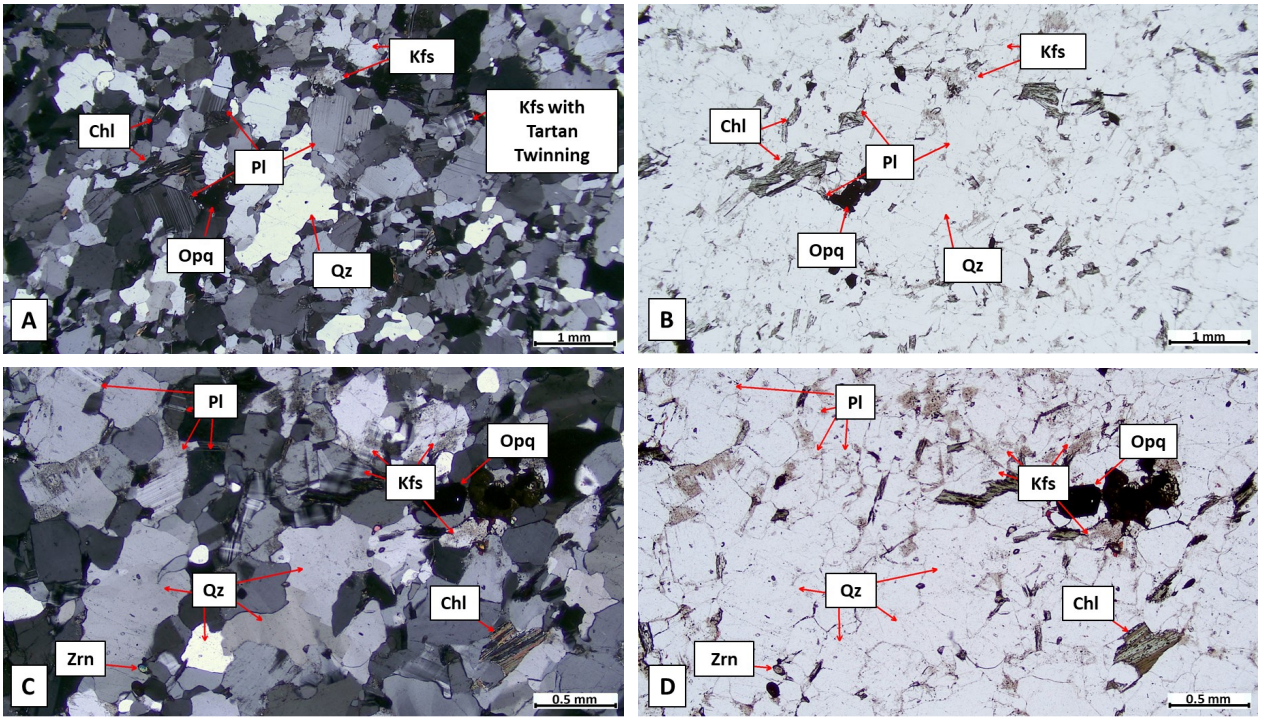

Figure 25: Photomicrographs of thin section MGO075117, located W of Röstånga. Thin section cut perpendicular to lineation. (A) and (C): XPL images. The grain boundaries are amoeboid, and the amount of rounded fine-grained minerals is increased. The quartz forms elongated grains and there is secondary chlorite. (B) and (D): PPL images. The mafic minerals are very sparse, and they are mostly consisted of chlorite and opaque minerals. The feldspars are altered to sericite.

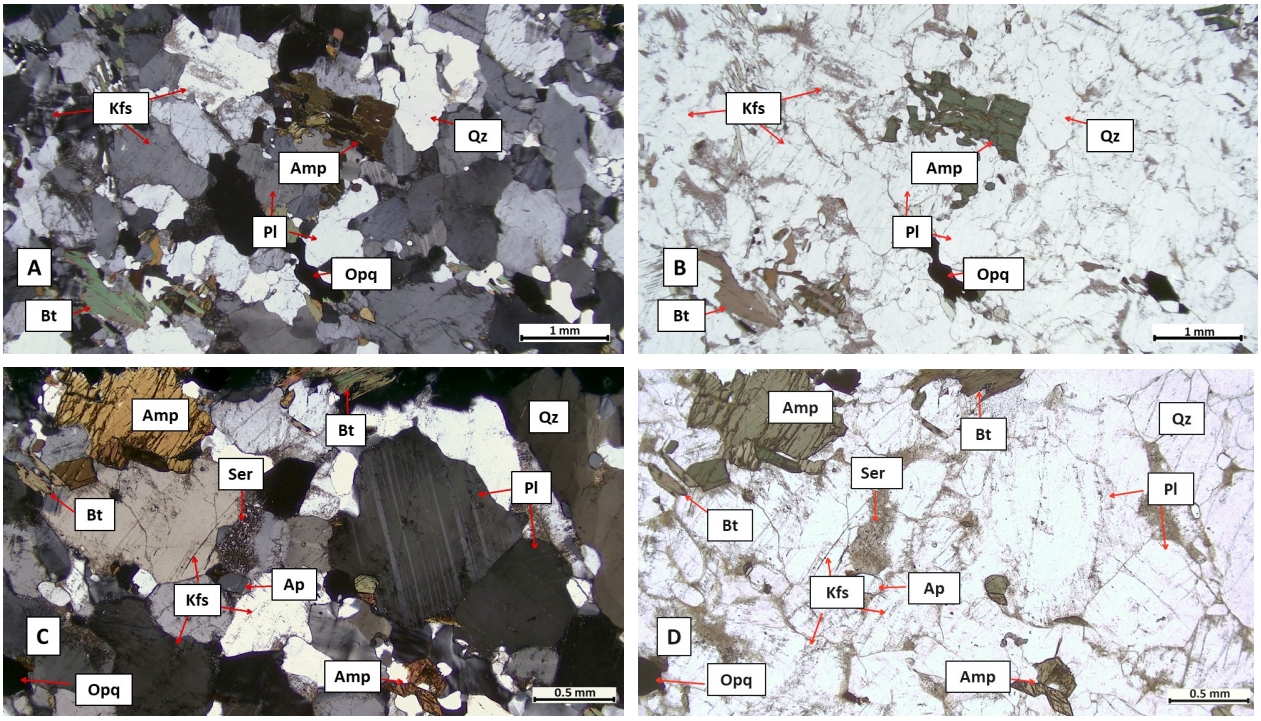

Figure 26: Photomicrographs of thin section MEK070523, located E of N Vram. (A) and (C): XPL images. The sample has many feldspar crystals that are partially or entirely sericitized. The sericitization is more intense on the K-feldspars than on the plagioclase. (B) and (D): PPL images. The mafic minerals are not oriented, and there is no clear fabric in this sample. There is accessory apatite and many opaque minerals.

Sample MEK070519, granitic gneiss east of Riseberga

The sample MEK070519 (Figure 27) is a fine- to medium-grained granitic gneiss with a high percentage of amphibole (11%) compared to the samples of class 3. The sample has 19% of quartz, one of the lowest among all samples, but the percentage of feldspar (63%) is increased. The K-feldspar appears either with tartan twinning (11%) or with perthitic exsolution (4%) or with a combination of the two (5%). The percentage of biotite is 4%, and it appears in small, elongated crystals (0.01-0.6 mm long) that are oriented randomly. There is high amount of fine-grained material in this sample, compared to the rest of the samples in class 3 (50% of the grains are less than 0.5 mm long). There is low alteration of biotite in chlorite (0.8%) and the sericitization of the feldspar is also limited (1%). The accessory minerals are apatite, titanite and opaque minerals.

Sample MEK070528, granitic gneiss at Riseberga

The sample MEK070528 (Figure 28) is a medium-grained granitic gneiss with high percentage of feldspar minerals (65%). The percentage of K-feldspar is very high (51%) compared to the rest of the samples of class 3 and appears either tartan twinned (18%) or with perthitic exsolution (6%) or as a combination between the two (4%). The rock lacks amphibole and the percentage of biotite is 4%. The quartz and feldspar grains can reach up to 4 and 3.5 mm long, respectively, and they have sutured grain boundaries with high complexity. The rock has low amount of fine-grained material, with only 10% of the grains being less than 0.5 mm long. There are some microfractures along the felsic minerals that are visible with the polarizing microscope (Figure 28D). There is some sericite forming as alteration product of feldspar (4%). The accessory minerals are zircon, titanite and opaque minerals.

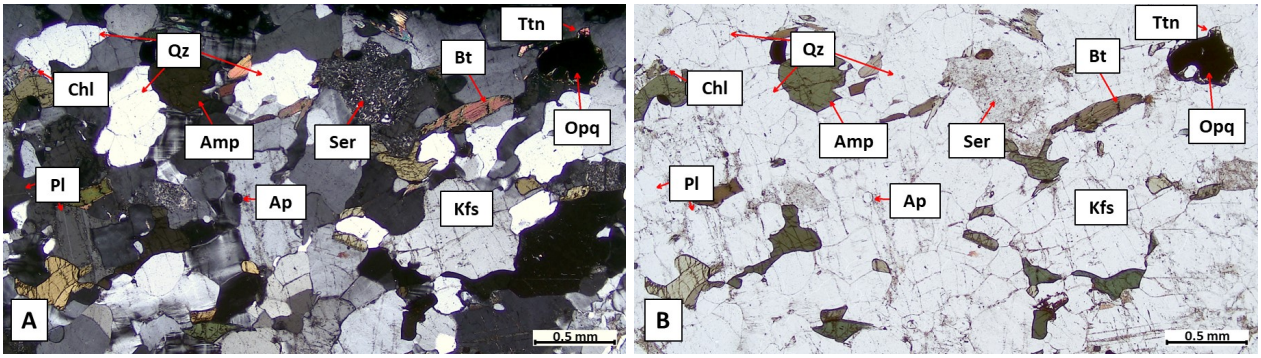

Figure 27: Photomicrographs of thin section MEK070519, E of Riseberga. Thin section cut perpendicular to lineation. (A): XPL image. the rock has more K-feldspar with tartan twinning and less perthitic K-feldspar. Around the opaque minerals, a titanite rim is formed. There is partial or total alteration of feldspar to sericite (B): PPL image. The rock does not show a foliation fabric, and the mafic minerals are scattered randomly in the rock.

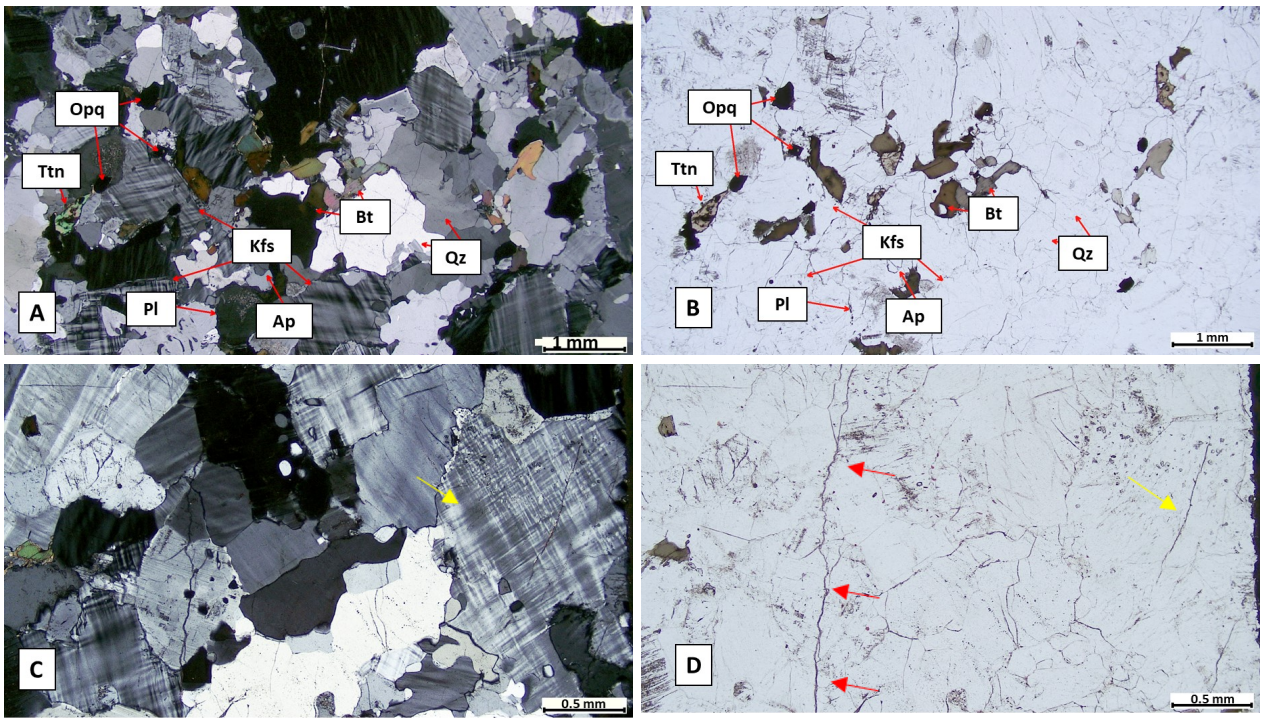

Figure 28: Photomicrographs of thin section MEK070528, in Riseberga. (A): XPL image. The rock is medium-grained, and the grains have quite complex grain boundaries. The mafic minerals are biotite and opaque minerals with titanite rim. (B): PPL image. The mafic minerals are oriented randomly in the sample and they are small in size. (C): XPL image. The tartan twinned K-feldspar (yellow arrow) shows (micro) perthitic exsolution. Very sparse, we can find some antiperthitic plagioclase (red arrow). (D): PPL image. the rock has some intragranular (yellow arrow) and intergranular (red arrows) fractures that are visible with a polarizing microscope.

Sample MEK070518, granitic gneiss south of Riseberga

The sample MEK070518 (Figure 29) is a medium- to coarse-grained granitic gneiss with very high amount of feldspar (53%). The K-feldspar (37%) has perthitic exsolution (28%) and the percentage of quartz is 21%. The percentages of biotite and amphibole are 1% and 12%, respectively, with the amphibole content being the highest compared to all samples in class 3. The rock is uneven grained, having up to 5 mm long, recrystallized quartz and feldspar crystals with very sutured grain boundaries, together with small (0.05 – 0.2 mm length), rounded garnet (10%). The garnet is usually found surrounding the amphibole crystals, forming small patches of dark minerals between the quartz and feldspar. There is rare alteration of biotite to chlorite. The accessory minerals are zircon, apatite and opaque minerals.

Sample MGO075116, granitic gneiss at Skäralid

The sample MGO075116 (Figure 30) is a medium- to coarse-grained granitic gneiss with high percentage of quartz (34%) compared to the samples in class 3. The percentage of feldspar is 57% (45% K-feldspar and 12% plagioclase). The K-feldspar has perthitic exsolution (38%). The biotite and amphibole percentages are around 3% and they are located in thin bands, together with fine-grained garnet (1%). Quartz crystals have an amoeboid shape and the complex boundaries. The length of quartz and feldspar can reach up to 5.1 and 4.2 mm, respectively. There is few chlorite (<0.5%). The accessory minerals are zircon, titanite and opaque minerals.

Sample MEK070520, granitic gneiss east of Klåveröd

The sample MEK070520 (Figure 31) is a fine- to medium-grained granitic gneiss with high percentage of quartz (30%) compared to the samples in class 3. The total percentage of feldspar is very high (68%), and the plagioclase percentage is 21%. The K-feldspar (47%) appears mostly tartan-twinned (24%), but it can also have perthitic exsolution (3 %) or a combination between the two (5 %). Biotite and amphibole are absent. The rock has a very weak fabric, and the percentage of fine-grained material is low (16% of the grains are less than 0.5 mm long). There is very low amount of chlorite (<1 %) and some accessory opaque minerals.

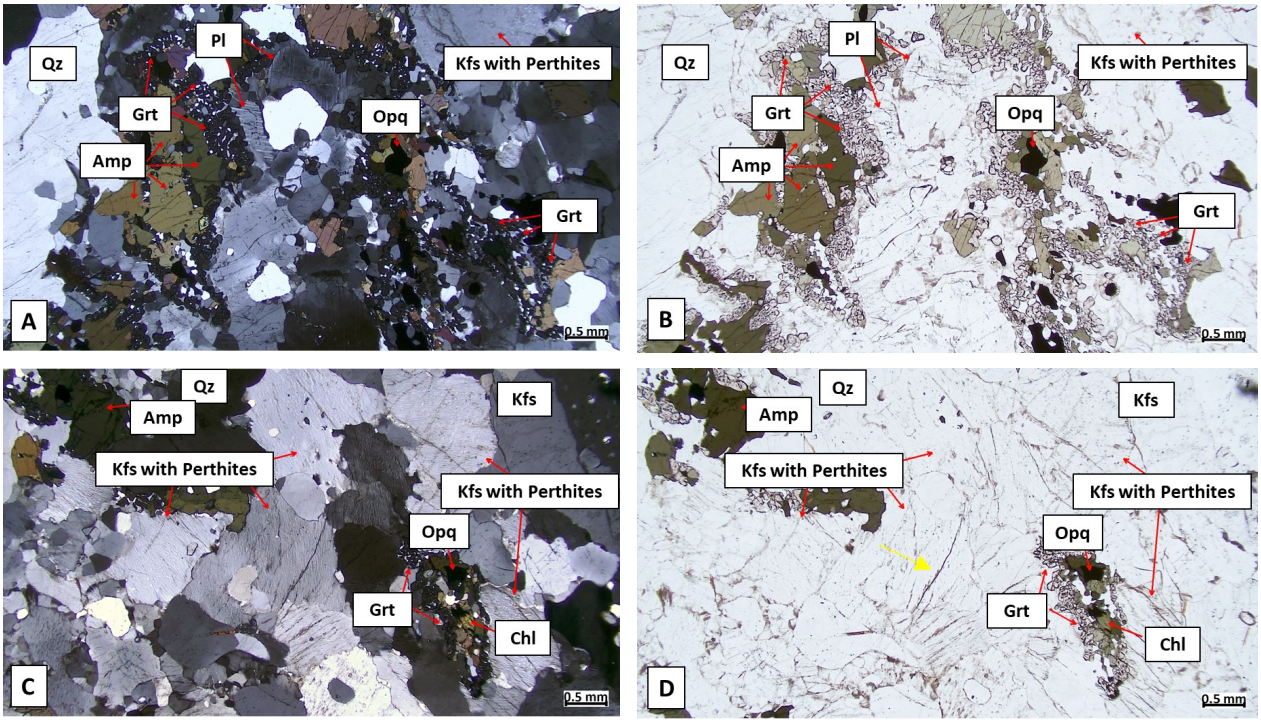

Figure 29: Photomicrographs of thin section MEK070518, S of Riseberga. (A) and (C): XPL images. The feldspar and quartz crystals form big grains, and the small garnet crystals are crystallized around the amphibole and the opaque minerals. The K-feldspar have (micro) perthites. They can be up to 5 mm long. The biotite is altered to chlorite. (B) and (D): PPL images. The main mafic minerals are amphibole and garnet, together with some opaque minerals. The mafic assemblages from elongated aggregates. The rock has a high percentage of Fe- and Mg- rich minerals. The feldspars have wide microfractures that are visible with polarizing microscope (yellow arrow in Figure 29D).

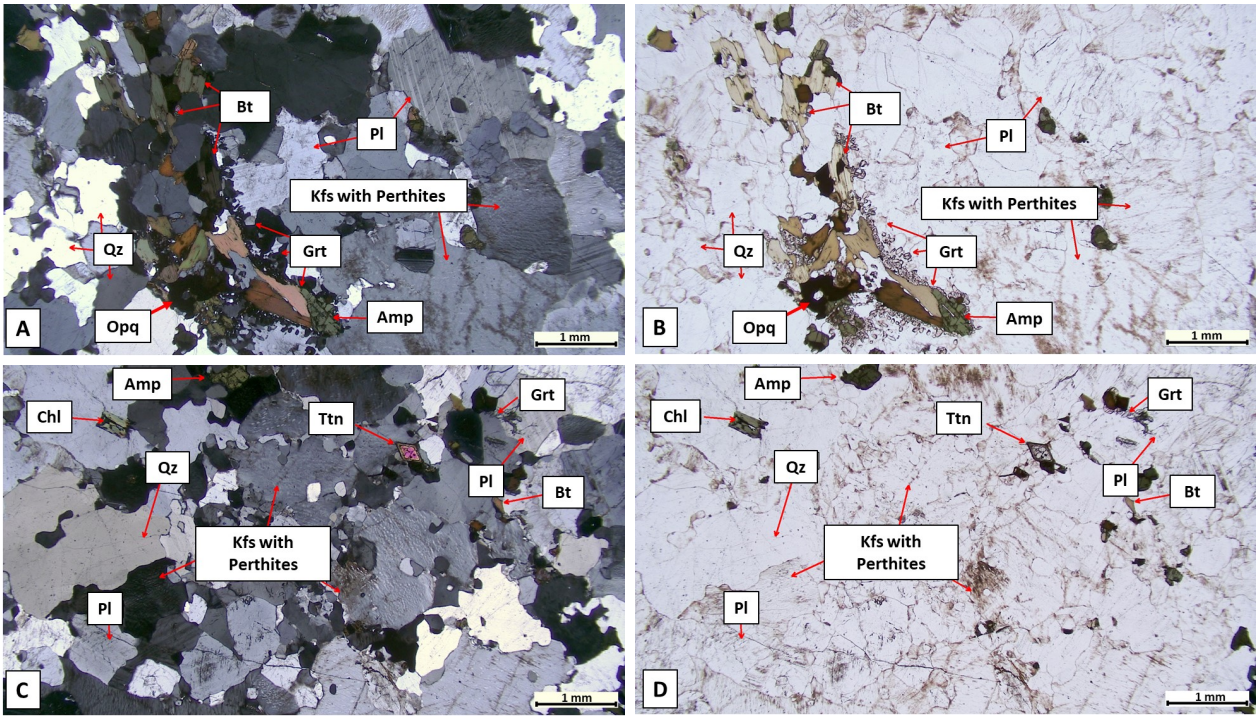

Figure 30: Photomicrographs of thin section MGO075116, located in Skäralid. (A) and (C): XPL images. The rock has a high percentage of quartz and feldspar. Quartz forms grains with sutured grain boundaries. The K-feldspar crystals have perthitic exsolution. (B) and (D): PPL images. The mafic minerals (amphibole and biotite) are low in content and they are crystallized in small assemblages. In figure (D) there is a beautiful diamond-shaped titanite.

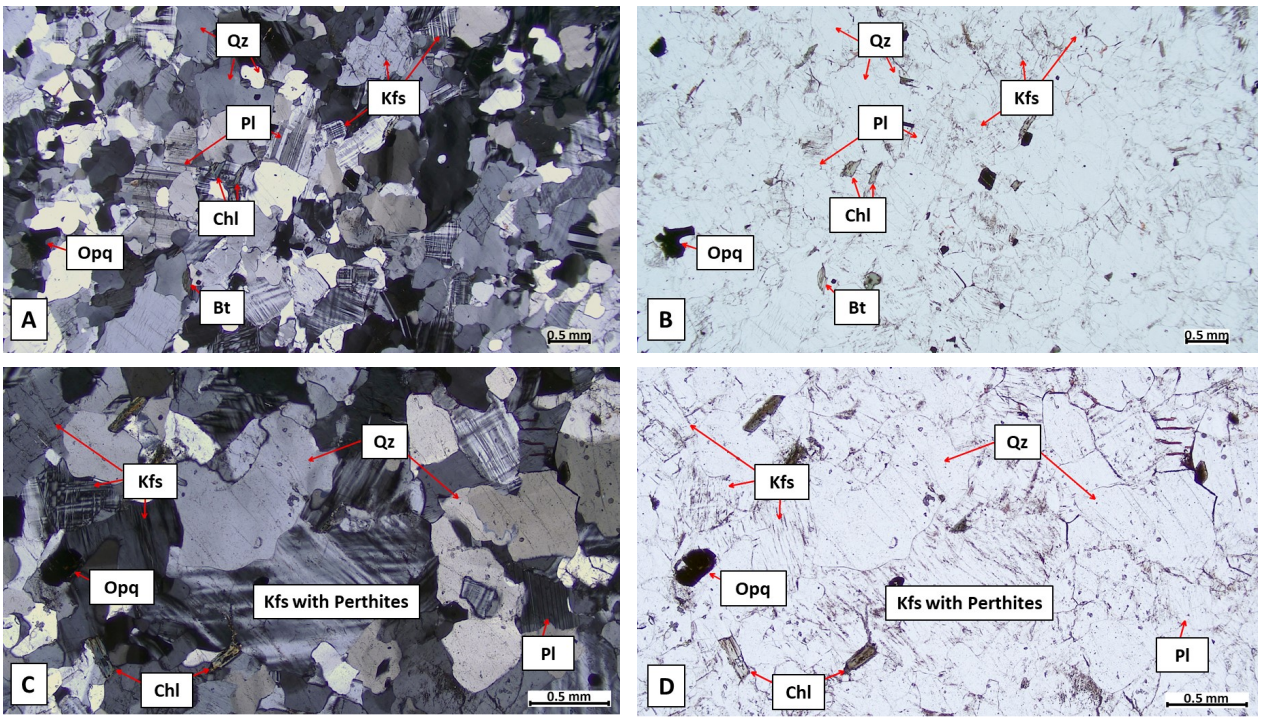

Figure 31: Photomicrographs of thin section MEK070520, located E of Klåveröd. (A) and (C): XPL images. The rock contains very little mafic minerals that are oriented randomly (chlorite, opaque minerals ± biotite). It has a small number of very fine-grained minerals. There are some K-feldspar crystals with tartan twinning and perthitic exsolution. (B) and (D): PPL images. The sample is almost leucocratic. The rare mafic minerals are of very small size and are quite sparse in the rock.

4.2.4 Metagabbro

The sample MEK070524 (Figure 32) is a fine- to medium-grained metagabbro. It consists of plagioclase with antiperthitic exsolution, amphibole, ortho- and clino-pyroxenes, biotite, sericite, garnet, with little quartz and apatite. The presence of the orthopyroxenes indicates very high metamorphic conditions, but there are signs of partial amphibolitization of the pyroxenes, probably due to retrogressive metamorphic conditions in a later stage.

whereas in zone 6 the samples lack titanite and the majority of them include fine-grained garnet. Moreover, in zone 6 there is higher percentage of perthitic exsolution in K-feldspar and lower tartan twinning in feldspar, than in zone 5. Biotite and amphibole percentages present a small decrease with decreasing quality, however there are some individual samples that lack these minerals. Lastly, apatite is more abundant in the samples of the metamorphic zone 6.

The sericitization of feldspars is lower in class 3, and

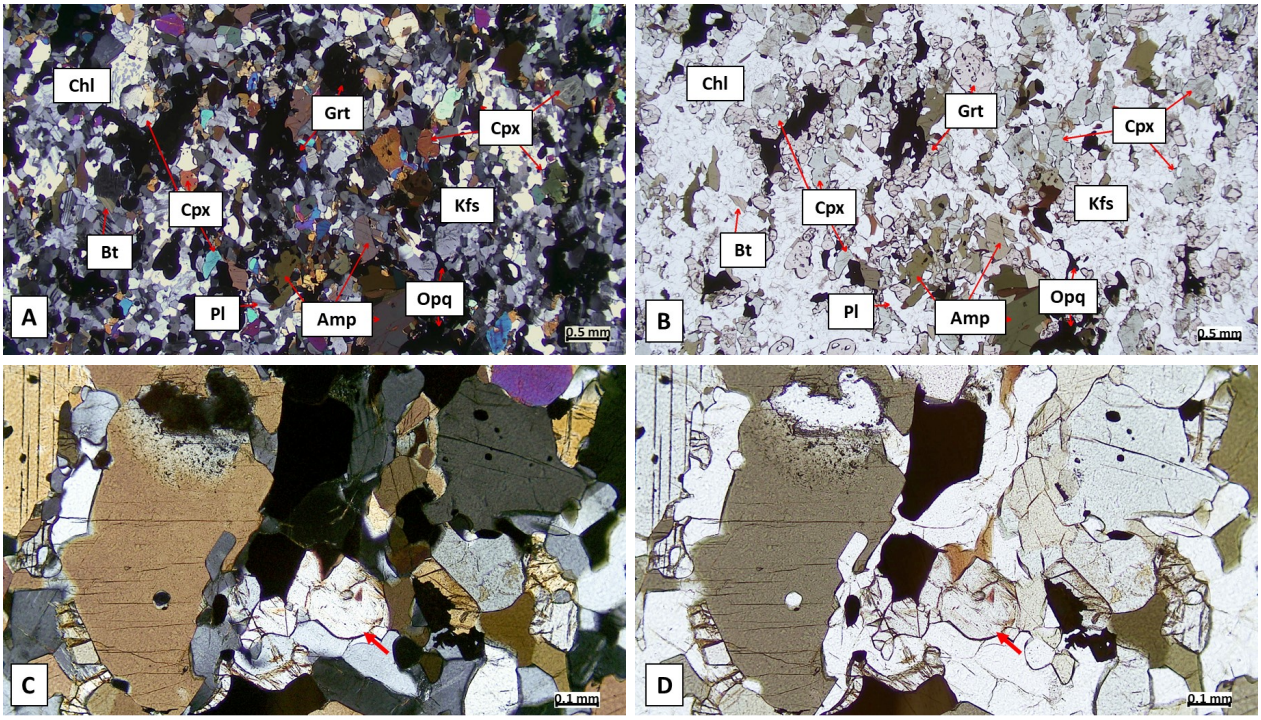

Figure 32: Photomicrographs of thin section MEK070524, a mafic rock located E of Munka Ljungby. (A): XPL image. The sample is fine- to medium-grained and has a granulitic texture. (B): PPL image. The felsic part is mainly consisted of Ca-rich plagioclase with antiperthitic exsolution. (C): XPL image. The red arrow shows an orthopyroxene crystal. It has very small grain size and it has first order birefringence colors (based on the Michel – Levy birefringence chart) and it is rather subhedral. (D): PPL image. The orthopyroxene crystal can be recognized by the high relief and the slight pleochroism with red-green colors.

4.3 Point counting

The results from the point counting of the thin sections are summarized in Figure 33. The color coding is green for class 1 samples, blue for class 2 samples and red for class 3 samples. Table 3 shows the average percentage for each mineral per class 1-3. The tables with the composition for each sample are presented in the Appendix.

The results from the point counting (Figure 33, Table 3) show that the percentage of quartz is higher in class 1 than in classes 2 and 3, and this decrease is accompanied by an increase in feldspar from class 1 to 3. Plagioclase is increased in class 3 in comparison to the other classes. What is noticeable is that the samples located in the metamorphic zone 5 (Figures 4, 5B) have higher occurrence of titanite and lower garnet, the chloritization of biotite follows the same trend. Opaque minerals are increased in class 2, and garnet is almost absent in classes 1 and 2, whereas in class 3 the average percentage is almost 2%.

4.4 Grain size analysis and grain complexity

Previous studies have shown that grain size has a great influence on mechanical properties. A fine-grained rock is more durable than a coarse-grained (Lundqvist & Göransson, 2001). Mechanical properties, such as resistance to abrasion and resistance to brittle fragmentation, tend to decrease with the increase of mean grain size, particularly for rocks with the grain size lower than 1 mm (Sun et al., 2017). For the orthogneisses, the analysis has been conducted using image analysis software and measuring manually the grain perimeter

along a traverse line. The results have been analyzed below.

4.4.1 Feret's diameter (minimum, maximum)

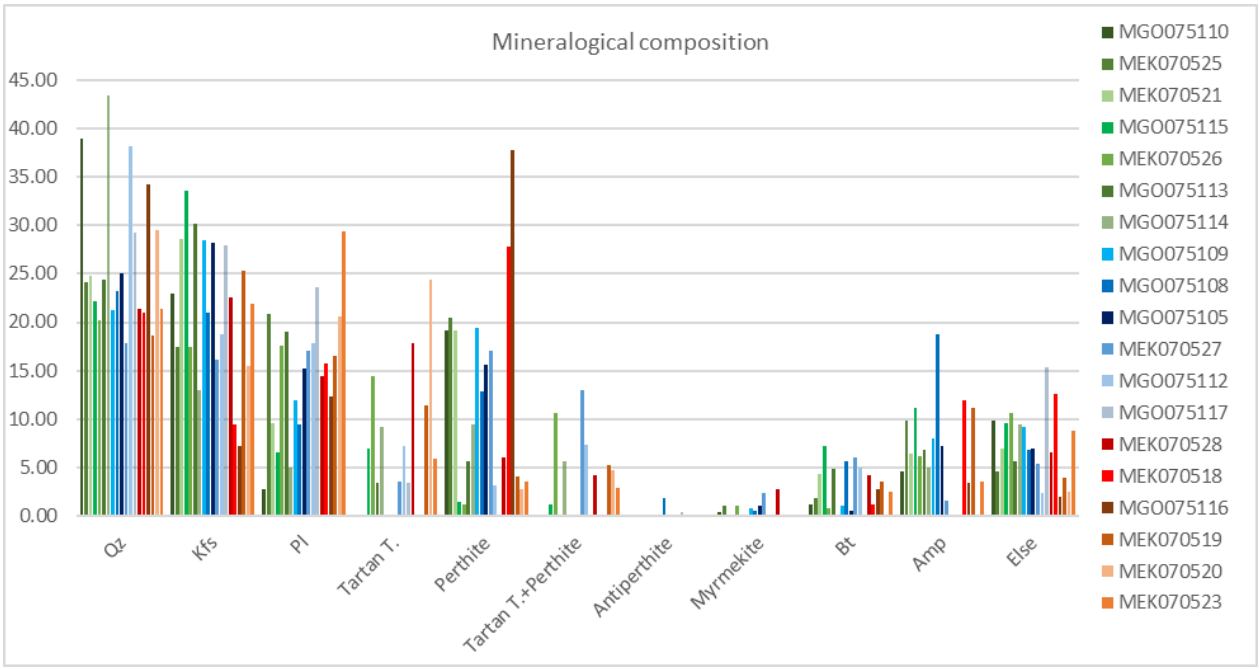

Figure 33: Chart with the mineralogical composition of each sample for the main phases, after the point counting method. Green = class 1, blue = class 2, red = class 3 samples.

	Minerals	Class 1	Class 2	Class 3
Main phases	Qz	28.3	25.8	24.3
	Kfs	41.6	40.5	43.5
	Pl	11.6	15.8	18.2
	Bt	2.9	3.0	2.4
	Amp	7.1	5.9	5.0
	Else	8.1	7.7	6.1
	Total Feldspar	53.2	56.2	62.2
Else = Associate minerals	Ser	3.7	2.1	1.7
	Chl	1.6	2.4	0.3
	Zrn	0.3	0.2	0.3
	Opq	1.8	2.3	1.5
	Ap	0.2	0.3	0.2
	Grt	0.2	0.2	1.8
	Ttn	0.3	0.2	0.1

Table 3: Average percentages of the different mineral phases per rock class.

The Feret's diameter represents the distance between two parallel tangents of an object (Ersoy & Waller, 1995). The Feret's maximum diameter represents the longest distance of the object, whereas the Feret's minimum diameter the shortest distance (Figure 34).

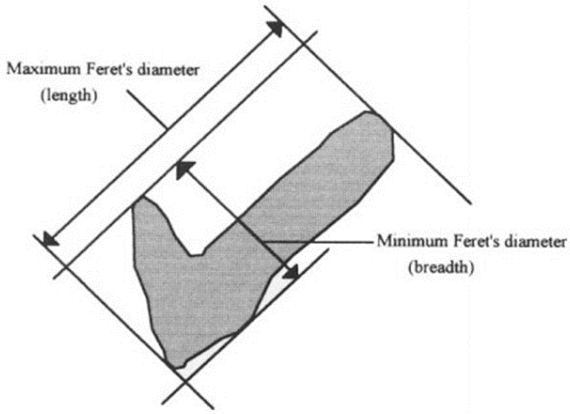

Figure 34: Illustration of minimum and maximum Feret's diameter (Ersoy & Waller, 1995). The length and the breadth are not always perpendicular to each other.

The average value of the maximum Feret's diameter depicts whether a rock is fine-grained or coarse-grained. The Standard Deviation (SD) is a measure of the amount of dispersion of the set of values. Higher values of SD indicate that the sample has a variety of grain sizes. The values of average Feret and SD for each sample are presented in Table 4.

It is derived from Table 4 that, although all samples have an average maximum Feret value of <1 mm, the variations in some cases are quite high. More specifically, samples MEK070518, MEK070528, MGO075109 and MGO075116 have the highest SD,

Sample	Class	Average Feret Value	Standard Deviation
MEK070521	1	0.26	0.16
MGO075108	2	0.28	0.28
MGO075115	1	0.28	0.17
MGO075113	1	0.28	0.20
MGO075105	2	0.30	0.25
MGO075110	1	0.37	0.34
MEK070519	3	0.41	0.27
MGO075117	2	0.41	0.30
MGO075109	2	0.42	0.66
MEK070526	1	0.43	0.34
MEK070525	1	0.44	0.38
MGO075114	1	0.45	0.50
MGO075112	2	0.45	0.41
MEK070518	3	0.60	0.87
MEK070527	2	0.63	0.56
MEK070523	3	0.65	0.53
MEK070520	3	0.70	0.39
MEK070528	3	0.77	0.66
MGO075116	3	0.93	0.96

Table 4: Average Feret values and Standard Deviation for each sample.

meaning that the variation of grain size in these samples is great, whereas samples MEK070521, MGO075113 and MGO075115 seem to have a rather low variation of grain size, based on the SD values. In order to validate these assumptions, the grain sizes were normalized and plotted in a cumulative plot (Figure 35A). Additionally, a cumulative plot with the minimum Feret's diameter measured from the same grains is presented in Figure 35B. The minimum Feret's diameter is helpful in determining the width of the grains. A sample with high values in both the minimum Feret's diameter and the maximum Feret's diameter corresponds to grains with increased size, whereas a foliated rock would have high maximum Feret's and rather smaller minimum Feret's diameter, due to the high amount of elongated grains.

The results of the cumulative plot agree with the average grain size. It is interesting to note here that the samples with high variations in grain size are primarily from class 3 and they are more coarse-grained. On the contrary, the samples with low variations in grain size are mainly from class 1 and they are more fine-grained. This result follows the rule that a fine-grained rock has better technical properties than a coarse-grained rock. Despite the general trend, there are some samples that do now follow this trend. These samples (MEK070519, MGO075114) show the opposite than expected from their technical quality.

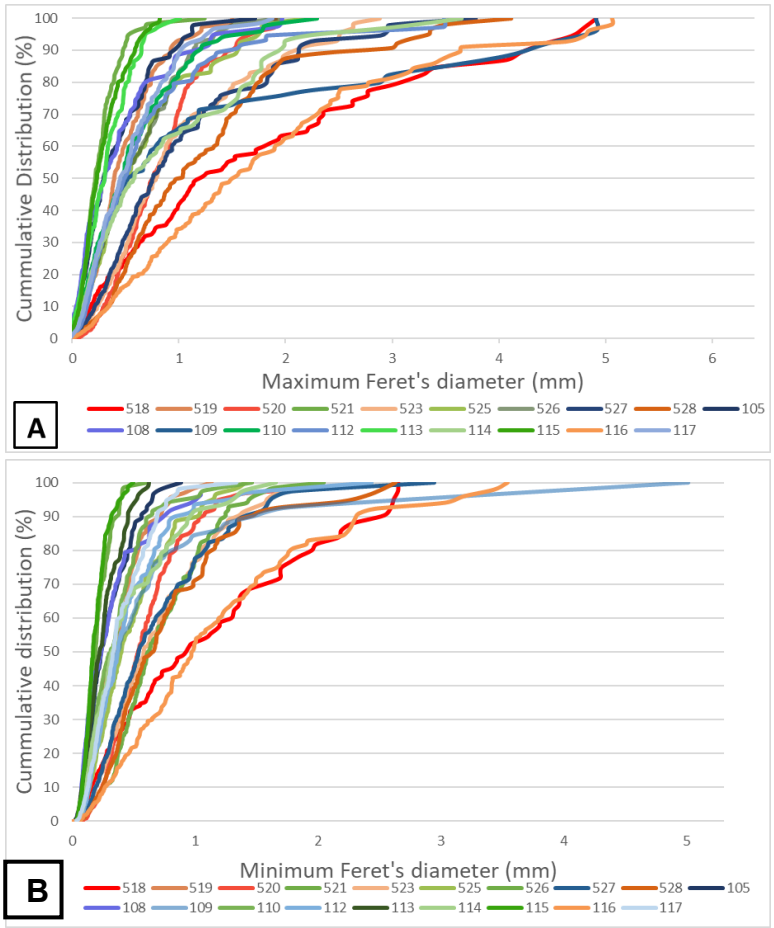

Figure 35: (A) Cumulative mineral grain size distribution for every sample, based on the Feret's diameter. (B) Cumulative plot of minimum Feret's diameter. The color coding is: green=class 1, blue=class 2, red=class 3.

4.4.2 “Grain Shape Complexity (GSC)”

The “Grain Shape Complexity” factor was invented while trying to understand how the perimeter and the length of a grain are affected in case of a rounded or a complex grain, respectively. This number increases with the decrease of grain size, or with the increase of the perimeter of the grain. The reason that the minimum Feret’s diameter was chosen here is due to the fact that the increase of the perimeter is not always dependent on the grain width. The fraction of the grain perimeter versus the minimum Feret diameter can reveal the irregularity of the grains; the equation of this factor is:

$$GSC_i = \frac{Perimeter\ of\ grain\ i\ (mm)}{Minimum\ Feret\ value\ of\ grain\ i\ (mm)}$$

High values of GSC correspond to grains with high complexity (more sutured or amoeboid grain boundaries), whereas low values indicate more rounded grains (granoblastic texture). The GSC factor for all samples was calculated based on the grain size analysis and the results were normalized and plotted in a cumulative plot (Figure 36).

As derived from the plot, the samples with the highest complexity are found in class 1 (green) and the samples with the lowest complexity in class 3 (red). The samples with the highest values of GSC are MGO075115 and MEK070521 from class 1, MGO075109 from class 2 and MEK070519 from class 3. The samples with the lowest values of GSC are MEK070525 form class 1 and MEK070520, MGO075116 from class 3. The samples that present unexpected values are MEK070519 and MEK070525, the former because high complexity is generally correlated with good technical values and the latter because low complexity is generally correlated with bad technical values.

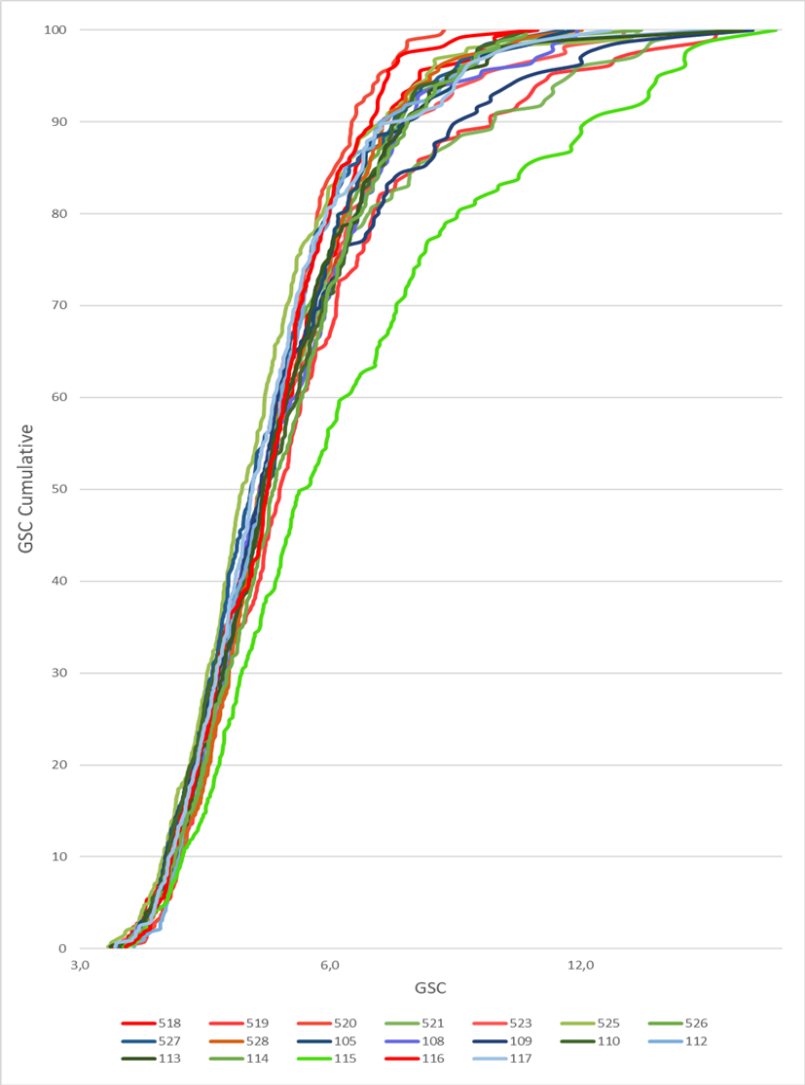

Figure 36: Logarithmic plot of the Grain Shape Complexity.

4.4.3 Circularity

Circularity is a measure of the degree of roundness of a circular object (Wojnar et al., 2004). The value of circularity ranges from 0 to 1, 1 being a mathematically perfect circle. Circularity applies in two dimensions, and the analogue in three dimensions is sphericity. The value of circularity in these samples was calculated automatically from the software after the measurement of the grain perimeter, following the equation:

$$Circularity_i = 4\pi \frac{Area\ of\ grain\ i\ (mm^2)}{(Perimeter\ of\ grain\ i\ (mm))^2}$$

The results from the circularity measurements are presented in Figure 37.

In this figure, there was a random choice of the limits in each column. Circularity values lower than 0.5 correspond to grains with irregular grain boundaries, whereas circularity values higher than 0.8 correspond to almost rounded grains. There is no obvious trend in this case, but generally the amount of grains with high circularity tends to increase with lower technical quality (this figure is arranged in relation to the Los Angeles values), and vice versa for the grains with low circularity.

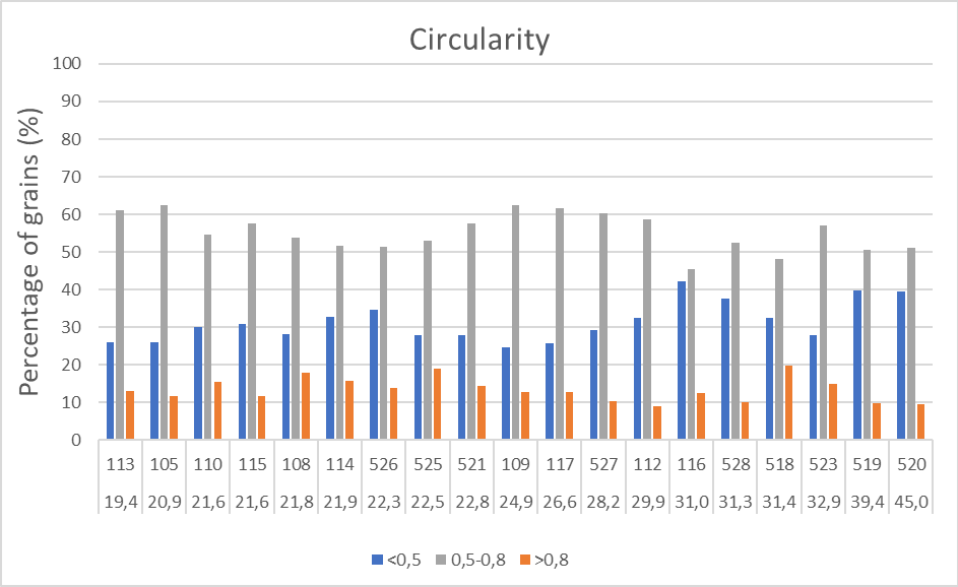

Figure 37: Diagram of circularity for all samples. Low circularity indicates grains with complex boundaries. The upper number on the horizontal axis corresponds to the sample code (last three digits) and the lower number to the LA value of the sample.

4.4.4 Aspect Ratio (AR)

The Aspect Ratio (AR) of a geometric shape in two dimensions is the ratio of its shorter side to its longer side (Wojnar et al., 2004). In this study, the aspect ratio is calculated based on the maximum and minimum Feret diameter of the grain, following the equation:

$$AR = \frac{minimum\ Feret\ of\ grain\ i\ (mm)}{maximum\ Feret\ of\ grain\ i\ (mm)}$$

The values vary from 0 to 1, 1 being an equiaxed grain. The results from the AR calculations for the samples are presented in Figure 38.

The Aspect Ratio is another tool to determine whether a rock is deformed. Highly deformed rocks present an increased amount of grains with very low AR. The general trend in the orthogneisses of the study area is that the amount of very elongated grains decreases with decrease in technical quality, as derived from Figure 38. The blue column (amount of grains with AR<0.5 – very elongated grains) is decreasing with an increase in LA values. This agrees with the metamorphic conditions of the study area, as the degree of deformation increases from SE to NW, especially when crossing the "border" from the metamorphic zone 5 to zone 6 (after Möller & Andersson, 2018). In other words, the increase of metamorphic conditions here corresponds to highly elongated grains and as a result, better technical properties.

4.4.5 Area

The area of the grains was measured using the grain shape measurements. This is the true area of the grains, as it is calculated from the pixels that each grain covers. Higher amount of fine-grained material indicates better quality. The results from the area calculations are presented in Figure 39.

The general trend here is that the very small grains (<0.01 mm^2) tend to increase with higher quality, whereas the grains over 1.0 mm^2 increase with lower quality. This follows the rule that a finer-grained rock tends to have better technical properties than a coarser-grained rock.

4.5 Visual Classification of Grain Boundary Complexity (VC)

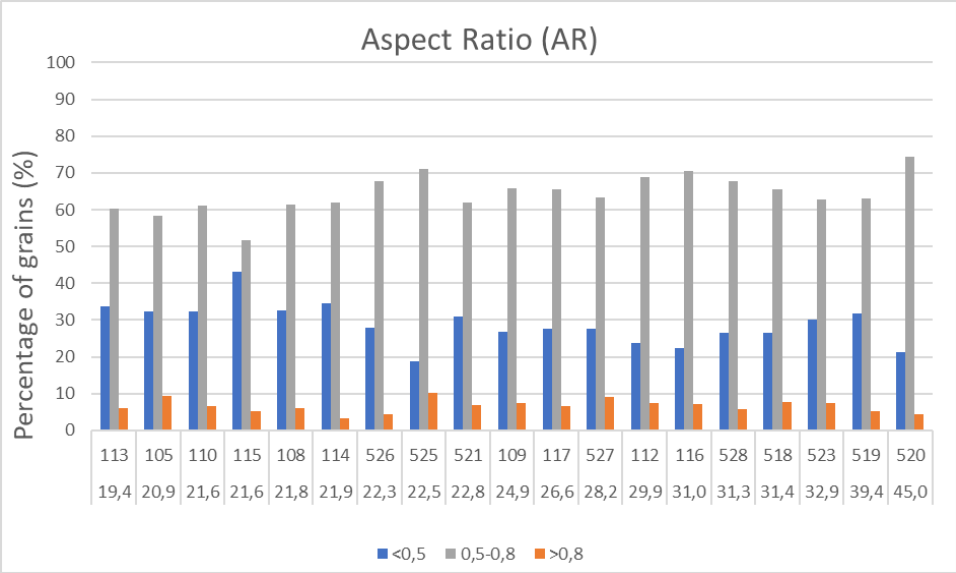

Figure 38: Diagram of aspect ratio for all samples, based on minimum and maximum Feret's diameter. Lower AR indicates more elongated grains. The upper number on the horizontal axis corresponds to the sample code (last three digits) and the lower number to the LA value of the sample.

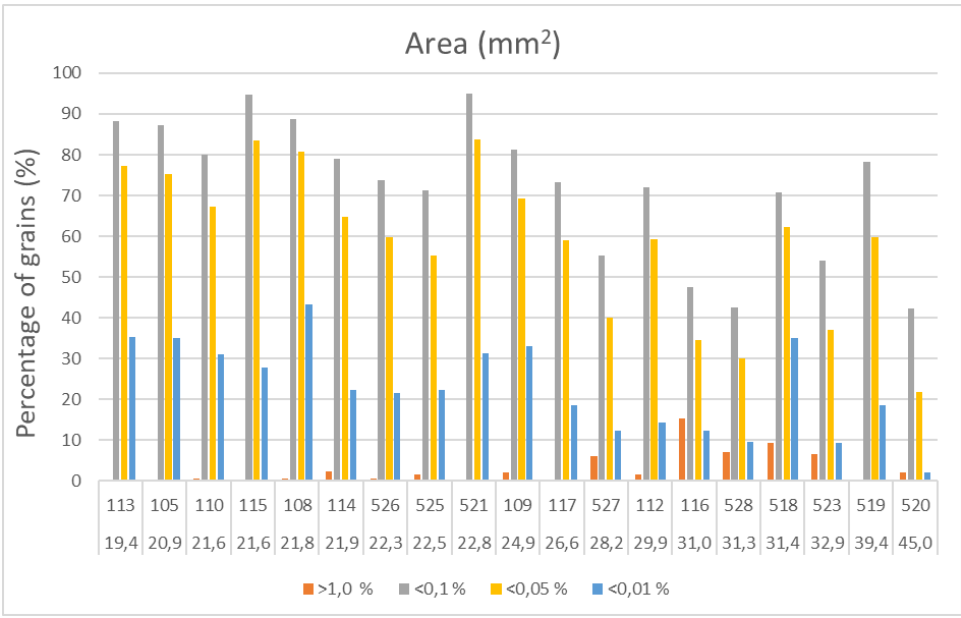

Figure 39: Diagram of grain sample area in mm² (%), based on the grain shape measurements. The upper number on the horizontal axis corresponds to the sample code (last three digits) and the lower number to the LA value of the sample.

The results from the classification are presented in Table 5. The classification was conducted twice, once for the coarse-grained grains and once for the fine-grained grains of the samples. After using the Model for Evaluation of Grain Boundaries (Figure 7), the results show that there is no clear trend of the grain boundary complexity using the Visual Classification. The coarse-grained minerals in all three classes have more complex boundaries than the fine-grained minerals (which is expected) but generally, the range of the grade in the coarse-grained material is from 3 to 4 in all three classes.

4.6 Microfracture analysis

The samples analyzed for microcracks were chosen based on two factors, the technical properties and the average grain size. Two coarser-grained samples (one from class 1 and one from class 3, Figures 40, 41) and two finer-grained samples (one from class 1 and one from class 3, Figures 42, 43) were analyzed. The preliminary results show that microcracks occur in all four samples analyzed, and there is no correlation between the grain size variations and the microcrack propagation.

In the first case of the two coarser-grained samples, the microcracks are present and they are usually transgranular (from one grain boundary and across the grain). They mostly appear to be along the quartz and feldspars, but sometimes they penetrate minerals with higher specific weight (light gray color in photos) like biotite, opaque minerals, amphiboles. In Figure 40, both samples have rather straight microcracks that are interconnected. However in Figure 41, the same samples have a very different appearance. Figure 41A is of sample MEK070523 (class 3) and the microfractures are almost parallel to each other, whereas Figure 41B is of sample MGO075114, and the microcracks here are puzzle-like shaped with high complexity. In this case, a possible connection of the microcracks to the technical properties might be valid, as microcracks

Class 1	VC - F	VC - C	Class 2	VC - F	VC - C	Class 3	VC - F	VC - C
MEK070521[2]	1	2	MEK070527	1	2	MEK070523	1	3
MEK070525	1	3	MGO075105[2]	2	3	MEK070519	2	3
MGO075114	1	4	MGO075108	2	3	MEK070520	1	3
MGO075115[2]	1	3	MGO075117	3	3	MGO075116[1]	1	4
MGO075109	2	3	MGO075112	3	4	MEK070528[1]	2	4
MGO075113[2]	2	3	MGO075109	2	3	MEK070518[1]	1	4
MEK070526	2	4						
MGO075110	2	4						

Table 5: Visual classification of grain boundary complexity in the orthogneisses from NW Skåne. The scale range is from 1 to 5, with 5 having the highest grain boundary complexity. VC-F=Visual Classification for the fine-grained grains, VC-C=Visual Classification for the coarse-grained grains. 1=very little or no fine-grained material, 2=high amount of fine-grained material.

with complex shape might actually increase the rock's brittleness by providing better interlocking of the grains.

In the second case of the two finer-grained samples, the microcracks are also transgranular in both samples. In some cases they seem to terminate when reaching a mineral with high specific weight, meaning that these minerals act as barriers in the microcrack propagation. However, in other cases the microcracks are penetrating these minerals. In Figure 42A, the sample MEK070519 has abundant microcracks that are quite straight. In Figure 42B, the sample MGO075113 has also many microcracks with slightly higher complexity. However in Figure 43, the sample of class 3 (Figure 43A) shows very complex, puzzle-like transgranular microcracks, whereas the sample of class 1 (Figure 43B) has microcracks with low-medium complexity.

The interpretation of these data is quite hard to explain, due to the limited amount of data used in this method. Further investigation should be conducted in order to have more reliable results.

5. Discussion

5.1 Metamorphic conditions of the area and association with rock quality

What is noticeable from Figure 5A is that the majority of samples with lower quality (class 2, class 3) are located in the southeastern part of the study area, whereas the higher quality samples (class 1) are found in the north and northwestern part. The approximate boundary between zones 5 and 6, together with the samples classified with gradient colors related to their LA values, are presented in Figure 5B, showing that the lower quality samples are located in zone 5, whereas the higher quality samples are in zone 6, which has higher metamorphic conditions. It is suggested that the metamorphic grade plays a major role in the development of the microstructure that steers the technical

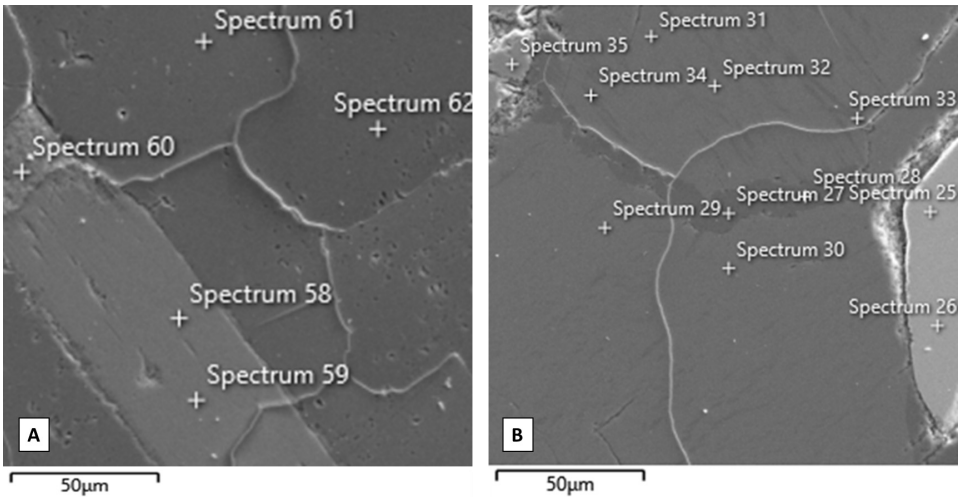

Figure 40: (A) Secondary electron image (SE-image) of sample MEK070523. The microcracks are transgranular, penetrating the biotite on the lower left corner. (B) SE-image of sample MGO075114. Here the microcracks are also transgranular, following the grain boundary of the perthitic K-feldspar on the top left corner and crossing the lower mineral.

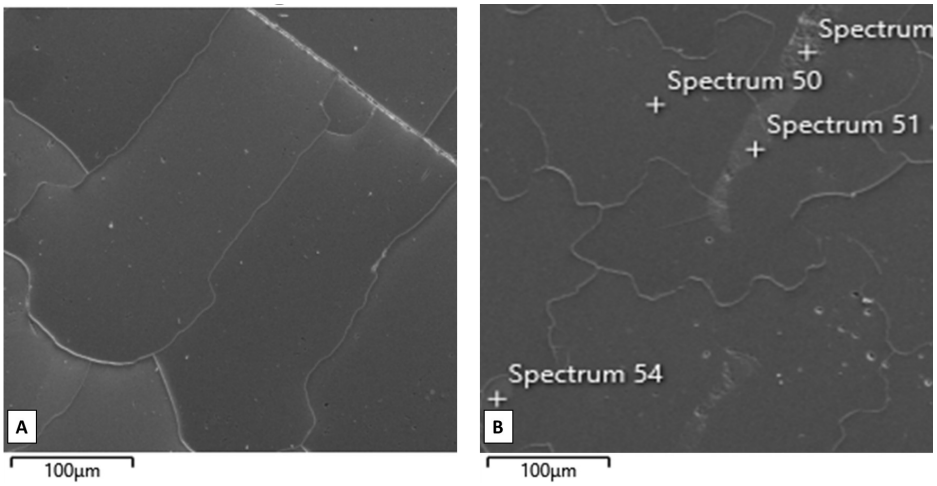

Figure 41: (A) SE-image of sample MEK070523. The microcracks are either intergranular or transgranular (the SEM does not reflect the grain boundaries of two grains of the same mineral). They are almost straight, a fact that might explain the low technical values of the sample. (B) SE-image of sample MGO075114. Here the microcracks are transgranular, crossing the different mineral phases. In comparison to the left photo, these microcracks look quite jagged so they have good interlocking.

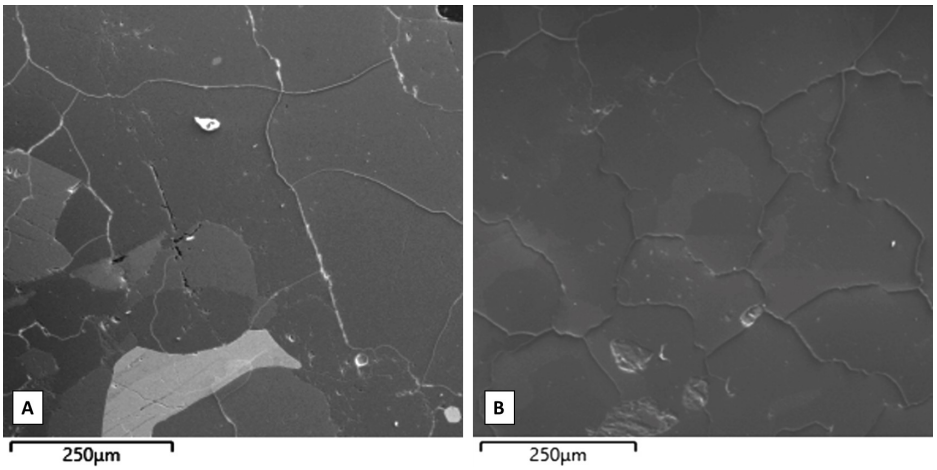

Figure 42: (A) SE-image of sample MEK070519. The microcracks are transgranular, but they seem to terminate on the bottom part of the photo, where a heavy mineral (very bright gray color – possibly an opaque mineral) is located. The cracks are almost straight here, a fact that should theoretically diminish the rock's strength. (B) SE-image of sample MGO075113. The microcracks are transgranular, crossing the different mineral phases. The triple points created from the microcracks could make the rock act as if having granoblastic texture.

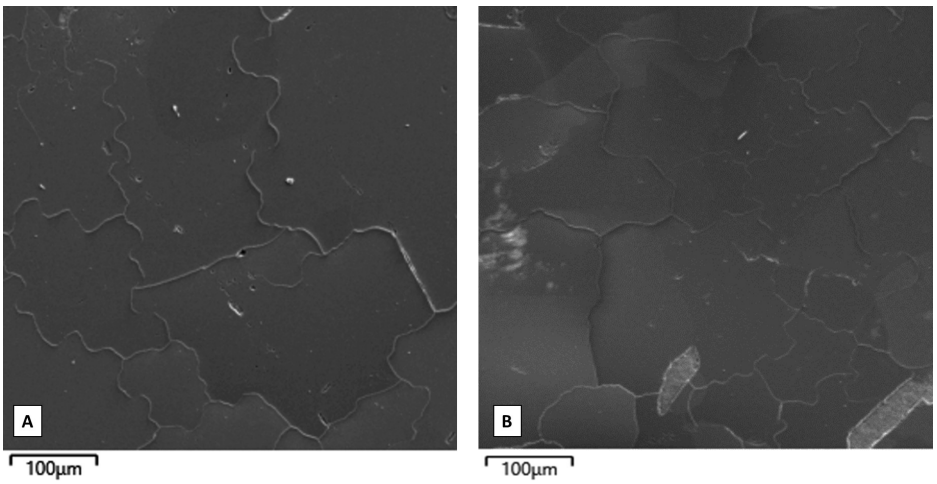

Figure 43: (A) SE-image of sample MEK070519. The microcracks are transgranular, having a puzzle-like shape. (B) SE-image of sample MGO075113. The microcracks are transgranular, crossing the different mineral phases. They are abundant in the sample.

values of these rocks. In this study the samples that have undergone higher metamorphic conditions have better technical properties.

What can also be derived from the study of the samples is that the degree of strain tends to increase with higher metamorphic conditions. Most of the samples from class 3 appear undeformed or with weak deformation, whereas almost all of the samples in class 1 are strongly deformed, mainly showing signs of plastic deformation and formation of lineation and foliation. Figure 44 shows the map area and the degree of deformation among the samples. The main question is: why is the increase of deformation good for the technical quality? Is there a correlation between highly deformed rocks and grain size/grain shape? If we compare the results from the Feret's diameter, the aspect ratio and the grain area, it is clear that the samples with higher quality (class 1) are more deformed with elongated grains, smaller grain size and lower mean area than the samples with lower quality. On the contrary, the majority of class 3 samples, even though the have very poor quality with higher grain size and they are not deformed, they appear to have a high amount of grains with low circularity, whereas most samples from class 1 have a lower amount of low circularity grains. This fact needs further investigation to be validated, but it could indicate that the grain size is of higher importance for the technical quality, in relation to the grain complexity.

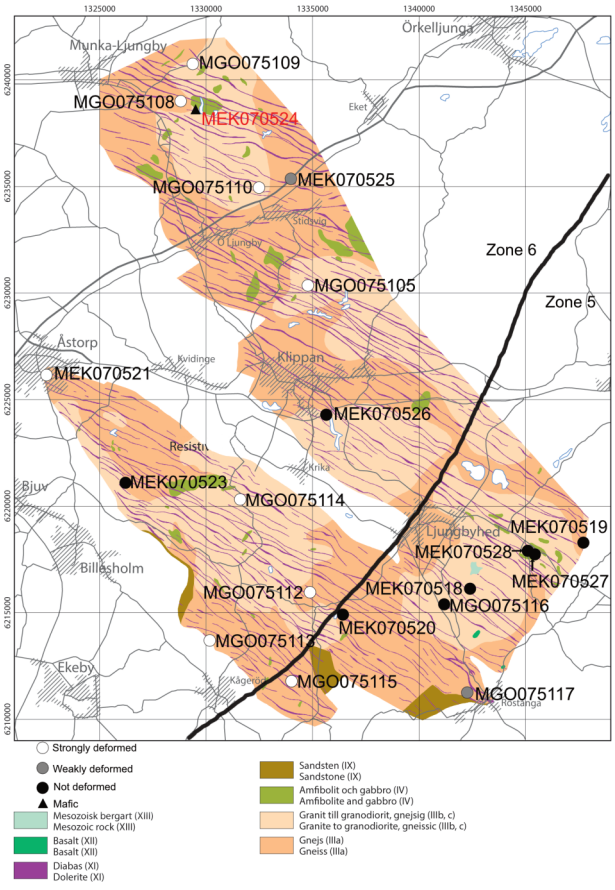

In terms of mineralogy, the samples that are located in zone 5 have lower percentage of quartz and higher feldspar content. The tartan twinning in feldspar is increased in these samples in comparison to the ones in zone 6. However, the appearance of perthitic exsolution in K-feldspars is higher in the samples of zone 6. These samples have little or no titanite and the majority of them include fine-grained rounded garnet crystals. Lastly, the rocks in zone 6 include accessory apatite, which is usually absent in zone 5.

5.2 Mineralogical and textural properties of each class

In this section, the technical properties of the samples are connected to the results from the quantitative mineralogical and microscopical examination. The aim is to try and explain in detail the reasons for these rocks of the same mineralogy having such diverse quality. This synopsis outlines which mineralogical and textural properties differentiate the samples with good technical quality from those with bad technical quality, together with a brief analysis of the samples that do not appear as expected.

5.2.1 Samples with good technical properties (Class 1)

Generally, the samples that have higher quality have high resistance to abrasion and brittle fragmentation and low LA (<30%), MDE (<7%), AN (<10%) values (Figure 6). They are fine-grained, and some have a high amount of grains with complex grain boundaries. The average percentage of biotite is approximately the same for all three classes (Table 3), and some samples contain a significant amount of sericite from the alteration of feldspars. The average percentage of quartz is 28% but some samples present quite higher amount of quartz. The amount of K-feldspar and plagioclase generally decreases with higher quality, in contrast to the amount of quartz that is higher for the samples of class 1. The samples of this class have been subjected to higher metamorphic conditions, and they are located in the north and northwest part of the study area (Figure 4A, 4B). The degree of deformation in these samples are higher in comparison to the rest of the samples (Figure 44), as depicted from the Aspect Ratio measurements; most of the samples have a high amount of elongated grains (Figure 38). The amount of fine-grained material is very high (Figure 39), but the circularity measurements show that the minerals in this class have high circularity, thus not very complex grain boundaries (Figures 36, 37). The reason for that

Figure 44: Map of the study area modified from Persson & Göransson (2010; based on Norling & Wikman (1990), Wikman et. al. (1993), Sivhed & Wikman (1986) and Wikman & Sivhed (1992)) with the samples colored according to their degree of deformation. The black line represents the approximate boundary between the metamorphic zones 5 and 6, after Möller & Andersson (2018).

could be because the higher metamorphic conditions and the deformation create smaller grains with low complexity.

Some samples in class 1 do not follow the general trend described above. For example, sample MGO075114, where there are many coarse-grained feldspar porphyroblasts and elongated quartz grains that might lower the total strength of the rock. However, the percentage of fine-grained material is quite high as well (68% of the grains are less than 0.5 mm long, Figure 35A). As a result, the quality of this rock increases.

5.2.2 Samples with medium technical properties (Class 2)

The 6 samples that are in class 2 are the ones that have increased values of AN (10-18%) and MDE (7-14%, Figure 6). These two technical tests measure the rock's resistance to abrasion. The LA values are slightly higher than in class 1, but they should be <30% (same limit as in class 1). The average percentage of quartz is lower in the class 2 samples (25.8%) in comparison to the class 1 samples, and the samples have increased amount of chlorite (2.4%) which lowers the resistance to abrasion. The total feldspar percentage is also higher in class 2, due to the higher percentage of plagioclase (15.8% in class 2 instead of 11.6% in class 1). The samples that belong in class 2 are not suitable for road aggregates, but they can be used for railroad construction or as aggregates (Table 2). The samples of this class are located both in the southeast and in the northern part of the study area (Figure 4A, 4B). The degree of strain in the north-northwestern part is higher in comparison to the southeastern part (Figure 44), and the results from the Aspect Ratio show that the samples that are in the northwestern part have higher amount of elongated grains, in comparison to the ones that are located in the southeast (Figure 38). The amount of fine-grained material is also higher in the samples that are located in the northwestern part of the study area (Figure 39), but the circularity measurements show that the samples in the southeast contain more grains with low circularity (Figure 37).

Some samples in class 2 do not follow the general trend described above. Sample MGO075109 for instance, has similar mineralogy to some samples in class 1, but the grain size plays a major role, as around 40% of the grains are over 1 mm long (Figure 35A), a factor that contributes significantly in lowering the rock's technical properties. Another example is sample MGO075112. The sample has high amount (22%) of grains over 1 mm long, high percentage of quartz and lacks amphiboles. Although there is high amount of fine-grained material in this sample, the lack of amphiboles and the grain size are the major factors that result in lowering the resistance to abrasion, and for that reason this rock is not suitable for road construction.

5.2.3 Samples with low technical properties (Class 3)

In general, the 6 samples that are in class 3 are the ones with the highest values of LA (>30%), AN (>18%) and MDE (>14%, Figure 6). The average percentage of amphibole and accessory minerals is lower than the other classes (Table 3). The average percentage of quartz is 24% but some samples present quite higher amount of quartz (Figure 33). The amount of K-feldspar and plagioclase is higher in the samples of class 3, in contrast to quartz. Moreover, the average percentage of garnet in these samples is much higher as it is for class 1 and class 2 samples. The samples are coarser grained, and they have a low amount of grains with complex grain boundaries; however, the samples of this class present the lowest values of circularity measurements (Figure 37). This is probably due to the lower degree of deformation, as the majority of the samples in class 3 are located in the southeastern part of the study area, where the metamorphic degree is lower (Figure 44). That is also be remarked from the Aspect Ratio measurements, since the samples of class 3 present the lowest amounts of elongated grains (Figure 38). The samples that belong in class 3 are not suitable for road aggregates or railways, but they can be used as aggregates (Table 2).

As in the previous two cases, some samples in class 3 do not follow the general trend described above. For instance, sample MEK070519 has the lowest percentage in quartz but is rather fine-grained (52% of the grains are less than 0.5 mm long). Also, the majority of the grains have high complexity. The reason that this orthogneiss is considered as not suitable for road and railway construction, regardless the low grain size, is probably due to the low amount of quartz since it increases the resistance to abrasion and to brittle fragmentation. Another example is sample MGO075116, where the case is the opposite than the previous sample. Here, the percentage of quartz is higher, in comparison to the rest of the samples in class 3; nonetheless, the grain size is rather high, as 70% of the grains are over 1 mm long (Figure 35A). The very high grain size in this sample is probably the most influential parameter of the technical quality.

6. Conclusions

The technical properties of the granitoid rocks are contingent of many factors; some of these are the mineralogy, the grain size and grain complexity, the presence of foliation, the presence of fine-grained matrix, the porosity, the presence of microfractures and others. In the present study, only some of these factors were analyzed in metamorphic orthogneisses. The results are restricted due to the small number of samples analyzed and the fact that not all these factors were taken into account. There is no clear distinction on which of the factors studied play the major role in the technical properties of these rocks, as derived from the results.

When examining in detail the samples that "do not follow the general trend", it is derived that none of the factors listed above is the dominant, but they complement each other.

The metamorphic degree is an important factor that affects the technical quality of the samples in the study area. The samples that underwent higher metamorphic conditions (northwest part of the study area) are more deformed and their technical quality is better than the samples that were in lower metamorphic conditions (southeast part of the study area). The degree of deformation follows the degree of metamorphism. The samples located in zone 6 are more deformed with a high amount of elongated grains, and their average grain size is smaller than the samples in zone 5, that are generally weakly deformed or undeformed.

In relation to mineralogy, it occurs that small variations of quartz and feldspar between the samples analyzed are associated with their quality. In particular, the higher the quartz percentage, the higher the technical properties, due to the fact that the presence of quartz lowers the Los Angeles, the Micro Deval and the Studded Tyre Test values. The feldspar tends to increase with the decrease in technical properties, because it increases in the expense of quartz. The presence of perthitic exsolution in K-feldspar is more intense in the samples that are located in zone 6 and have higher quality, and the presence of tartan twinning in these samples in lower. The average biotite and amphibole content are similar to all three classes. The samples that have lower quality include higher percentage of titanite and very low garnet and apatite, in contrast with the samples with higher quality.

The grain size is also strongly connected with the technical properties of these rocks. Generally, the rocks with good properties tend to have more fine-grained minerals, and they also appear even-grained. Additionally, the grain complexity is an important factor, because a rock that contains minerals with complex gain boundaries might have better interlocking than a rock with plain grain boundaries (i.e. granoblastic texture). In the majority of the samples, the grain size is more important than the circularity and the complexity of the grains, as most of the samples of class 3 have a high number of grains with low circularity, but the average grain size in that class is much higher than of class 1 samples.

The presence of microcracks in these rocks does not appear to have a major influence in their technical properties, since they are present in a consistent pattern in all four samples analyzed in the SEM. The microcracks have similar appearance in these samples, regardless their mean grain size. Since the restrictions in this study did not facilitate a comprehensive investigation of their properties, further analysis should be conducted in measuring their frequency, in order to have more reliable results.

7. Acknowledgement

I would like to thank my supervisor Charlotte Möller for her valuable help and the meticulous review of most parts of my thesis. Many thanks to my co-supervisors, Jenny Andersson and Mattias Göransson, for the constant guidance and the helpful advice. I would also like to thank Jan-Erik Lindqvist for all the suggestions and the important information he shared with me. Special thanks to my colleague Stylianos Karastergios, for all the encouragement and the endless discussions. Last but not least, I would like to thank my family and friends for all the love and support they gave to me during all this time.

8. References

Åkesson, U., Hansson, J. & Stigh, J., 2004: Characterization of microcracks in the Bohus granite, western Sweden, caused by uniaxial cyclic loading. *Engineering Geology 72*, pp. 131-142. doi: https://doi.org/10.1016/j.enggeo.2003.07.001

Andersson, J., Söderlund, U., Cornell, D., Johansson, L. & Möller, C., 1999: Sveconorwegian (-Grenvillian) deformation, metamorphism and leucosome formation in SW Sweden, SW Baltic Shield: Constraints from a Mesoproterozoic granite intrusion. *Precambrian Research 98*, pp. 151-171. doi: 10.1016/S0301-9268(99)00048-0

Bergerat, F., Angelier, J. & Andreasson, P.-G., 2007: Evolution of paleostress fields and brittle deformation of the Tornquist Zone in Scania (Sweden) during Permo-Mesozoic and Cenozoic times. *Tectonophysics 444*, pp. 93-110. doi: https://doi.org/10.1016/j.tecto.2007.08.005

Bingen, B., Nordgulen, Ø. & Viola, G., 2008: A four-phase model for the Sveconorwegian orogeny, SW Scandinavia. *Journal of Geology 88*, pp. 43-72.

Brattli, B., 1992: The influence of geological factors on the mechanical properties of basic igneous rocks used as road surface aggregates. *Engineering Geology 33*, pp. 31-44. doi: https://doi.org/10.1016/0013-7952(92)90033-U

Cawood, P. A., Nemchin, A. A., Strachan, R., Prave, T. & Krabbendam, M., 2007: Sedimentary basin and detrital zircon record along East Laurentia and Baltica during assembly and breakup of Rodinia. *Journal of the Geological Society 164*, pp. 257-275. doi: 10.1144/0016-76492006-115

Ersoy, A. & Waller, M. D., 1995: Textural characterization of rocks. *Engineering Geology 39*, pp. 123-136. doi: https://doi.org/10.1016/0013-7952(95)00005-Z

European Commission, 2019: Total length of the road network in Sweden in 2017, by road type (in kilometers). Statista Inc.

Föreningen För Asfaltsbeläggningar I Sverige, F.-M.-. 1998: Bestämning av kornstorleksfördelning genom siktningsanalys., Föreningen för asfaltbeläggningar i Sverige. p. 7

Goodman, R., 2020: Introduction to Rock Mechanics / R.E. Goodman.

Göransson, M., Bergström, U., Shomali, H., Claeson, D. & Hellström, F., 2008: Beskrivning till bergkvalitetskartan delar av Kungsbacka och Varbergs kommuner. *Sveriges geologiska undersökning K 96*, p. 37.

Hellman, F., Åkesson, U. & Eliasson, T., 2011. Kvantitativ petrografi sk analys av bergmaterial – en metodbeskrivning. VTI Report.

Högdahl, K., Andersson, U. B. & Eklund, O., 2004: *The Transscandinavian igneous belt in Sweden: a review of its character and evolution*. p. 125

Hubbard, F. H., 1978: Geochemistry of the Varberg granite gneisses. *Geologiska Föreningen i Stockholm Förhandlingar 100*, pp. 31-38. doi: 10.1080/11035897809448557

Johansson, E., 2011: *Technological properties of rock aggregates.*, Luleå Tekniska Universitet.

Johansson, L., Lindh, A. & Möller, C., 1991: Late Sveconorwegian (Grenville) high-pressure granulite facies metamorphism in southwest Sweden. *Journal of Metamorphic Geology 9*, pp. 283-292. doi: 10.1111/j.1525-1314.1991.tb00523.x

Kowallis, B. & Wang, H., 1983: Microcrack study of granitic cores from Illinois deep borehole UPH 3 (USA). *Journal of Geophysical Research 88*, pp. 7373-7380. doi: 10.1029/JB088iB09p07373

Kranz, R. L., 1983: Microcracks in rocks: A review. *Tectonophysics 100*, pp. 449-480. doi: https://doi.org/10.1016/0040-1951(83)90198-1

Lanin, E. S., Acker, C., Yu, Z., Sone, H. & Wang, B., 2019: Comparing Biotite Elastic Properties Recovered by Nano-Indentation With Molecular Simulation Predictions. *53rd U.S. Rock Mechanics/Geomechanics Symposium.* New York City, New York, American Rock Mechanics Association, p. 8

Larsson, D. & Söderlund, U., 2005: Lu–Hf apatite geochronology of mafic cumulates: An example from a Fe–Ti mineralization at Smålands Taberg, southern Sweden. *Chemical Geology - CHEM GEOL 224*, pp. 201-211. doi: 10.1016/j.chemgeo.2005.07.007

Laurent, A. T., Seydoux-Guillaume, A.-M., Duchene, S., Bingen, B., Bosse, V. & Datas, L., 2016: Sulphate incorporation in monazite lattice and dating the cycle of sulphur in metamorphic belts. *Contributions to Mineralogy and Petrology 171*, p. 94. doi: 10.1007/s00410-016-1301-5

Lindqvist, J. E., Åkesson, U. & Malaga, K., 2007: Microstructure and functional properties of rock materials. *Materials Characterization - MATER CHARACT 58*, pp. 1183-1188. doi: 10.1016/j.matchar.2007.04.012

Lundqvist & Göransson, 2001: Evaluation and Interpretation of Microscopic Parameters vs. Mechanical Properties of Precambrian Rocks from the Stockholm Region, Sweden. *Proceedings of the 8th Euroseminar Applied to Building Materials.* Athens, Greece. pp. 13-20

Lundqvist, T., 1979: The Precambrian of Sweden.

Merriam, R., Riekeiii, H. & Kim, Y., 1970: Tensile strength related to mineralogy and texture of some granitic rocks. *Engineering Geology - ENG GEOL 4*, pp. 155-160. doi: 10.1016/0013-7952(70)90010-4

Miskovsky, K., Duarte, M., Kou, S. & Lindqvist, P. A., 2004: Influence of the Mineralogical Composition and Textural Properties on the Quality of Coarse Aggregates. *Journal of Materials Engineering and Performance 13*, pp. 144-150. doi: 10.1361/10599490418334

Möller, C. & Andersson, J., 2018: Metamorphic zoning and behavior of an underthrusting continental plate. *Journal of Metamorphic Geology. 36*, pp. 567-589. doi: https://doi.org/10.1111/jmg.12304

Möller, C., Andersson, J., Dyck, B. & Antal Lundin, I., 2015: Exhumation of an eclogite terrane as a hot migmatitic nappe, Sveconorwegian orogen. *Lithos 226*, pp. 147-168. doi: https://doi.org/10.1016/j.lithos.2014.12.013

Möller, C., Andersson, J., Lundqvistt, I. & Hellström, F., 2007: Linking deformation, migmatite formation and zircon U–Pb geochronology in polymetamorphic orthogneisses, Sveconorwegian Province, Sweden. *Journal of Metamorphic Geology 25*, pp. 727-750. doi: 10.1111/j.1525-1314.2007.00726.x

Möller, C. & Söderlund, U., 1997: Age constraints on the regional deformation within the eastern segment, S. Sweden: Late sveconorwegian granite dyke intrusion and metamorphic-deformational relations. *GFF 119*, pp. 1-12. doi: 10.1080/11035899709546447

Norling, E. & Bergström, J., 1987: Mesozoic and Cenozoic tectonic evolution of Scania, southern Sweden. *Tectonophysics 137*, pp. 7-19.

Norling, E. & Wikman, H., 1990: Beskrivning till berggrundskarta Höganäs NO/Helsingborg NV. *Sveriges geologiska undersökning Af 129.* p. 123

Passchier, C. W. & Trouw, R. a. J., 1997: *Microtectonics*. Berlin. pp. 971-972

Persson, L. & Göransson, M., 2010: Beskrivning till bergkvalitetskartan, Söderåsens kommun. *In:* S. g. u. (SGU) (ed.).

Phillips, E. R., 1974: Myrmekite — one hundred years later. *Lithos 7*, pp. 181-194. doi: https://doi.org/10.1016/0024-4937(74)90029-2

Phillips, G. N., 1981: Water activity changes across an amphibolite-granulite facies transition, Broken Hill, Australia. *Contributions to Mineralogy and Petrology 75*, pp. 377-386. doi: 10.1007/BF00374721

Rivers, T., 2008: Assembly and preservation of lower, mid, and upper orogenic crust in the Grenville Province—Implications for the evolution of large hot long-duration orogens. *Precambrian Research 167*, pp. 237-259. doi: https://doi.org/10.1016/j.precamres.2008.08.005

Shelley, D., 1993: *Igneous and Metamorphic Rocks Under The Microscope. Classification, Textures, Microstructures and Mineral Preferred Orientations.* Cambridge University Press, p. 553

Simmons, G. & Richter, D., 1976: Microcracks in rocks. *Physics and Chemistry of Minerals and Rocks*, pp. 105-137.

Simpson, C. & Wintsch, R. P., 1989: Evidence for deformation-induced K-feldspar replacement by myrmekite. *Journal of Metamorphic Geology 7*, pp. 261-275. doi: 10.1111/j.1525-1314.1989.tb00588.x

Sivhed, U. & Wikman, H., 1986: Beskrivning till berggrundskarta Helsingborg SV. *Sveriges geologiska undersökning Af 149.* 108 p.

Smith, J. V., 1974: *Feldspar Minerals. Volume 1. Crystal Structure and Physical Properties.* Cambridge University Press. pp. 69-71

Söderlund, U. & Ask, R., 2006: Mesoproterozoic bimodal magmatism along the Protogine Zone, S Sweden: three magmatic pulses at 1.56, 1.22 and 1.205 Ga, and regional implications. *GFF 128*, pp. 303-310. doi: 10.1080/11035890601284303

Söderlund, U., Jarl, L.-G., Persson, P.-O., Stephens, M. B. & Wahlgren, C.-H., 1999: Protolith ages and timing of deformation in the eastern, marginal part of the Sveconorwegian orogen, southwestern Sweden. *Precambrian Research 94*, pp. 29-48. doi: https://doi.org/10.1016/S0301-9268(98)00104-1

Söderlund, U., Patchett, P. J., Vervoort, J. D. & Isachsen, C. E., 2004: The 176Lu decay constant determined by Lu–Hf and U–Pb isotope systematics of Precambrian mafic intrusions. *Earth and Planetary Science Letters 219*, pp. 311-324. doi: https://doi.org/10.1016/S0012-821X(04)00012-3

Sun W., W. L., Wang Y., 2017: Mechanical properties of rock materials with related to mineralogical characteristics and grain size through experimental investigation: a comprehensive review. Frontiers of Structural and Civil Engineering 11, 322. doi: 10.1007/s11709-017-0387-9

Sveriges Geologiska Undersökning, 2018: Grus, sand och krossberg 2016. *Periodiska publikationer 2017:2*, 38 p.

Swedish Standards Institute, S.-E.-. 1997a: Ballast – Mekaniska och fysikaliska egenskaper – Del 1: Bestämning av nötningsmotstånd (micro-Deval). Svensk Standard. 11 p.

Swedish Standards Institute, S.-E.-. 1997b: Ballast – Mekaniska och fysikaliska egenskaper – Del 2: Bestämning av motstånd mot sönderdelning. *Svensk Standard.* 29 p.

Swedish Standards Institute, S.-E.-. 2004: Ballast – Mekaniska och fysikaliska egenskaper – Del 9: Bestämning av motstånd mot nötning av dubbdäck (Nordiska kulkvarnsmetoden). Svensk Standard. 12 p.

Tavares, L. & Neves, P., 2008: Microstructure of quarry rocks and relationships to particle breakage and crushing. *International Journal of Mineral Processing - INT J MINER PROCESS 87*, pp. 28-41. doi: 10.1016/j.minpro.2008.01.007

Tugrul, A. & Zarif, I. H., 1999: Correlation of mineralogical and textural characteristics with engineering properties of selected granitic rocks from Turkey. *Engineering Geology 51*, pp. 303-317. doi: 10.1016/S0013-7952(98)00071-4

Vägverket, 2005a: Allmän teknisk beskrivning för vägkonstruktion. Kapitel E. Obundna material. ATB VÄG 2005. Publ. 2005:112. p. 105

Vägverket, 2005b: Allmän teknisk beskrivning för vägkonstruktion. Kapitel F. Bitumenbundna material. ATB VÄG 2005 Publ. 2005:112. p. 90

Whitney, D. & Bernard, E., 2010: Abbreviations for names of rock-forming minerals. *American Mineralogist 95*, pp. 185-187.

Wikman, H., Bergström, J. & U., S., 1993: 1993: Beskrivning till berggrundskarta Helsingborg SO. . *Sveriges geologiska undersökning Af 180*, pp. 22–28.

Wikman, H. & Sivhed, U., 1992: Beskrivning till berggrundskarta Helsingborg NO. *Sveriges geologiska undersökning Af 148*, pp. 22–28.

Wojnar, L., Kurzydłowski, K. J. & Szala, J., 2004: Quantitative Image Analysis. *Metallography and Microstructures.* ASM International.

Xiang-Dong, W. L., Anders, 1996: Temperature-pressure Investigation of the Southern Part of the Southwest Swedish Granulite Region. *European Journal of Mineralogy 8*, pp. 51-68. doi: 10.1127/ejm/8/1/0051

9. Appendices

Appendix 1: Ternary QAP diagram for granite rocks, based on the modal amounts for point counting. The felsic samples of this study are plotted on the diagram.

Appendix 2: Geographic coordinates and technical analyses of samples from the map area of Söderåsen. The coordinate system is RT90. AN = Studded Tyre test value, LA = Los Angeles value, MDE = micro-Deval value.

Appendix 3: Modal mineralogy of the orthogneisses from Söderåsen, sorted by class. The modal percentage was calculated using the point counting method.

Appendix 4: Table with the orthogneiss samples divided by the metamorphic zones and ordered with increasing LA value. The minerals and the exsolution textures are the ones that show the highest variation between the two zones.

Appendix 1: Ternary QAP diagram for granite rocks, based on the modal amounts for point counting. The felsic samples of this study are plotted on the diagram.

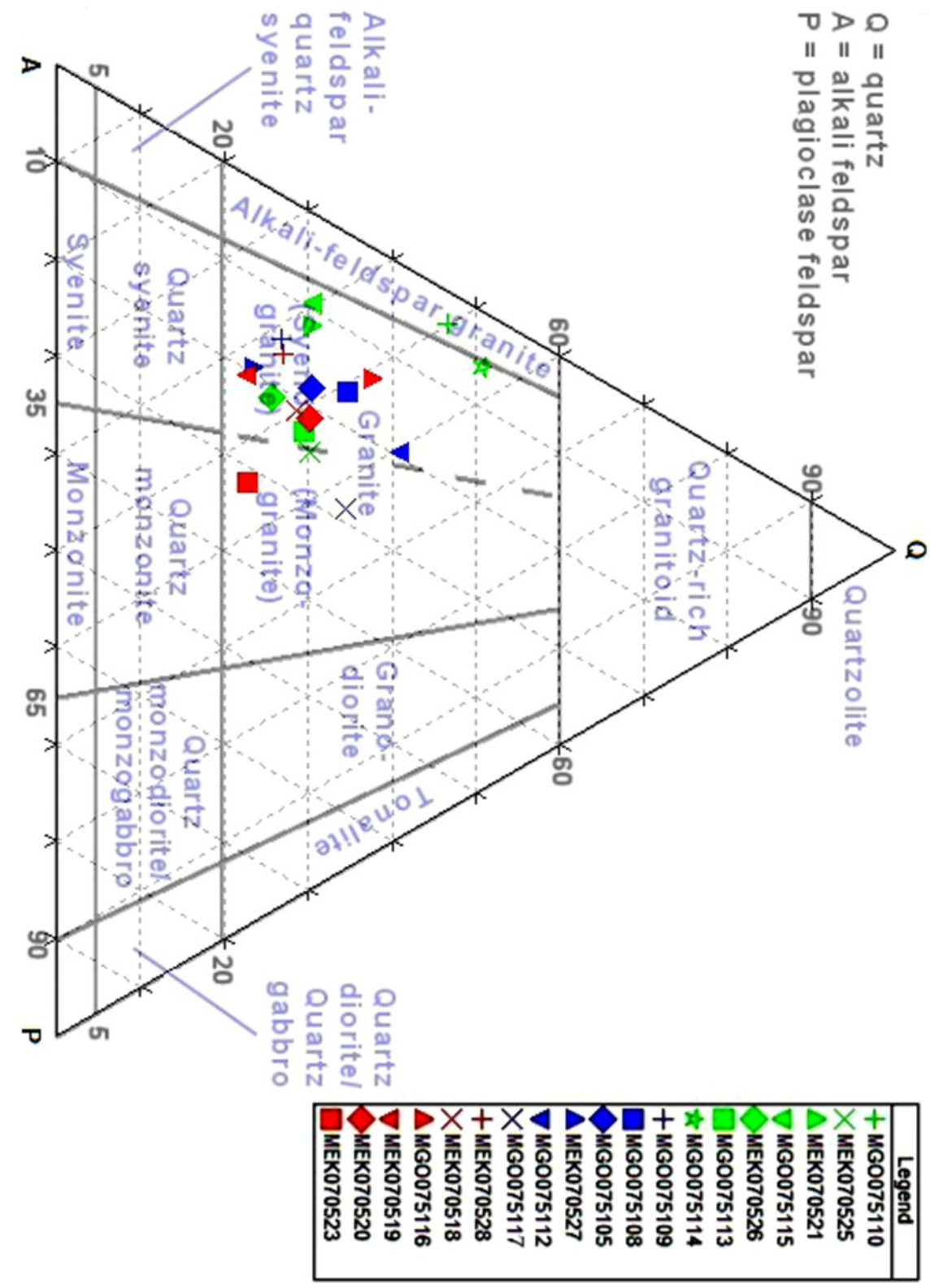

Appendix 2: Geographic coordinates and technical analyses of samples from the map area of Söderåsen. The coordinate system is RT90. AN = Studded Tyre test value, LA = Los Angeles value, MDE = micro-Deval value.

Sample	N-S coordinates	E-W coordinates	A_N %	LA %	M_{DE} %
Class 1					
MGO075113	6213694	1330241	9.1	19.4	5.9
MGO075110	6234953	1332424	8.6	21.6	5.3
MGO075115	6211798	1334055	9.9	21.6	6.6
MGO075114	6220279	1331642	9.3	21.9	5.8
MEK070526	6224280	1335730	9.4	22.3	6.0
MEK070525	6235288	1334046	9.3	22.5	6.0
MEK070521	6225722	1322716	8.8	22.8	5.6
Class 2					
MGO075105	6230270	1334827	10.3	20.9	6.6
MGO075108	6238971	1328735	10.1	21.8	6.6
MGO075109	6240770	1329439	11.1	24.9	7.5
MGO075117	6211164	1342247	11.4	26.6	8.0
MEK070527	6217902	1345054	12.3	28.2	7.2
MGO075112	6215953	1334800	11.7	29.9	8.2
Class 3					
MGO075116	6215386	1341162	11.7	31.0	7.2
MEK070528	6217900	1345072	11.5	31.3	7.1
MEK070518	6216112	1342350	12.0	31.4	8.0
MEK070523	6221085	1326271	13.9	32.9	9.3
MEK070519	6218308	1347723	14.0	39.4	9.2
MEK070520	6214865	1336446	14.5	45.0	8.6

Appendix 3: Modal mineralogy of the orthogneisses from Söderåsen, sorted by class. The modal percentage was calculated using the point counting method.

CLASS 1 SAMPLES							
Minerals	MGO075110	MEK070525	MEK070521	MGO075115	MEK070526	MGO075113	MGO075114
Quartz	39.0	24.2	24.8	22.2	20.2	24.4	43.4
Potassium Feldspar	23.0	17.4	28.6	33.6	17.4	30.2	13.0
Plagioclase Tartan Twinned	2.8	20.8	9.6	6.6	17.6	19.0	5.0
Kfs Perthitic	0.0	0.0	0.0	7.0	14.4	3.4	9.2
Kfs Tartan twinned & Perthitic	19.2	20.4	19.2	1.4	1.2	5.6	9.4
Kfs Antiperthitic Plagioclase	0.0	0.0	0.0	1.2	10.6	0.2	5.6
	0.0	0.0	0.0	0.0	0.0	0.0	0.0
Myrmekite	0.4	1.0	0.0	0.0	1.0	0.0	0.0
Biotite	1.2	1.8	4.4	7.2	0.8	4.8	0.0
Amphibole	4.6	9.8	6.4	11.2	6.2	6.8	5.0
Else	9.8	4.6	7.0	9.6	10.6	5.6	9.4
Total	**100.0**	**100.0**	**100.0**	**100.0**	**100.0**	**100.0**	**100.0**
Else							
Sericite	4.6	0.4	3.6	5.8	7.4	0.6	3.8
Chlorite	2.4	0.2	0.0	0.4	2.0	2.0	4.0
Zircon	0.6	0.4	0.4	0.0	0.2	0.2	0.2
Opaques	2.0	2.8	2.6	1.8	1.0	2.2	0.4
Apatite	0.0	0.4	0.0	0.0	0.0	0.6	0.4
Garnet	0.2	0.4	0.0	0.0	0.0	0.0	0.6
Titanite	0.0	0.0	0.4	1.6	0.0	0.0	0.0
Total	**9.8**	**4.6**	**7.0**	**9.6**	**10.6**	**5.6**	**9.4**

Appendix 3 (cont.)

CLASS 2 SAMPLES						
Minerals	MGO075109	MGO075108	MGO075105	MEK070527	MGO075112	MGO075117
Quartz	21.2	23.2	25.0	17.8	38.2	29.2
Potassium Feld-spar	28.4	21.0	28.2	16.2	18.8	28.0
Plagioclase	12.0	9.4	15.2	17.0	17.8	23.6
Tartan Twinned Kfs	0.0	0.0	0.0	3.6	7.2	3.4
Perthitic Kfs	19.4	12.8	15.6	17.0	3.2	0.0
Tartan twinned & Perthitic Kfs	0.0	0.0	0.0	13.0	7.4	0.0
Antiperthitic Pla-gioclase	0.0	1.8	0.2	0.0	0.0	0.4
Myrmekite	0.8	0.6	1.0	2.4	0.0	0.0
Biotite	1.0	5.6	0.6	6.0	5.0	0.0
Amphibole	8.0	18.8	7.2	1.6	0.0	0.0
Else	9.2	6.8	7.0	5.4	2.4	15.4
Total	**100.0**	**100.0**	**100.0**	**100.0**	**100.0**	**100.0**
Else						
Sericite	3.2	0.8	0.6	2.0	1.6	4.2
Chlorite	2.6	0.4	1.6	1.0	0.0	8.6
Zircon	0.4	0.0	0.0	0.6	0.0	0.0
Opaques	2.4	4.4	3.0	1.4	0.6	2.4
Apatite	0.6	0.2	1.2	0.0	0.0	0.0
Garnet	0.0	0.6	0.6	0.0	0.2	0.0
Titanite	0.0	0.4	0.0	0.4	0.0	0.2
Total	**9.2**	**6.8**	**7.0**	**5.4**	**2.4**	**15.4**

Appendix 3 (cont.)

CLASS 3 SAMPLES						
Minerals	MEK070528	MEK070518	MGO075116	MEK070519	MEK070520	MEK070523
Quartz	21.4	21.0	34.2	18.6	29.5	21.4
Potassium Feld-spar	22.6	9.4	7.2	25.3	15.5	22.0
Plagioclase	14.4	15.8	12.4	16.5	20.6	29.4
Tartan Twinned Kfs	17.8	0.0	0.0	11.4	24.4	5.9
Perthitic Kfs	6.0	27.8	37.8	4.1	2.8	3.6
Tartan twinned & Perthitic Kfs	4.2	0.0	0.0	5.3	4.7	2.9
Antiperthitic Plagioclase	0.0	0.0	0.0	0.2	0.0	0.2
Myrmekite	2.8	0.2	0.2	0.0	0.0	0.0
Biotite	4.2	1.2	2.8	3.5	0.0	2.6
Amphibole	0.0	12.0	3.4	11.2	0.0	3.5
Else	6.6	12.6	2.0	3.9	2.6	8.8
Total	**100.0**	**100.0**	**100.0**	**100.0**	**100.0**	**100.3**
Else						
Sericite	3.8	0.0	0.0	1.0	0.0	5.7
Chlorite	0.0	0.0	0.2	0.8	0.8	0.2
Zircon	0.6	0.4	0.4	0.0	0.0	0.2
Opaques	1.6	1.6	0.0	2.0	1.8	2.0
Apatite	0.0	0.6	0.0	0.2	0.0	0.2
Garnet	0.0	10.0	1.0	0.0	0.0	0.0
Titanite	0.6	0.0	0.4	0.0	0.0	0.0
Total	**6.6**	**12.6**	**2.0**	**3.9**	**2.6**	**8.2**

Appendix 4: Table with the orthogneiss samples divided by the metamorphic zones and ordered with increasing LA value. The minerals and the exsolution textures are the ones that show the highest variation between the two zones.

	Sample	Class	LA %	Perthite	Tartan twinning	Tartan t. + Perthites	Tit	Grt	Ap
Zone 5	MGO075115	1	21.6		✓		✓		
	MGO075117	2	26.6		✓		✓		
	MEK070527	2	28.2	✓	✓	✓	✓		
	MGO075116	3	31	✓			✓	✓	
	MEK070528	3	31.3	✓	✓	✓	✓		
	MEK070518	3	31.4	✓				✓	✓
	MEK070519	3	39.4		✓	✓	✓		✓
	MEK070520	3	45		✓	✓			
Zone 6	MGO075113	1	19.4	✓					✓
	MGO075105	2	20.9	✓				✓	✓
	MGO075110	1	21.6	✓				✓	
	MGO075108	2	21.8	✓			✓	✓	✓
	MGO075114	1	21.9	✓	✓	✓		✓	✓
	MEK070526	1	22.3		✓	✓			
	MEK070525	1	22.5	✓				✓	✓
	MEK070521	1	22.8	✓			✓		
	MGO075109	2	24.9	✓					✓
	MGO075112	2	29.9	✓	✓	✓		✓	
	MEK070523	3	32.9	✓	✓				✓

Tidigare skrifter i serien ”Examensarbeten i Geologi vid Lunds universitet”:

553. Hernnäs, Tove, 2018: Garnet amphibolite in the internal Eastern Segment, Sveconorwegian Province: monitors of metamorphic recrystallization at high temperature and pressure during Sveconorwegian orogeny. (45 hp)
554. Halling, Jenny, 2019: Characterization of black rust in reinforced concrete structures: analyses of field samples from southern Sweden. (45 hp)
555. Stevic, Marijana, 2019: Stratigraphy and dating of a lake sediment record from Lyngsjön, eastern Scania - human impact and aeolian sand deposition during the last millennium. (45 hp)
556. Rabanser, Monika, 2019: Processes of Lateral Moraine Formation at a Debris-covered Glacier, Suldenferner (Vedretta di Solda), Italy. (45 hp)
557. Nilsson, Hanna, 2019: Records of environmental change and sedimentation processes over the last century in a Baltic coastal inlet. (45 hp)
558. Ingered, Mimmi, 2019: Zircon U-Pb constraints on the timing of Sveconorwegian migmatite formation in the Western and Median Segments of the Idefjorden terrane, SW Sweden. (45 hp)
559. Hjorth, Ingeborg, 2019: Paleomagnetisk undersökning av vulkanen Rangitoto, Nya Zeeland, för att bestämma dess utbrottshistoria. (15 hp)
560. Westberg, Märta, 2019: Enigmatic worm-like fossils from the Silurian Waukesha Lagerstätte, Wisconsin, USA. (15 hp)
561. Björn, Julia, 2019: Undersökning av påverkan på hydraulisk konduktivitet i förorenat område efter in situ-saneringsförsök. (15 hp)
562. Faraj, Haider, 2019: Tolkning av georadarprofiler över grundvattenmagasinet Verveln - Gullringen i Kalmar län. (15 hp)
563. Bjermo, Tim, 2019: Eoliska avlagringar och vindriktningar under holocen i och kring Store Mosse, södra Sverige. (15 hp)
564. Langkjaer, Henrik, 2019: Analys av Östergötlands kommande grundvattenresurser ur ett klimtperspektiv - med fokus på förstärkt grundvattenbildning. (15 hp)
565. Johansson, Marcus, 2019: Hur öppet var landskapet i södra Sverige under Atlantisk tid? (15 hp)
566. Molin, Emmy, 2019: Litologi, sedimentologi och kolisotopstratigrafi över krita–paleogen-gränsintervallet i borrningen Limhamn-2018. (15 hp)
567. Schroeder, Mimmi, 2019: The history of European hemp cultivation. (15 hp)
568. Damber, Maja, 2019: Granens invandring i sydvästa Sverige, belyst genom pollenanalys från Skottenesjön. (15 hp)
569. Lundgren Sassner, Lykke, 2019: Strandmorfologi, stranderosion och stranddeposition, med en fallstudie på Tylösand sandstrand, Halland. (15 hp)
570. Greiff, Johannes, 2019: Mesozoiska konglomerat och Skånes tektoniska utveckling. (15 hp)
571. Persson, Eric, 2019: An Enigmatic Cerapodian Dentary from the Cretaceous of southern Sweden. (15 hp)
572. Aldenius, Erik, 2019: Subsurface characterization of the Lund Sandstone – 3D model of the sandstone reservoir and evaluation of the geoenergy storage potential, SW Skåne, South Sweden. (45 hp)
573. Juliusson, Oscar, 2019: Impacts of subglacial processes on underlying bedrock. (15 hp)
574. Sartell, Anna, 2019: Metamorphic paragenesis and P-T conditions in garnet amphibolite from the Median Segment of the Idefjorden Terrane, Lilla Edet. (15 hp)
575. Végvári, Fanni, 2019: Vulkanisk inverkan på klimatet och atmorsfärcirkulationen: En litterarurstudie som jämför vulkanism på låg respektive hög latitud. (15 hp)
576. Gustafsson, Jon, 2019: Petrology of platinum-group element mineralization in the Koillismaa intrusion, Finland. (45 hp)
577. Wahlquist, Per, 2019: Undersökning av mindre förkastningar för vattenuttag i sedimentärt berg kring Kingelstad och Tjutebro. (15 hp)
578. Gaitan Valencia, Camilo Esteban, 2019: Unravelling the timing and distribution of Paleoproterozoic dyke swarms in the eastern Kaapvaal Craton, South Africa. (45 hp)
579. Eggert, David, 2019: Using Very-Low-Frequency Electromagnetics (VLF-EM) for geophysical exploration at the Albertine Graben, Uganda - A new CAD approach for 3D data blending. (45 hp)
580. Plan, Anders, 2020: Resolving temporal links between the Högberget granite and the Wigström tungsten skarn deposit in Bergslagen (Sweden) using trace elements and U-Pb LA-ICPMS on complex zircons. (45 hp)
581. Pilser, Hannes, 2020: A geophysical survey in the Chocaya Basin in the central Valley of Cochabamba, Bolivia, using ERT and TEM. (45 hp)
582. Leopardi, Dino, 2020: Temporal and genetical constraints of the Cu-Co Vena-

Dampetorp deposit, Bergslagen, Sweden. (45 hp)

583. Lagerstam Lorien, Clarence, 2020: Neck mobility versus mode of locomotion – in what way did neck length affect swimming performance among Mesozoic plesiosaurs (Reptilia, Sauropterygia)? (45 hp)
584. Davies, James, 2020: Geochronology of gneisses adjacent to the Mylonite Zone in southwestern Sweden: evidence of a tectonic window? (45 hp)
585. Foyn, Alex, 2020: Foreland evolution of Blåisen, Norway, over the course of an ablation season. (45 hp)
586. van Wees, Roos, 2020: Combining luminescence dating and sedimentary analysis to derive the landscape dynamics of the Velická Valley in the High Tatra Mountains, Slovakia. (45 hp)
587. Rettig, Lukas, 2020: Implications of a rapidly thinning ice-margin for annual moraine formation at Gornergletscher, Switzerland. (45 hp)
588. Bejarano Arias, Ingrid, 2020: Determination of depositional environment and luminescence dating of Pleistocene deposits in the Biely Váh valley, southern foothills of the Tatra Mountains, Slovakia. (45 hp)
589. Olla, Daniel, 2020: Petrografisk beskrivning av Prekambriska ortognejser i den undre delen av Särvskollan, mellersta delen av Skollenheten, Kaledonska orogenen. (15 hp)
590. Friberg, Nils, 2020: Är den sydatlantiska magnetiska anomalin ett återkommande fenomen? (15 hp)
591. Brakebusch, Linus, 2020: Klimat och väder i Nordatlanten-regionen under det senaste årtusendet. (15 hp)
592. Boestam, Max, 2020: Stränder med erosion och ackumulation längs kuststräckan Trelleborg - Abbekås under perioden 2007-2018. (15 hp)
593. Agudelo Motta, Laura Catalina, 2020: Methods for rockfall risk assessment and estimation of runout zones: A case study in Gothenburg, SW Sweden. (45 hp)
594. Johansson, Jonna, 2020: Potentiella nedslagskratrar i Sverige med fokus på Östersjön och östkusten. (15 hp)
595. Haag, Vendela, 2020: Studying magmatic systems through chemical analyses on clinopyroxene - a look into the history of the Teno ankaramites, Tenerife. (45 hp)
596. Kryffin, Isidora, 2020: Kan benceller bevaras över miljontals år? (15 hp)
597. Halvarsson, Ellinor, 2020: Sökande efter nedslagskratrar i Sverige, med fokus på avtryck i berggrunden. (15 hp)
598. Jirdén, Elin, 2020: Kustprocesser i Arktis – med en fallstudie på Prins Karls Forland, Svalbard. (15 hp)
599. Chonewicz, Julia, 2020: The Eemian Baltic Sea hydrography and paleoenvironment based on foraminiferal geochemistry. (45 hp)
600. Paradeisis-Stathis, Savvas, 2020: Holocene lake-level changes in the Siljan Lake District – Towards validation of von Post's drainage scenario. (45 hp)
601. Johansson, Adam, 2020: Groundwater flow modelling to address hydrogeological response of a contaminated site to remediation measures at Hjortsberga, southern Sweden. (15 hp)
602. Barrett, Aodhan, 2020: Major and trace element geochemical analysis of norites in the Hakefjorden Complex to constrain magma source and magma plumbing systems. (45 hp)
603. Lundqvist, Jennie, 2020: "Man fyller det med information helt enkelt": en fenomenografisk studie om studenters upplevelse av geologisk tid. (45 hp)
604. Zachén, Gabriel, 2020: Classification of four mesosiderites and implications for their formation. (45 hp)
605. Viðarsdóttir, Halla Margrét, 2020: Assessing the biodiversity crisis whitin the Triassic-Jurassic boundary interval using redox sensitive trace metals and stable carbon isotope geochemistry. (45 hp)
606. Tan, Brian, 2020: Nordvästra Skånes prekambriska geologiska utveckling. (15 hp)
607. Taxopoulou, Maria Eleni, 2020: Metamorphic micro-textures and mineral assemblages in orthogneisses in NW Skåne – how do they correlate with technical properties? (45 hp)

LUNDS UNIVERSITET

Geologiska institutionen
Lunds universitet
Sölvegatan 12, 223 62 Lund